

© Copyright 2006

Philip Edward Higuera



Late Glacial and Holocene Fire History in the Southcentral Brooks Range, Alaska: Direct  
and Indirect Impacts of Climatic Change on Fire Regimes

Philip Edward Higuera

A dissertation submitted in partial fulfillment of the  
requirements for the degree of

Doctor of Philosophy

University of Washington

2006

Program Authorized to Offer Degree:  
College of Forest Resources



University of Washington  
Graduate School

This is to certify that I have examined this copy of a doctoral dissertation by

Philip Edward Higuera

and have found that it is complete and satisfactory in all respects,  
and that any and all revisions required by the final  
examining committee have been made.

Chair of the Supervisory Committee:

---

Linda B. Brubaker

Reading Committee:

---

Linda B. Brubaker

---

Daniel G. Gavin

---

Douglas G. Sprugel

Date: \_\_\_\_\_



In presenting this dissertation in partial fulfillment of the requirements for the doctoral degree at the University of Washington, I agree that the Library shall make its copies freely available for inspection. I further agree that extensive copying of the dissertation is allowable only for scholarly purposes, consistent with "fair use" as prescribed in the U.S. Copyright Law. Requests for copying or reproduction of this dissertation may be referred to ProQuest Information and Learning, 300 North Zeeb Road, Ann Arbor, MI 48106-1346, 1-800-521-0600, or to the author.

Signature \_\_\_\_\_

Date \_\_\_\_\_



University of Washington

**Abstract**

Late Glacial and Holocene Fire History in the Southcentral Brooks Range, Alaska: Direct and Indirect Impacts of Climatic Change on Fire Regimes

Philip Edward Higuera

Chair of the Supervisory Committee:  
Professor Linda B. Brubaker  
College of Forest Resources

Fire-history records have important implications for understanding the controls of modern and future fire regimes in arctic and boreal Alaska. Charcoal in lake sediments provides a means to reconstruct past fires across different climatic and vegetational periods in this region, but interpreting charcoal stratigraphy is challenging because little information exists linking charcoal production to charcoal accumulation in sediment cores. I present a numerical model that simulates the major processes in this pathway and illustrate its use as a tool to evaluate the assumptions of charcoal dispersal and taphonomy and the merits of different approaches for analyzing charcoal records. This model suggests that existing assumptions of charcoal dispersal distances are too simplistic but supports the use of current analytical techniques for decomposing charcoal series to infer local fire occurrence. I also use lake sediment records to reconstruct fire return intervals (FRIs; the inverse of fire frequency) across a 150 km-wide study area in the southcentral Brooks Range of Alaska over the past 15,000 years. Fossil pollen, stomata, and modern analog analyses document four major shifts in vegetation over this period. At millennial time scales, fire-regime changes showed greater correspondence to changes in vegetation than to changes in inferred climate. For example, FRIs increased with climatic warming associated with a shift to deciduous forest c. 10,500 years ago, and FRIs decreased with climatic cooling associated with the development of the modern boreal forest c. 5500 years ago. These patterns suggest that vegetation strongly mediated the direct impacts of millennial-scale climatic change by modifying landscape



flammability. Within the boreal forest period (5500-0 years ago), fire histories reveal varying sensitivities of the fire regime to moisture and/or temperature changes. A subtle but statistically significant decrease in FRIs is associated with a shift from drier to moister conditions 2700 years ago; fire regimes were insensitive to a climatic shift c. 1200 years ago; and mean FRIs increased by 50% with the onset of Little Ice Age cooling 450 years ago. These varying responses emphasize the need for a rigorous understanding of climatic and non-climatic variables to anticipate fire regimes under future climatic scenarios.

# TABLE OF CONTENTS

List of Figures.....	iii
List of Tables .....	v
Chapter 1: Background, motivation, and overview .....	1
Chapter 2: Understanding the origin and analysis of sediment-charcoal records with a simulation model.....	10
Summary .....	10
Introduction.....	11
Methods and Rationale .....	14
Results.....	24
Discussion.....	27
Chapter 3: Vegetation-mediated impacts of climatic change on late glacial and Holocene fire regimes in the southcentral Brooks Range, Alaska.....	46
Summary .....	46
Introduction.....	47
Study Lakes and Regional Setting .....	49
Late Glacial and Holocene Climatic and Vegetational History.....	50
Methods and Rationale .....	51
Results.....	55
Discussion.....	60
Chapter 4: Impacts of centennial and millennial-scale climatic change on boreal forest fire regimes in the southcentral Brooks Range, Alaska.....	83
Summary .....	83
Introduction.....	84
Study Lakes and Regional Vegetation, Fire, and Climate History .....	86

Methods and Rationale .....	88
Results.....	91
Discussion.....	93
References.....	112
Appendix A: Evaluation and expansion of a Gaussian plume model for quantifying the source area of macroscopic charcoal .....	129
Appendix B: Sensitivity to assumptions on wind direction and the distribution of injection heights .....	148
Appendix C: Modern analog analysis with fossil pollen samples .....	151
Appendix D: Detecting changes in fire-frequency regimes: sample size and statistical power .....	154
Introduction.....	154
Methods.....	160
Results.....	162
Conclusions.....	163
Matlab function for the likelihood ratio test .....	172

## LIST OF FIGURES

Figure Number	Page
1.1 Aerial photograph of the Erickson Creek Fire.....	5
1.2 Geographic pattern of Alaskan wildfires, 1950-2004.....	6
1.3 Annual area burned in Alaska, 1950-2004.....	7
1.4 Simplified schematic of climatic influences on fire regimes.....	8
1.5 Controls of fire occurrence at different spatial and temporal scales.....	9
2.1 Components of a simulated sediment charcoal record.....	38
2.2 Characteristics of dispersal tables used in the Charcoal Simulation Model.....	39
2.3 Contrasting definitions of low-frequency trends in charcoal accumulation.....	40
2.4 Sources of variability in simulated charcoal records.....	41
2.5 Comparisons between simulated and empirical charcoal records.....	42
2.6 Correlation between charcoal accumulation and area burned in simulated charcoal records.....	43
2.7 Maximum correlation of sampled charcoal accumulation in simulated records, as a function of mixing and sampling intervals.....	44
2.8 Maximum accuracy of peak identification in simulated records, as a function of smoothing and sampling intervals.....	45
3.1 Map of Alaska and the study area, including recent fire history.....	74
3.2 Age-depth models for Ruppert, Xindi, Code, and Wild Tussock lakes.....	75
3.3 (a-d) Pollen, stomata, and charcoal stratigraphy for Ruppert, Xindi, Code, and Wild Tussock lakes, with modern analog analysis and vegetation zones.....	76
3.4 Box plots of charcoal accumulation rates within vegetation zones for Ruppert, Xindi, Code, and Wild Tussock lakes.....	80
3.5 Interpolated charcoal records and peak identification for Ruppert, Xindi, Code, and Wild Tussock lakes.....	81
3.6 Distribution of fire return intervals for each vegetation zone for Ruppert, Xindi, Code, and Wild Tussock lakes.....	82

4.1 Map of Alaska and the study area, including recent fire history .....	101
4.2 Age-depth model for Last Chance Lake .....	102
4.3 Analytical framework for inferring impacts of climatic change on historic fire regimes .....	103
4.4 (a-d) Pollen, stomata, and charcoal stratigraphy for Ruppert, Code, Wild Tussock, and Last Chance lakes, with modern analog analysis and vegetation zones .....	104
4.5 Interpolated charcoal record and peak identification for Last Chance Lake .....	108
4.6 Fire return intervals for each climatic period for Ruppert, Code, Wild Tussock, and Last Chance lakes.....	109
4.7 Composite fire return intervals and unique Weibull distributions for each climatic period .....	110
4.8 Summary of fire and climatic history for the study area or region.....	111
6.1 Sensitivity of the correlation of airborne charcoal accumulation and area burned to wind and injection-height assumptions.....	150
7.1 Pollen samples from the NAPD dataset used in modern analog analysis.....	152
7.2 Within- and between-biome comparisons using the NAPD dataset.....	153
8.1 Random fire occurrence data and an example of the likelihood ratio test with different sample sizes.....	166
8.2 Statistical power as a function of sample size for alternative methods for comparing distributions of fire return intervals .....	167
8.3 Statistical power as a function of sample size and Weibull $c$ parameter for the likelihood ratio test. ....	171

## LIST OF TABLES

Table Number	Page
2.1 Components of the Charcoal Simulation Model.....	35
2.2 Parameters used in the Charcoal Simulation Model.....	36
2.3 Parameters for comparisons between simulated and empirical charcoal records.....	37
3.1 Summary of late glacial and Holocene climatic and vegetational change in northcentral Alaska.....	69
3.2 Location, characteristics, and record quality for Ruppert, Xindi, Code, and Wild Tussock lakes.....	70
3.3 AMS <sup>14</sup> C dates for Ruppert, Xindi, Code, and Wild Tussock lakes.....	71
3.4 Probability of Type-I error for comparisons between fire-return-interval distributions within and between vegetation zones and sites.....	72
3.5 Sensitivity of fire-return-interval distributions to peak identification criterion.....	73
4.1 AMS <sup>14</sup> C dates for Last Chance Lake.....	99
4.2 Probability of Type-I error for comparisons between fire-return-interval distributions within and between climatic periods and sites.....	100

## ACKNOWLEDGEMENTS

Funding for this dissertation came from the National Science Foundation's Arctic Systems Science program via grant number 0112586 awarded to Linda Brubaker, Patricia Anderson, Feng Sheng Hu, Thomas Brown, and Scott Rupp in 2001 and through a National Science Foundation Graduate Research Fellowship awarded to the author in 1999 (utilized from 2003-2005). Sampling was conducted under permit from Gates of the Arctic National Park and the Bureau of Land Management. I thank Kate Shick and John Mauro for help with field work during 2002 and 2003. I thank Ethan Cudaback, Amy Lilienthal (Yambor), Jennifer Leach, Jason Smith, and Emily Spaulding for carrying out most of the laboratory work required for this research. The pollen samples from Ruppert and Xindi lakes were counted by Linda Brubaker and Patricia Anderson. The majority of charcoal samples was counted by Claire Adam and Jennifer Leach, with contributions also from Emily Spaulding and the author.

My years as a graduate student at the University of Washington have been extremely rewarding both academically and personally, thanks in large part to the guidance, friendship and support of those mentioned below. First and foremost, I give my heartfelt thanks to Linda Brubaker for providing the opportunities, training, encouragement, freedom, and endless constructive feedback that was integral to my intellectual development. Linda's commitment to rigorous science, her deep respect for individuals, and her ability to keep life in perspective have made her an exceptional mentor. I am also sincerely grateful to Doug Sprugel. Through many discussions over the years, Doug has always offered insightful feedback on my ideas, kept me honest, and helped me communicate my thoughts effectively. I thank Dan Gavin for joining my committee from outside the University and providing significant intellectual feedback on both the methodological and ecological questions I pursued in my work. I thank my other committee members, Jim Agee and Patricia Anderson, for providing important advice along the way and for reviewing this dissertation.

I thank Mathew Peters, first a ski partner, then a close friend, and finally a collaborator. Matt was instrumental in the development of CharSim (Chapter 2) and

served as an unofficial research mentor for this component of my dissertation. His intellectual curiosity, patience, and unselfish pursuit of understanding were inspirational and provided a valuable component of my graduate studies.

Former members of the Paleoecology Lab, including Shelley Crausbay, Heather Heuser, Wyatt Oswald, and Alecia Spooner, provided important advice, feedback and perspective during my graduate studies. I am also thankful for the friendship and feedback from fellow graduate students, including Mike Keim, Jeremy Littell, Dan Perrakis, and Carol Volk. I thank my friends and family in Seattle and beyond for encouragement, support, and a wonderful life outside of graduate school. The myriad of trips in the mountains of Washington and the region sustained me and will remain some of the most memorable and meaningful experiences of my life. I am especially grateful for the patience, understanding, and encouragement of my closest friends and family over the last few months of my program.

Finally, I thank my wife, Claire Adam, for enduring the residual stresses of my Ph.D. program, always making me smile, and helping me keep life in perspective. Your love, support, encouragement, and companionship have made all the difference in the world.

## **DEDICATION**

I dedicate this dissertation to my parents, Margaret and Gilberto Higuera, for their never-ending love, support, and commitment to my education.

## CHAPTER 1: BACKGROUND, MOTIVATION, AND OVERVIEW

Arctic and boreal regions of Alaska stand in sharp contrast to more populated lower latitudes of North America. Vast areas are roadless, grizzly bear and wolf still populate the landscape, and wildfires burn largely unsuppressed (Bureau of Land Management 2005; Fig. 1.1, 1.2). Between 1950-2004, Alaskan wildfires burned about 344,000 ha annually (Alaska Fire Service 2005; Fig. 1.3), an area larger than the state of Rhode Island. Alaska and other arctic and boreal regions of the world also differ from lower latitudes in their sensitivity to recent and predicted climate change (IPCC 2001). Models of future climate (AICI 2004) and recent observations (Serreze et al. 2000) indicate that the earliest and most pronounced warming due to increased atmospheric CO<sub>2</sub> concentrations will occur in northern high latitudes. Biological and physical responses to recent warming in Alaska are becoming clearer with each passing year: e.g. boreal forest expansion, increased shrub densities in tundra, deeper permafrost thawing, and longer snow-free seasons (see Hinzman et al. 2005 for a review). In the boreal forests of Canada, annual area burned has increased over the past 50 years (Stocks et al. 2002), and the record-setting 2004 fire season in Alaska (2.7 million ha burned representing 14% of the total area burned since 1950; Fig. 1.3) is consistent with this trend.

The magnitude of predicted warming, plus the impacts of fire on vegetation (Dyrness et al. 1986, Bonan 1989, Johnson 1992), the global carbon cycle (Harden et al. 2000) and human livelihoods (Chapin et al. 2003), motivate studies of the effects of climatic change on fire regimes in arctic and boreal regions. These effects are often depicted by a simple conceptual model of climate-vegetation-fire relationships (Fig. 1.4). Climate directly impacts the probability of fire ignition and spread by influencing relative moisture, lightning, and wind patterns. Climate indirectly influences the probability of fire through its control of vegetation assemblages over large spatial and temporal scales. The understanding of these interactions will inherently benefit from the perspective of historic studies. For example, interpretations of Alaskan fire data from 1950-2001 (Kasischke et al. 2002; Fig. 1.2) emphasize that fire regimes are controlled primarily by mean summer temperatures and precipitation, and secondarily by vegetation (Fig. 1.4 a). This short-term view predicts that annual area burned in boreal forests will increase with future

warming and drying (Flannigan et al. 2005). On the other hand, reconstructions of fire regimes over longer time periods (e.g. Lynch et al. 2002, Lynch et al. 2004b) suggest that vegetational change can strongly modify direct climatic impacts on fire regimes through changes in landscape flammability (Fig. 1.4 b). In this scenario, fire occurrence may depend more strongly upon the nature of vegetation (i.e. fuels) rather than the climatic conditions necessary for fire (i.e. drying, ignitions, winds).

These two perspectives of fire-climate-vegetation interactions are not mutually exclusive. However, one perspective may be more realistic than the other depending on the spatial or temporal scale considered, because climatic (e.g., weather) and vegetational (e.g., fuels) effects vary across time and space (Fig. 1.5). At short time scales and small spatial scales (i.e. days to decades, stands to landscapes; dashed lines in Fig. 1.5), climatic (weather) variability may be more influential than vegetational change, but at longer time scales and over larger spatial scales (i.e. centuries to millennia, landscapes to regions; solid lines in Fig. 1.5) both climate and vegetation can strongly influence fire regimes. Studies on the modern landscape tend to focus on processes operating at short time scales but over broad spatial scales. In contrast, paleoecological studies tend to focus on processes operating over long time scales, but at smaller spatial scales (Fig. 1.5).

The overall goal of my dissertation research is to improve the current understanding of direct and indirect impacts of climatic change on fire regimes in Alaska. I use a paleoecological approach to reconstruct fire and vegetation history over the past 15,000 years in the southcentral Brooks Range, where historic fire regimes are poorly understood. The paucity of fire history records in this region and generally across Alaska reflects the difficulty of reconstructing fire history in systems with infrequent, stand-replacing fires. Only recently has macroscopic charcoal in lake sediments been used to quantify millennial-scale fire history in Alaskan and Canadian boreal forests (Carcaillet et al. 2001a, Lynch et al. 2002, Lynch et al. 2004b). These studies, along with others from non-boreal regions have helped develop analytical techniques for inferring past fire occurrence based on the identification of charcoal peaks in sediment records (see Whitlock and Anderson 2003). This approach is virtually the only tool available for inferring historic fire regimes in arctic and boreal landscapes.

Chapter 2 focuses on the use of sediment charcoal records as a tool for reconstructing fire history. Despite the increased use of charcoal records to interpret past fire regimes, the field of charcoal analysis still struggles with fundamental questions about the spatial scale of these records, ways to analyze charcoal stratigraphy, and the accuracy of inferred fire histories. To improve the current understanding of processes creating sediment charcoal records, I developed a numerical model that simulates fire regimes, charcoal dispersal, and charcoal taphonomy. The model is the first of its kind and offers a means to assess key assumptions of charcoal analysis and the merits of different analytical techniques. By placing realistically-sized fires on a landscape and making basic assumptions about charcoal dispersal, the model illustrates that charcoal accumulation in a lake mainly reflects area burned within the charcoal source area, and that variability in charcoal peak heights can be explained largely by the size of charcoal source areas relative to the size of fires. The model produces records similar in appearance to sediment-charcoal records from Alaskan boreal forests, and based on this similarity, I suggest that charcoal source areas are larger than previously inferred from experimental dispersal data but consistent with charcoal dispersal from wildfires. I further illustrate how sediment mixing, sediment sampling, and analytical techniques that isolate charcoal peaks emphasizes fire occurrence at smaller spatial scales, despite long-distance charcoal dispersal.

Chapter 3 focuses on late-glacial and Holocene fire and vegetation history in the southcentral Brooks Range, reconstructed based on charcoal, pollen, and stomata in the sediments of four lakes. I take advantage of previous interpretations of climatic and vegetational history in the region to infer the direct and indirect impacts of climatic change on fire regimes. Over the past 15,000 years, millennial-scale climates have included a wide range of temperature and moisture conditions, and vegetation assemblages have varied from tundra to deciduous and evergreen forests. I present a method to objectively identify charcoal peaks in sediment records to infer local fire occurrence and apply this to each of the four records. Based on estimated fires, I characterize regimes with the distribution of fire return intervals (FRIs; the inverse of fire frequency) within each vegetation zone, and I statistically compare these regimes using a

likelihood ratio test. Reconstructing fire history across past changes in climate and vegetation provides insights into both the fire ecology of arctic and boreal systems and their potential response to future climate change. The findings of Chapter 3 specifically point to the importance of vegetation in modifying the direct impacts of climatic change on fire regimes.

Chapter 4 addresses changes in boreal fire regimes associated with shifts in temperature and/or relative moisture over the past 5000 years. I quantify fire regimes at four lakes using the same methods as in Chapter 3, and I compare fire regimes between independently documented climatic zones. I employ a method for pooling fire-history data that allows detection of subtle changes in fire regimes at millennial and centennial time scales. The pooled fire-history dataset indicates that boreal forest fire regimes were sensitive to certain climatic changes over the past 5000 years, but insensitive to others. Inferences into the mechanisms behind these changes are limited by a poor understanding of past sub-centennial climate variability. Additional records of climate, fire, and vegetation at fine spatial and temporal scales are required to advance the understanding of climatic influence on fire regimes over the past 5000 years.

Overall, my dissertation research has important methodological implications for reconstructing fire regimes with sediment charcoal records and provides the first quantitative records of fire history in interior Alaska over the past 15,000 years. The patterns of fire history in the region suggest the importance of both direct and indirect influences of climatic change on fire regimes. With additional records from central Alaska, the results here should contribute to a rigorous understanding of the direct and indirect effects of climate change on arctic and boreal fire regimes.



**Figure 1.1.** The Erickson Creek Fire, an unsuppressed fire burning across the Dalton Highway in June 2003.

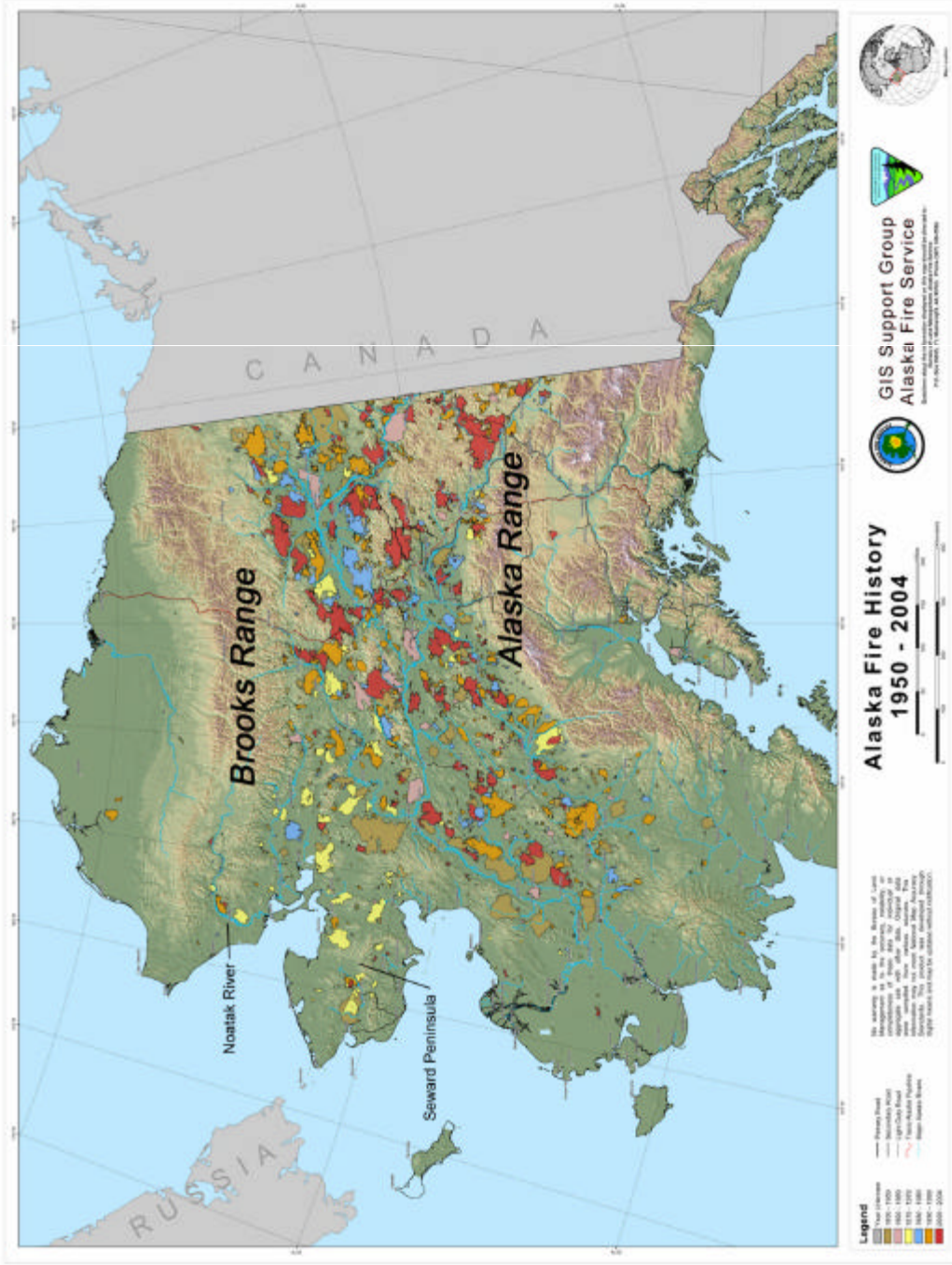


**Figure 1.2.** Alaskan fire history, 1950-2004. Fires are primarily restricted to the region north of the Alaska Range and south of the Brooks Range. Just over 5% of the area burned occurred in tundra, most on the Seward Peninsula and along the Noatak River.

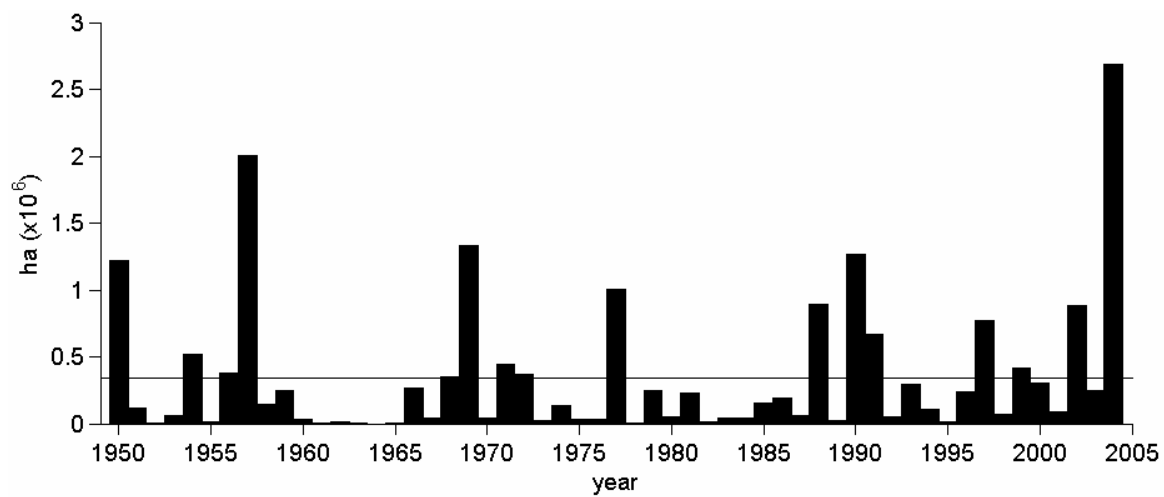
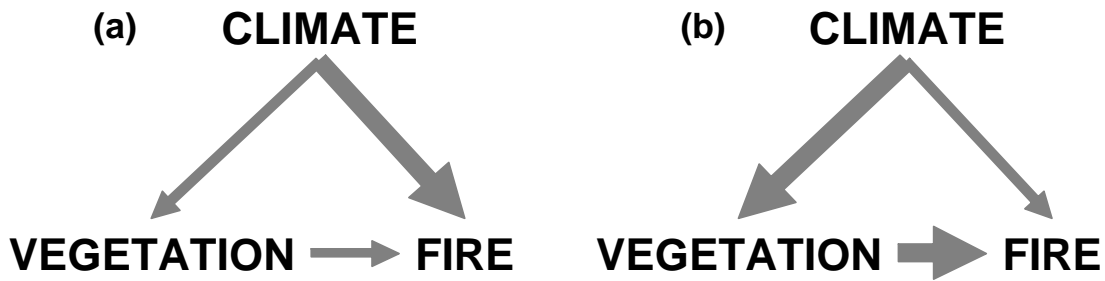


**Figure 1.3.** Annual area burned in Alaska based on observational records maintained by the Alaska Fire Service. The horizontal line is the 1950-2004 average of 344,000 ha.



**CLIMATE:** temperature, moisture, ignition, wind

**FIRE:** frequency, size, intensity, severity

**VEGETATION:** species assemblages, age, density

**Figure 14.** Simplified model of direct and indirect pathways for climatic changes to impact fire regimes. The arrow width represents the importance of each pathway. (a) Fire is controlled more by climatic than vegetational changes, as in the modern boreal forest, for example. (b) Fire is controlled more by vegetational changes, as in the fuel-limited ponderosa pine forests of the southwestern U.S., for example.

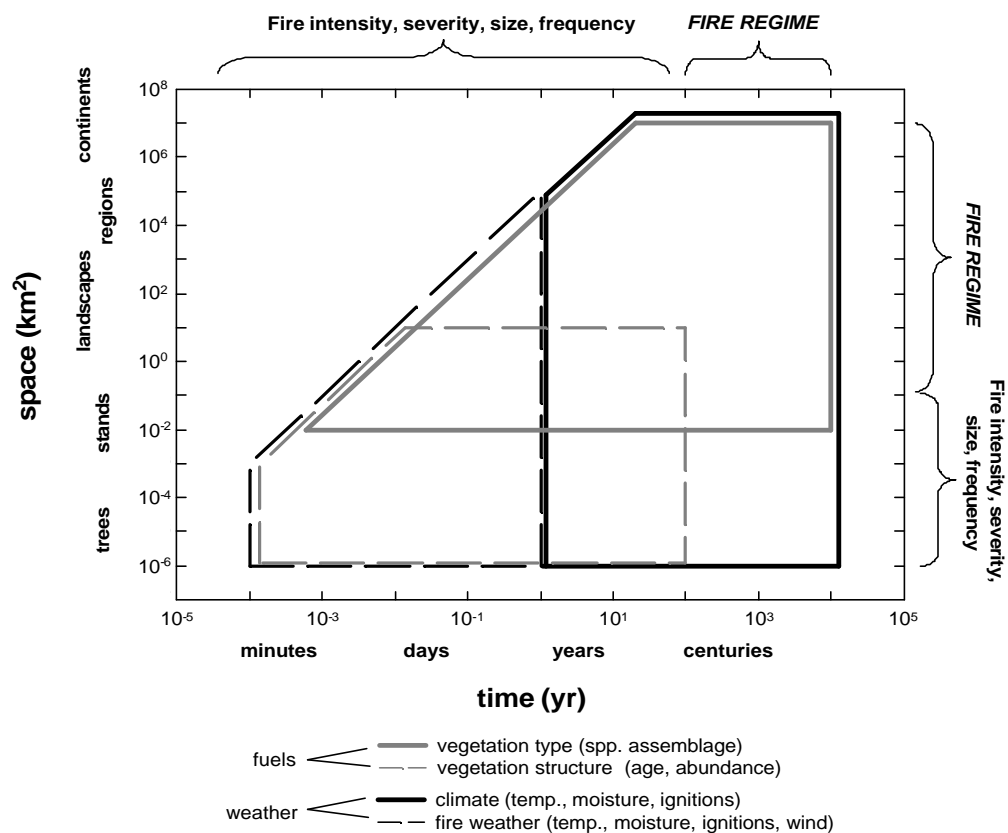


**Figure 1.5.** (from Hu et al. 2006) The timing of fire at any one point in space and time is controlled by different aspects of fuels (vegetation) and weather. While topography is an important control of fire occurrence, its stability over centuries to millennia is assumed in paleoecological research. Scaling prevents events from happening simultaneously at short time scale and large spatial scale (e.g. the void in the upper left). The fire regime concept takes form only at larger spatial and temporal scales, while metrics specific to individual fires operate at smaller scales. Paleoecological research can provide records of fire occurrence at stand to regional spatial scales and centennial to millennial temporal scales. It is thus well suited for investigating the role of climate and vegetation type in controlling fire regimes.

## CHAPTER 2: UNDERSTANDING THE ORIGIN AND ANALYSIS OF SEDIMENT-CHARCOAL RECORDS WITH A SIMULATION MODEL

Philip E. Higuera<sup>1</sup>, Matthew E. Peters<sup>2,3</sup>, Linda B. Brubaker<sup>1</sup>, and Daniel Gavin<sup>4</sup>

<sup>1</sup>College of Forest Resources, University of Washington, Seattle, WA

<sup>2</sup>Department of Applied Mathematics and Department of Atmospheric Science,  
University of Washington, Seattle, WA

<sup>3</sup>Current address: Department of Earth and Planetary Sciences, Harvard University,  
Cambridge, MA

<sup>4</sup>Department of Geography, University of Oregon, Eugene, OR

### SUMMARY

Interpreting sediment-charcoal records is challenging because there is little information linking charcoal production from fires to charcoal accumulation in lakes. We present a numerical model simulating the major processes involved in this pathway. The model incorporates the size, location, and timing of fires, primary and secondary charcoal transport, sediment mixing, and sediment sampling. We use the model as a tool to evaluate assumptions of charcoal dispersal and taphonomy and to assess the merits of inferring local and regional fire history by decomposing charcoal records into low-frequency ('background') and high-frequency ('peak') components. Under specific dispersal scenarios, the model generates records similar in appearance to sediment-charcoal records from Alaskan boreal forests. These scenarios require long-distance dispersal (e.g. 1-10s km), consistent with observations from wildfires but longer than previously inferred from experimental dispersal data. More generally, charcoal accumulation in simulated records mainly reflects area burned within the charcoal source area. Variability in charcoal peak heights is primarily explained by the size of charcoal source areas relative to the size of simulated fires, with an increase in this ratio resulting in increased variability in peak heights. Mixing and multi-year sampling add noise to charcoal records, obscuring the relationship between area burned and charcoal accumulation. This noise highlights the need for statistical treatments of charcoal records. Using simulated records we demonstrate that long-term averages of charcoal

accumulation ( $> 10 \times$  mean fire return interval) correlate well with area burned within the entire charcoal source area. We further demonstrate how decomposing simulated records to isolate the peak component emphasizes fire occurrence at smaller spatial scales ( $< 1$  km radius). Together, these results provide theoretical support for the analysis of charcoal records using the decomposition approach.

## INTRODUCTION

Interpreting fire history from sediment charcoal records depends upon understanding the processes controlling charcoal accumulation and the use of analytical methods that appropriately reflect these processes. Over the past two decades, a number of empirical and theoretical studies has helped identify key assumptions about charcoal-dispersal and taphonomic processes affecting sediment charcoal records (Clark 1988a, MacDonald et al. 1991, Clark and Royall 1995a, Bradbury 1996, Whitlock and Millspaugh 1996, Clark and Patterson 1997, Clark et al. 1998, Blackford 2000, Mohr et al. 2000, Carcaillet et al. 2001b, Lynch et al. 2004a, Whitlock et al. 2004, Higuera et al. 2005b). These assumptions provide a rationale for developing analytical frameworks to interpret fire occurrence from continuous records of macroscopic charcoal<sup>1</sup> (e.g. Clark 1988a, Clark 1990, Clark et al. 1996, Long et al. 1998, Carcaillet et al. 2001a, Gavin et al. 2003). Nevertheless, evaluating the assumptions of charcoal analysis and developing appropriate analytical techniques remain two important research goals for interpreting the characteristics and variability of past fire regimes (Whitlock and Anderson 2003). Modeling sediment charcoal records provides a tool that can help in both respects. Here we describe a model that translates the current understanding of charcoal dispersal and taphonomy into a numerical framework that simulates lake sediment-charcoal records. Assumptions of charcoal analysis are evaluated by comparing simulated records to empirical records from Alaskan lakes, and the merits of analytical approaches are examined by comparing simulated charcoal records with the known (simulated) fire histories that created them.

---

<sup>1</sup> Unless otherwise noted, "charcoal" refers to macroscopic charcoal particles, typically those  $> 100 \mu\text{m}$  in diameter.

The interpretation of fire history from sediment charcoal rests upon three main assumptions about charcoal dispersal, taphonomy and sampling. First, most macroscopic charcoal falls close to its source, such that peaks in sedimentary charcoal represent “local” fire occurrence. This assumption was originally considered by Clark (1988a), who used a Gaussian plume model to argue that macroscopic charcoal should be deposited within  $10^1$ - $10^3$  m of its source. Studies of charcoal deposition from experimental fires agree with these theoretical considerations and suggest that “local” could be defined as within several tens to hundreds of meters of a sedimentary basin (Clark et al. 1998, Blackford 2000, Ohlson and Tryterud 2000, Lynch et al. 2004a). This spatial scale is also supported by studies matching charcoal peaks to known fire events (e.g. Clark 1990, Whitlock and Millspaugh 1996, Gavin et al. 2003, Lynch et al. 2004a, Higuera et al. 2005b). On the other hand, several studies have shown that macroscopic charcoal can travel several to tens of kilometers away from wild fires (Pisaric 2002, Tinner et al. 2006) and create distinct charcoal peaks in sediment records (Whitlock and Millspaugh 1996, Gardner and Whitlock 2001, Hallett et al. 2003). The unknown impacts of such widely varying dispersal distances make the spatial scale of sediment records difficult to understand.

Second, interpreting fire history from charcoal stratigraphy assumes that secondary charcoal deposition via slope wash or within-lake redeposition does not obscure patterns of primary charcoal deposition. This assumption is supported by the physical properties of macroscopic charcoal (size, shape, and density), which suggest that redistribution across the landscape should be minimal (Clark 1988a, Clark and Patterson 1997). In addition, empirical work (Bradbury 1996, Whitlock and Millspaugh 1996) indicates that charcoal peaks from known fires remain distinct despite within-lake redistribution of charcoal in non-fire years. Thus, existing evidence indicates that primary charcoal deposition should remain the dominant signal in charcoal records, in at least in some sedimentary basins.

Third, interpreting fire occurrence assumes that sediment mixing and sampling provide adequate temporal resolution for detecting local fire occurrence. Clark (1988a) used a simple sediment mixing model to suggest that sampling intervals should be  $< 0.2$

times the fire-return-interval of interest to resolve individual charcoal peaks (i.e.  $\text{yr sample}^{-1} \leq 0.2 \text{ yr fire}^{-1}$ ).

From these assumptions come the rationale for analyzing charcoal records by decomposing a charcoal series ( $C_{raw}$ ) into “background” ( $C_{background}$ ) and “peak” ( $C_{peak}$ ) components (e.g. Clark et al. 1996, Long et al. 1998, Carcaillet et al. 2001a, Lynch et al. 2002, Gavin et al. 2003, Hallett et al. 2003). Clark and Royal (1995b) originally used the terms “background” and “peak” to discriminate between the low-frequency trends in abundant, small charcoal ( $< 100 \mu\text{m}$  diameter) and higher-frequency trends in less abundant, large charcoal ( $> 100 \mu\text{m}$  diameter). Clark and co-authors emphasized the different spatial scales of these components: peak and background charcoal represent local and regional source areas, respectively (Clark and Royall 1995a, Clark et al. 1996, Clark and Patterson 1997). Long et al. (1998) applied these terms to purely macroscopic charcoal records and expanded the definition of background to include the effects of charcoal production per fire and secondary charcoal transport, which could change with changing vegetation and geomorphic regimes. Thus the term “background” has been used differently in the literature to account for both ecological and physical processes that can cause low-frequency variations in sediment charcoal accumulation. Peak charcoal is assumed to represent primary charcoal deposition from “local” fires and analytical and naturally occurring noise from all sources of charcoal deposition. A threshold separates charcoal samples representing noise from those mainly representing “local” fires.

In this paper, we describe a numerical model (the Charcoal Simulation Model, CharSim) developed as a tool for evaluating assumptions of charcoal dispersal and taphonomy and for assessing the merits of analytical techniques for inferring fire history. Through model description and comparisons between simulated and Alaskan sediment charcoal records, we illustrate the major processes creating variability in sediment charcoal records. We use comparisons between simulated records and their underlying fire histories to assess the impacts of different taphonomic and analytical scenarios on interpretations of fire-history using the decomposition approach.

## METHODS AND RATIONALE

### The Charcoal Simulation Model (CharSim)

CharSim simulates and links (1) the spatial and temporal pattern of fire regimes, (2) charcoal production, dispersal, and primary deposition, (3) secondary deposition, (4) sediment mixing, and (5) sediment sampling (Table 2.1). Each component is potentially important in creating sediment-charcoal records, although some processes are difficult to parameterize due to a lack of empirical data. We parameterized CharSim to represent fire regimes and lake sediment records from interior Alaska, an area dominated by black spruce boreal forest and large, high-severity fires (e.g. Kasischke et al. 2002). The model code (MatLab Version 7.0.0 and C) is available from the authors upon request.

The following sections describe the processes contained within any conceptual model of charcoal production, transport, and deposition, the components and design of CharSim, and the technical details of the model. Figure 2.1 illustrates each step of the model, from airborne charcoal deposition to charcoal in a sampled sediment core.

### Fire Regime

CharSim simulates burning on a homogenous landscape represented by 100 x 100 m (1 ha) pixels. Fires start within a circular “study area” of 50-km radius (i.e. 78,540 km<sup>2</sup> area) with a “lake” at its center (represented by a single 1-ha pixel). The number of fires occurring in any year is determined by a Poisson probability distribution with a prescribed mean number of fires per year ( $\lambda$ ). Fires start at random locations on the landscape and grow to a size based on a normal probability density function (PDF) fit to log-transformed fire sizes from Alaska (n = 1058, 1988-2003 data; Alaska Fire Service, 2004; Table 2.1). The size of each fire,  $FS_i$  is randomly selected from this PDF. The minimum and maximum fire size recorded in the Alaskan dataset are 11 and 236,128 hectares, so the spatial extent of CharSim can include > 99% of the fire sizes contained within the Alaskan-derived fire-size distribution. Fires grow in a circular shape, excluding any areas that have burned within 50 years (representing low flammability of

early successional stands) until they reach their size,  $FS_i$ . Fires start in the study area but grow outside it as necessary.

### Primary Charcoal Deposition

For each time year,  $T$ , burned pixels contribute airborne charcoal,  $C_{air}$ , to the lake and to the eight pixels immediately surrounding the lake based on a charcoal dispersal table (Fig. 2.2). Charcoal abundance is represented as a proportion, relative to the total amount of charcoal from all burned pixels. A charcoal dispersal table indicates the quantity of charcoal deposited at one pixel (e.g. the lake or pixel adjacent to the lake) given that another pixel burns. When constructed from the perspective of the lake, the charcoal dispersal table is a visual representation of the total area from which charcoal deposited at the lake originates, termed “the potential charcoal source area” (PCSA; see Appendix A). Each dispersal table represents the average conditions during a fire that affect the amount of charcoal reaching the lake.

A dispersal table can incorporate any number of assumptions and does not depend on a single dispersal model. A chief benefit of using dispersal tables, rather than dispersal curves (“kernels”), is their modularity. Tables can be modified to reflect future knowledge or different assumption and easily substituted within CharSim for existing ones. In addition, dispersal tables insulate CharSim from the assumptions used to make the tables, since CharSim depends only on the table itself. In fact, the behavior of CharSim can be understood to a large extent based simply on the table (i.e. the size and shape of the source area) without knowledge of the dispersal model.

Charcoal dispersal tables were calculated based on a Gaussian dispersal model developed by Sutton (1947a), modified by Chamberlain (1953), and applied to charcoal analysis by Clark (1988). In previous work, Peters and Higuera (Appendix A) modified the model to a two-dimensional form and expanded it to simulate multiple injection heights (the height at which charcoal is released from a buoyant plume) and multiple wind. The dispersal model parameters are discussed by Peters and Higuera (Appendix A).

Dispersal distances in the modified model are a function of a single fall speed, a single wind speed, and an empirical or theoretical PDF of wind direction and injection heights. We constrained fall speeds to the average measured in the International Crown Fire Modeling Experiment (ICFME) experimental burn in boreal Canada ( $1.56 \text{ m s}^{-1}$ ; Appendix A; Lynch et al. 2004a) and wind speed to the highest 10-m wind speeds measured during several fires from the ICFME ( $10 \text{ m s}^{-1}$ , Taylor et al. 2004). Although it may be unrealistic to use a single wind speed and fall speed represent average conditions during burning, Peters and Higuera (Appendix A) found that the dispersal model is relatively insensitive to variations in these parameters. Injection heights and wind direction are much more critical, and these are simulated by PDFs to provide appropriate variation. To simulate multiple injection heights, we assume a distribution of injection heights during a single fire that has a negative skewness, with a peak at large injection heights and a long tail at smaller heights (Fig. 2.2, row 1). In contrast to a situation where all charcoal is injected at a single height, this model produces a dispersal table with a strong local bias in charcoal dispersal and no or minimal skip distance (Appendix A). The sensitivity of CharSim to assumptions on injection-height distributions is described in Appendix B. To simulate varying wind directions we create a dispersal table with multiple wind directions and then weight each direction based on an empirical PDF of June-August wind directions from Bettles, Alaska (representing the study area from where empirical records were collected, Chapter 4; Table 2.1). This produces a circular dispersal table with higher values along dominant wind directions (Fig. 2.2, row 3)

We used four injection-height scenarios, characterized by the modal injection height  $h_{mode}$ , which spans a range of realistic injection heights from wildland fires (e.g. Clark 1988a, Clark et al. 1998, Samsonov et al. 2005). Each scenario represents a different PCSA. In each of the first three scenarios, a single dispersal table was used, based on a specific  $h_{mode}$  of 10, 100, or 1000 m. The 10 m  $h_{mode}$  scenario gives two-dimensional results similar to empirical data collected from an experimental fire in boreal Canada by Lynch et al. (2004a; Appendix A), while the 100 m and 1000 m  $h_{mode}$  scenarios simulate fires with taller plumes (e.g. from larger and/or more intense fires). The fourth scenario was a mixed scenario representing the assumption that injection

heights scale with fire size. In the mixed scenario  $h_{mode}$  varied with the log of fire size, with each 20<sup>th</sup> percentile of the log-transformed fire-size distribution calling on a different injection height and dispersal table. Thus, for the smallest 20% of the fires the modal injection height was 10 m; for the next 20%, 50 m; then 100 m; then 500 m, and for the largest 20%, 1000 m.

With a mode and distribution of injection heights selected, there are two ways to portray the PCSA (Fig. 2.2). Assuming a fire of infinite size, one can consider charcoal deposition at a lake originating from different distances (i.e. radii), as graphically illustrated by the cumulative proportion of total charcoal deposited at increasingly larger radii (Fig. 2.2, row 2). The PCSA is associated with the radius at which 100% of charcoal originates. A second, more geographic approach is to map the density of charcoal originating in each part of the PCSA (the charcoal dispersal table, Fig. 2.2, row 3). This illustrates the two-dimensional variations in charcoal dispersal that result from variations in both injection height and wind directions.

### Secondary Charcoal Deposition

Secondary charcoal deposition comes from (1) charcoal deposited on the landscape immediately adjacent to the lake (i.e. the eight pixels surrounding the lake), introduced via slope-wash processes (via water or wind), and (2) charcoal on the lake sediment surface, which is transported to the “center” of the lake, defined as 10% of the lake area, via within-lake redeposition. Both processes are minimally understood. We simulate these processes with a simple negative exponential die-off curve, which moves a given proportion of charcoal from its source (landscape or lake sediment surface) to its end point (lake or lake center) over a certain time frame.

Limited quantitative data are available for selecting parameters for secondary charcoal processes. We assume only a small proportion of charcoal on the landscape surface is transported into a lake basin by slopewash or otherwise (Clark and Patterson 1997, Lynch et al. 2004a), and that these processes last until the re-growth of vegetation within the watershed (Clark 1988a, Whitlock and Millsbaugh 1996, Lynch et al. 2004a).

It was also assumed that within-lake redeposition focuses charcoal in the center of a basin, and that charcoal remains mobile for several decades after a fire (Bradbury 1996, Whitlock and Millspaugh 1996). To minimize modeling errors associated with these uncertain processes, we selected secondary transport values that are conservative with respect to the amount of charcoal moved by slope wash and within-lake redeposition. Specifically, slope-wash parameters were set to move 1% of all landscape charcoal into the lake basin, with 90% and 99% of the deposition occurring within 20 and 50 years of airborne charcoal deposition (Table 2.2; Fig. 2.1c). Within-lake redeposition parameters were set to move 10% of the charcoal from the outer 90% of the lake-sediment surface to the center of the lake, with 90% and 99% of redeposition occurring within 10 and 20 years, respectively (Table 2.2; Fig. 2.1e).

The amount of charcoal deposited on the lake-sediment surface in any year due to slope-wash processes,  $C_{sw, T}$ , is given by:

$$C_{sw, T} = p_{sw} \sum_{t=0}^{N_{sw}} sw_t C_{ls, T-t} \quad (1)$$

where  $C_{ls, T-t}$  is the amount of charcoal on the pixels immediately surrounding the lake for each year  $T-t$  though  $T$ ,  $sw_t$  describes the negative-exponential PDF with mean  $\mu_{sw}$  (Fig. 2.1 b-c), and  $p_{sw}$  is the proportion of landscape charcoal moved into the lake. Only the most recent  $N_{sw}$  years contribute charcoal in this fashion. Charcoal on the pixels surrounding the lake,  $C_{ls}$ , originates from airborne charcoal deposition and *in situ* charcoal production when these pixels burn. Airborne deposition is determined in the same fashion as for primary charcoal deposition on the lake (described above). *In situ* charcoal production is defined to be 10 times greater than the total amount of airborne charcoal produced during a fire. This is consistent with a one- to two-order of magnitude difference between charcoal deposition inside and outside experimental fires in boreal forests (Clark et al. 1998, Ohlson and Tryterud 2000, Lynch et al. 2004a).

Finally, total charcoal deposition on the lake-sediment surface in year  $T$ ,  $C_{lake, T}$  (Fig. 2.1 d) is the sum of airborne charcoal,  $C_{air}$  (i.e. primary deposition) and secondary charcoal deposition,  $C_{sw}$ :

$$C_{lake, T} = C_{air, T} + C_{sw, T} \quad (2)$$

Analogous to (1), total charcoal transport to the center of the lake is:

$$C_{lake\_center,T} = \mathbf{a}C_{lake,T} + (1-\mathbf{a})p_{re} \sum_{t=0}^{N_{re}} re_t C_{lake,T-t} \quad (3)$$

where  $re_t$  describes the negative-exponential PDF with mean  $\mu_{re}$  (Table 2.2; Fig. 2.1 e, f).  $p_{re}$  is the proportion of charcoal on the non-center portion of the lake-sediment surface which is later redeposited in the center of the lake.  $N_{re}$  is the number of years over which within-lake redeposition occurs, and  $\alpha$  is the percentage of lake defined to be the center.

### Sediment Mixing and Sediment Sampling

A sediment accumulation rate  $s$  determines the depth of sediment represented by each year of the model. Charcoal deposited in the center of the lake in year  $T$ ,  $C_{lake\_center,T}$ , is mixed into the surrounding strata between mixing depths  $md_u$  and  $md_l$  above and below each stratum to define charcoal abundance in the core in year  $T$ ,  $C_{core,T}$  (Fig. 2.1 h). The sediment accumulation rate  $s$  and mixing depth,  $md$  ( $= md_u + md_l$ ), define a mixing time window,  $t_l \leq t \leq t_u$ , over which charcoal deposited at time  $T$  is mixed. Charcoal in the simulated core at year  $T$  is computed, after the core is “made”, by mixing charcoal from sediments above and below the depositional strata in this time window, weighted by a Weibull PDF:

$$C_{core,T} = \sum_{t_l \leq t \leq t_u} C_{lake\_center,t} \Psi_{I_m,T-t} \quad (5)$$

Here,  $\Psi_{I_m,t}$  represents the PDF of the Weibull distribution with mode  $I_m$  shifted such that the mode occurs at year  $t$ . The Weibull distribution, with shape parameter set to 2.5, slightly biases mixing towards the uppermost sediments (Fig. 2.1 g).

Charcoal abundance in the simulated core is summed across a given sampling depth,  $d_{sample}$ , which is translated into an upper and lower sampling time,  $st_u$  and  $st_l$ , by dividing by the sediment accumulation rate,  $s$ . The units of charcoal abundance  $C$  until this point have been a proportion, which we can convert into a charcoal count, charcoal area or another measure of abundance. In order to directly compare with Alaskan records, we chose to use charcoal counts in this paper, consistent with the assumptions underlying

the dispersal tables (see Appendix A). Charcoal counts in each sample are divided by the volume of the sample,  $v$  ( $\text{cm}^3$ ; assuming a 7.5-cm diameter circular core), to calculate charcoal concentration ( $\# \text{cm}^{-3}$ ). The sediment accumulation rate  $s$  ( $\text{cm yr}^{-1}$ ) is multiplied by charcoal concentration to obtain the charcoal accumulation rate (CHAR) for each sample,  $C_{sample,i}$  ( $\# \text{cm}^{-2} \text{yr}^{-1}$ ):

$$C_{sample,i} = \frac{s}{v_{sample}} \sum_{st}^{st_{iu}} C_{core,T} \quad (6)$$

Finally, to facilitate comparisons between real and simulated records we standardize charcoal accumulation rates by dividing each value by the mean value for the series. We present this as a unitless CHAR index (Fig. 2.1 i).

We selected mixing and sampling parameters that correspond to recent fire history records from lakes in the southcentral Brooks Range, Alaska (Chapter 4). The presence of laminations, other stratigraphic layers  $> 1.0$  cm, and charcoal stratigraphy in these records suggest that sediment mixing influences roughly between 0.5 and 2 cm (PEH personal observation); sediment accumulation rates over the past 4500 years range between 0.012-0.150  $\text{cm yr}^{-1}$ . Sampling distances between 0.25-0.50-cm sections yield sample intervals between 2-42 years (Chapter 4).

### Comparing CharSim and Alaskan Charcoal Records

To evaluate the parameter choices in CharSim, we compared several charcoal records from the southern Brooks Range, Alaska (Ruppert Lake, 67°04'16" N, 154°14'45" W; Code Lake, 67°09'29" N, 151°51'40" W; Wild Tussock Lake, 67°07'40" N, 151°22'55" W; Last Chance Lake, 67°04'45" N, 150°45'08" W; unofficial names; Chapter 3), to simulated records generated using the four  $h_{mode}$  scenarios (Table 2.3) and parameters described in Table 2.2. To the extent that simulated records produce variability in charcoal series that are similar to empirical records, the representation of processes in the model represents at least one scenario that could explain the creation of actual charcoal records. To the extent that simulated records differ from real records, CharSim is misrepresenting or missing processes that are operating on the empirical

records. We recognize that different processes could lead to the same pattern, so similarity between simulated and observed records in itself is not a rigorous validation of CharSim. A more robust validation requires studies quantifying secondary charcoal transport and comparisons to records with known fire histories at a range of spatial scales.

By comparing a single CharSim record to an empirical record we assume the processes creating the empirical record are stationary in time. We thus restrict our comparisons with Alaskan records to the last 3000-4500 yr, which represents a stationary period in the pollen and charcoal history of each record (Chapter 3, 4). We evaluated similarity visually with quantile-quantile plots and statistically using a two-sample Kolmogorov-Smirnov test comparing the cumulative distributions of equally sampled CharSim and Alaskan records (Zar 1999). Alaskan records were standardized to their mean CHAR and, like CharSim records, are expressed as a CHAR index.

### **Inferring Different Aspects of a Fire Regime**

Modeling sediment charcoal records allows one to ask questions that are otherwise impractical or impossible to address empirically. Using CharSim records we addressed two sets of questions that are relevant to the interpretation of sediment charcoal records: (1) how well does airborne and sampled CHAR ( $C_{air}$  and  $C_{sample}$ ) correlate with area burned at different spatial scales, and (2) how well do identifiable charcoal peaks reflect fire occurrence at different spatial scales? For each set of questions we also evaluated how mixing and sampling intervals modify these relationships to ultimately define our ability to infer area burned and/or fire timing in sampled sediment-charcoal records.

#### Area Burned

In CharSim, the annual accumulation of airborne charcoal in the lake is related to area burned in that year, weighted by some function incorporating the distance between the area burned and the lake. Thus charcoal records should represent a distance-weighted

index of area burned. To examine such a relationship, we compared both airborne charcoal accumulation,  $C_{air}$ , and sampled charcoal accumulation,  $C_{sample}$  (using a sampling interval of 20 yr), to annual area burned at multiple radii from the lake using 20,000-yr records generated from the 10- 100- and 1000-m  $h_{mode}$  scenarios (Table 2.2). We use these scenarios to informally test two hypotheses about the relationship between  $C_{air}$  and area burned: (1) for any  $h_{mode}$  scenario the correlation between annual area burned and  $C_{air}$  is maximized at a radius close to that defining the PCSA for that scenario, and (2) the distance of maximum correlation should vary between scenarios. Because the correlation between  $C_{sample}$  and area burned differs depending on both sampling interval and mixing interval, we also examined this correlation for 12 sampling intervals from 1 to 2400 years (0.008 to 20 fires per sample) and 10 mixing intervals from 1 to 150 mm (0.07 to 1 fire(s) per mixing interval), using the 1000-m  $h_{mode}$  scenario. For each of these 120 comparisons, we recorded the maximum correlation and radius at which the maximum correlation occurred (termed the “optimum spatial scale”).

### “Local” Fire Occurrence

An alternative approach for interpreting fire history from sediment-charcoal records is to focus on high-frequency, high-magnitude variations (i.e. charcoal peaks). This widely-used approach relies on the decomposition of charcoal series into high- and low-frequency components, termed "peak charcoal" and "background charcoal" in the literature (e.g. Whitlock and Anderson, 2003). Ultimately, decomposition turns a charcoal series into a binary record where each sample is categorized into one of two groups: "fire" or "no fire". We evaluated the ability to reconstruct fire occurrence at a range of spatial scales across a range of sampling intervals by analyzing simulated records using the decomposition approach.

To identify charcoal peaks we used the decomposition method in which a smoothed charcoal series representing low-frequency variability is subtracted from the raw series to obtain the residual, or peak charcoal series (Fig. 2.3). This approach assumes an additive relationship between peak and background components of a charcoal

record (e.g. Clark and Royall 1996). An analyst must select both a smoothing function to define the low frequency average, and a threshold value to split the peak series into “fire” and “non-fire” samples. As each CharSim record is associated with a known fire history, it is possible to objectively select the most accurate threshold to infer fires. Specifically, the threshold is placed at a value that maximizes accuracy, defined to be the proportion of true positive peaks (peaks correctly identified as fires) minus the proportion of false-positive peaks (peaks incorrectly identified as fires; see Higuera et al. 2005b). Furthermore, this measure of accuracy may be calculated for fires within different radii from the lake. We can thus identify the radius at which the charcoal peaks most accurately represent the fire history by finding the radius at which accuracy is maximized (defining the ‘optimal spatial scale’).

Using this method to identify charcoal peaks, we evaluated the relationship between (1) sampling interval, (2) smoothing interval, (3) maximum accuracy, and (4) the optimal spatial scale of a record. Starting from a single 20,000-year record of airborne charcoal deposition from the 1000-m  $h_{mode}$  scenario, we created six records of sampled charcoal using sampling intervals from 2 to 60 years (0.015 to 0.48 fires per sample) and a mixing interval of 30 years (0.25 fires per mixing-interval), with parameters otherwise described in Table 2.2. Each of these six records was decomposed using six different smoothing functions (locally weighted regression robust to outliers, Cleveland 1979). These functions varied in length from 0 years (i.e. no smoothing done) to 1200 years (10 fires per smoothing-window). For each of the 36 total records we recorded the accuracy and the optimal spatial scale, representing the best possible interpretation of the record. To test the sensitivity of these results to our assumptions on secondary charcoal transport, we performed the same simulations with secondary charcoal transport eliminated (i.e.  $P_{sw} = P_{re} = 0$ ).

## RESULTS

### CharSim Simulations: Sources of Variation and Sensitivity

#### Parameters Controlling Primary Charcoal Deposition

The variability in peak heights in CharSim records is most sensitive to the size of the PCSA relative to the fire size (the “source-area to fire-size ratio”): if the source-area to fire-size ratio is large, peak heights vary broadly, while if the source-area to fire-size ratio is small, all peaks are about the same size. Two relationships account for this result. First, if fires frequently cover large portions of the PCSA (i.e. small source-area to fire-size ratio), the resulting record of charcoal accumulation is approximately binary. This is the case for the 100-m (Fig. 2.4 a) and 10-m (not shown)  $h_{mode}$  scenarios. However, with the same fire size distribution and increasing PCSA (1000-m  $h_{mode}$  scenario; Fig. 2.4 b), smaller portions of the source area burn in any single fire. Thus the greater variability in fire location within the source area creates variability in charcoal peak heights. Second, the variability in fire sizes within the PCSA causes variability in simulated charcoal records. For example, if the distribution of fire sizes from the Alaskan database is replaced with a uniform distribution such that the total area burned remains relatively constant, the variability in charcoal peak heights decreases by roughly a factor of four (Fig 4c) for the 1000-m  $h_{mode}$  dispersal scenario. In contrast, variability in wind direction, as modeled here, has only minor effects on the variation in charcoal accumulation (see Appendix B).

#### Parameters Controlling Secondary Charcoal Deposition

In the scenarios, the transport of 1% of landscape charcoal from fires burning adjacent to the lake had a minor but visible impact on peak heights (Fig. 2.1b vs. d). In addition to modifying peak heights, slope-wash added charcoal to sediments in years after primary charcoal deposition (Fig. 2.1d). Within-lake redeposition also distributed charcoal to years following primary deposition, but this process did not affect relative peak heights (Fig. 2.1, d, f).

### Parameters Controlling Sediment Mixing and Sampling

Sediment mixing and sampling had large impacts on the patterns of airborne charcoal deposition. Because these processes act on all charcoal within any given stratigraphic level, they spread charcoal out across multiple years of sediment accumulation (in this case approximately 20), thereby modifying peak heights (as much as a factor of four), combining adjacent peaks, and erasing small peaks (e.g. Fig. 2.1 b-f vs. h, i). Below, we analyze the relationship between mixing and sampling intervals and how the choice of sampling interval affects our interpretation of sediment records.

### **Comparing CharSim and Alaskan Charcoal Records**

Only the 1000-m and mixed  $h_{mode}$  scenarios (charcoal dispersal distances up to ca. 20 km) captured the variation of charcoal accumulation in the Alaskan records, with the mixed scenarios generally providing closer fits to empirical data (Table 2.3). The variability in peak magnitude within the Alaskan records, particularly at the highest CHARs, was least well-represented in the simulated records (Fig. 2.5). For example, the poorest fit between Alaskan and CharSim records was from Ruppert Lake (Table 2.3), which contains two peaks 1.5 and 2 times larger than the largest peaks in the CharSim record (Fig. 2.5). The 10- and 100-m  $h_{mode}$  scenarios, with charcoal dispersal distances of approximately 0.25 and 2 km, respectively (Fig. 2.2), created nearly binary records with variations unlike the Alaskan records (Fig. 2.4).

### **Inferring Different Aspects of a Fire Regime**

#### Area Burned

Airborne charcoal accumulation  $C_{air}$  and annual area burned within a given radius are significantly correlated ( $p < 0.05$ ,  $r^2 > 0.90$ ) at radii close to the radius defining of the PCSA (c.  $10 \times h_{mode}$ ; Fig. 2.6, filled symbols). In comparison, the correlations between

sampled charcoal accumulation  $C_{sample}$  and area burned were much lower ( $r^2 < 0.50$ ) and less sensitive to different radii (Fig. 2.6, open symbols).

Correlations between  $C_{sample}$  and area burned increased with sampling intervals, reaching a maximum of 0.80 when sampling intervals included an average of 11 fires per sample (i.e. the sampling interval was 11 times the mean fire return interval; Fig. 2.7). Optimum spatial scales at these sampling intervals approached the scale defined by the PCSA and were either 16,000 m ( $n = 49$ ; 45%) or 8,000 m ( $n = 61$ ; 55%). Mixing affected the correlation between  $C_{sample}$  and area burned primarily at shorter sampling intervals (Fig. 2.7).

### “Local” Fire Occurrence

For a given mixing rate, the accuracy of identifying local fire occurrence is a function of the spatial scale of the record, the smoothing window, and the sampling resolution relative to the mean fire return interval (mFRI). Maximum accuracy occurred when sampling intervals were  $< 0.12$  times the mean fire return interval (mFRI; e.g. 12 yr for a 100 yr mFRI) and was sensitive to the smoothing windows at these intervals. Optimal smoothing windows were generally 2-5 times the mFRI (Fig. 2.8), which is shorter than the smoothing window maximizing the correlation between sampled charcoal  $C_{sample}$  and area burned. At larger sampling intervals, accuracy was less sensitive to smoothing windows, although smoothing windows shorter than the mFRI were associated with low accuracy (Fig. 2.8). Very long smoothing windows failed to remove short-term variations associated with secondary transport and mixing, resulting in reduced accuracy due to false-positives. Short smoothing windows tracked peak heights too closely and resulted in reduced accuracy because of lowered true-positive rates (data not shown).

The maximum accuracy of fire identification occurred at much smaller spatial scales than those maximizing the correlation between  $C_{air}$  and area burned. Of the 36 records analyzed for accuracy, the optimal spatial scale was defined by a 100 ( $n = 35$ ) or 250 ( $n = 1$ ) m radius (data not shown). When secondary charcoal transport was

eliminated (i.e.  $P_{sw} = P_{re} = 0$ ), optimal spatial scales were defined by only slightly larger radii, at 100 m ( $n = 16$ ; 44%), 250 m ( $n = 19$ ; 53%) or 500 m ( $n = 1$ ; 3%; data not presented graphically). Accuracy in all scenarios was less than 0.85 and limited by lower true-positive rates rather than by higher false-positive rates. For example, while no false positives occurred at the optimal threshold values, sediment mixing combined peaks from fires closely spaced in time (e.g.  $< 20$  yr, data not shown) so that some fires were not detected.

## DISCUSSION

### Assessment of CharSim

The simulation results show that the random placement of realistically sized fires on a homogenous landscape and a few basic assumptions about charcoal dispersal and taphonomy create charcoal records consistent with Alaskan sediment records. Nevertheless, CharSim is limited by a lack of empirical data and an incomplete understanding of key processes. Therefore, we couch our interpretations with several constraints. First, although charcoal dispersal is simulated with a physically based dispersal model that successfully reproduces data from an experimental fire (Appendix A), we lack a strong empirical or theoretical basis for choosing the distributions of injection heights. Given the hypothetical nature of the dispersal scenarios, the dispersal distances, PCSAs, and optimal spatial scales should be interpreted as first order estimates. Despite this caution, the general conclusions about the relative roles of PCSA and fire size are robust to a variety of assumptions concerning the form of the distribution of injection heights and wind direction (Appendix B). Second, we know little about the rates and variability of charcoal input via slope wash and redeposition. While the simulations address the role of these secondary transport processes, our inferences rely on minimally-constrained assumptions. For example, we did not model scenarios in which the variability of secondary charcoal input was high enough to create variability in simulated records similar to that observed in airborne charcoal deposition. While possible, this scenario seems unlikely because it requires extremely high, short-term variations in processes delivering secondary charcoal to sampling sites. Such questions

highlight the need for additional research on the effects of secondary charcoal transport. Third, we do not consider variations in topography, vegetation, and charcoal production. Besides being inherently challenging and time consuming to model, these factors involve an unwarranted level of complexity for an initial modeling attempt. Finally, we have not addressed the effect of lake size, which, as shown in modeled and empirical pollen data (e.g. Sugita 1993), is likely an important determinant of depositional patterns. We expect future development to include this variable.

### **Processes Creating Variability in Sediment Charcoal Records**

We compared simulated charcoal records to Alaskan sediment records primarily to provide insights into the processes that can create realistic variability in sediment charcoal records. Below we discuss the major conclusions from the model that relate to the processes of charcoal dispersal and taphonomy.

#### Primary Charcoal Deposition

At the most fundamental level, the amount of primary charcoal deposited in a lake is a function of the size and location of burned areas within the PCSA. If the PCSA captures only a small portion of the variability in fire size and location, airborne charcoal deposition will vary little between fire events. This is the case in the small PCSA scenarios ( $h_{mode} = 10$  and  $100$  m;  $\sim 0.2$  and  $13$  km<sup>2</sup>, respectively), which show little variation in charcoal deposition among fires because most fires either cover the entire PCSA or miss it completely. In these scenarios, airborne charcoal deposition creates a nearly binary pattern of charcoal accumulation through time (Fig. 2.4 a). However, as PCSA size increases ( $h_{mode} = 1000$  m;  $1300$  km<sup>2</sup>), variability in primary charcoal deposition increases because there is greater variability in the locations and sizes of fires within the source area.

Because the fire sizes in CharSim are well constrained by the Alaskan fire database, the results allow inferences about charcoal source areas in boreal forests of this region. In particular, the correspondence between CharSim simulations and empirical

records (Fig. 2.5, Table 2.3) suggests that charcoal dispersal distances exceed 10 km (source areas  $> 300 \text{ km}^2$ ). This finding contrasts with evidence from experimental fires in boreal forests (Clark et al. 1998, Ohlson and Tryterud 2000, Lynch et al. 2004a), which suggest that macroscopic charcoal travels much shorter distances (e.g. 10's to 100's of meter; source areas  $< 3 \text{ km}^2$ ). When CharSim simulations are based on these smaller dispersal distances (10- and 100-m  $h_{mode}$  scenarios), unrealistic binary charcoal records are produced that contain distinct peaks and little charcoal otherwise (e.g. Fig. 2.4 a, e). High-magnitude, short-term variations in secondary charcoal delivery is a possible mechanisms through which a simple, binary records could be modified, but this scenario seems unlikely for the reasons discussed above (see “Assessment of CharSim”). The larger charcoal dispersal distances suggested by CharSim are also consistent with studies documenting charcoal deposition (Pisaric 2002, Tinner et al. 2006) or charcoal peaks in lakes that are several kilometers away from wildfires (e.g. Whitlock and Millspaugh 1996; Gardner and Whitlock, 2001; Hallett *et al.*, 2003). Furthermore, the large injection heights (e.g. up to 1000 m) required to simulate large charcoal source areas are tenable given plume heights of 2000-5000 m in observed wildfires (Clark et al. 1998, Samsonov et al. 2005).

#### Secondary Charcoal Deposition, Sediment Mixing, and Sediment Sampling

Secondary transport, mixing, and sampling have variable effects on sediment charcoal records. These processes confound the relationship between primary deposition and annual area burned because they erase or combine small, closely spaced peaks by spreading charcoal across time periods before and after primary charcoal input. Although in the simulations, none of these processes (alone or in combination) could create the variability seen in the Alaskan sediment records, they were necessary to produce records that visually resemble empirical records (e.g. Fig. 2.2 b vs. g). Thus one interpretation suggested by CharSim simulations is that the variability in charcoal records originates through mechanisms controlling primary deposition and taphonomic processes and sampling intervals temporally smooth these series. On the other hand, the simulations

also show that secondary transport can add variability to charcoal peaks that is unrelated to primary input. This occurs when slopewash from burned pixels immediately surrounding the lake (even at minimal rates of 1% per 50 years) increases the size of charcoal peaks relative to peaks created from more distant fires (Fig. 2.2 a vs. b). This result is a consequence of the assumption that charcoal deposition within a fire is 10 times greater than charcoal deposition beyond a burned area (Clark et al. 1998, Ohlson and Tryterud 2000, Lynch et al. 2004a). Thus abundant charcoal on a burned landscape represents a potentially important source of charcoal input to sediment records, and erosional inputs from the surrounding landscape could magnify the local bias of sediment charcoal records (Clark and Patterson 1997).

### **Methodological Implications: Analyzing Sediment Charcoal Records via Decomposition**

Given the known fire history creating each simulated charcoal record, simulated records provide an opportunity to examine assumptions and interpretations of the decomposition approach to sediment-charcoal analysis. The correlation between low-frequency trends in charcoal accumulation and area burned within relatively long distances from the lake (e.g. > 5 km) provides support for previous interpretations of background charcoal. Results also indicate that charcoal records can be analyzed in a manner that faithfully represents “local” fire occurrence. Overall, the results lend theoretical support to two main assumptions of sediment charcoal analysis (e.g. Clark and Royall 1996, Clark and Patterson 1997, Long et al. 1998): that charcoal records contain (1) low frequency (long term) trends reflecting area burned at large spatial scales and (2) high frequency (short term) variations that reflect fire occurrence at small spatial scales.

#### Area Burned

The result that low-frequency summaries (> 10 x the mFRI) of charcoal records can accurately reflect area burned within the PCSA (Fig. 2.7) is consistent with the original concept of “background” charcoal (Clark and Royall 1995b, Clark and Royall

1996, Clark et al. 1996, Clark and Patterson 1997). While airborne charcoal deposition at a lake can be highly correlated with area burned in annual times scales (Fig. 2.6), secondary transport, mixing, and sampling, distribute annual charcoal deposition over longer time periods in sediments, resulting in poor short-term, but strong long term correlations between sampled charcoal and area burned (Fig. 2.7). If secondary transport, mixing and/or sampling vary at shorter time scales than the smoothing window used to define “background” charcoal, then long-term summaries of charcoal accumulation should be accurate descriptions of area burned, although inherently with low temporal resolution. However, the relationship between “background” charcoal and area burned assumes that the amount of charcoal produced per unit area burned and secondary deposition is constant. If charcoal production increased (from changing vegetation type) or secondary deposition increased (from changing sedimentation regime), there would be an overall increase in charcoal accumulation, even if fire frequency or size did not change. In general, though, the interpretation of low-frequency trends in charcoal accumulation is a potentially valuable way to infer regional burning patterns over multi-centennial to multi-millennial time scales (e.g. Marlon 2003).

#### “Local” Fire Occurrence

The results suggest that the optimal sampling interval for detecting individual fires is  $< 0.2$  times the mFRI (Fig. 2.8), with the ability to detect fires decreasing quickly at larger intervals because charcoal peaks from distinct fires are combined. This finding is similar to conclusions of Clark (1988), who recommended sampling intervals  $< 0.2$  times the return interval of interest, based on visual analysis of charcoal peaks in simple simulated records with different sampling intervals.

We found that charcoal peak identification in simulated records most accurately reflects fire occurrence within 500 m of the lake (Fig. 2.8). This result is consistent with Gavin et al.’s (2003) finding that the maximum correspondence (analogous to accuracy) between charcoal peaks and fires occurred when fires burned within 500 m of a lake on Vancouver Island, Canada. More generally, the results imply that long-distance charcoal

transport does not preclude the accurate detection of local fires. For example, the PCSA in the 1000-m  $h_{mode}$  scenario extends to 20 km from the lake, yet charcoal peaks most accurately reflect fires within 500 m. What then explains the bias of charcoal peaks to local fires? First, the distance-weighting inherent in charcoal dispersal results in local fires always creating larger charcoal peaks than more distant fires. Second, secondary transport, mixing and sampling “mute” small charcoal peaks, while large charcoal peaks are robust to these processes. Third, the decomposition approach, which removes low frequency trends, emphasizes large charcoal peaks and thereby amplifies the inherent biases against small and/or distant fires. However, other decomposition techniques can amplify small peaks.

#### Concepts of “background” and smoothing windows

The concept of “background” charcoal is represented by a low-frequency summary of a charcoal series over some time window, defined by the “smoothing window” (Fig. 2.3). This representation of background has been used in two distinct ways in the charcoal literature, each with theoretical justification and support from the CharSim simulations. First, background charcoal has been interpreted to represent area burned at large temporal and spatial scales. This definition of background is justified in CharSim by the high correlation between area burned and charcoal accumulation for sampling intervals  $> 10 \times$  the mFRI. Thus the smoothing window used to depict this definition of background should be greater than  $10 \times$  the inferred mFRI. Although background charcoal could also reflect changing vegetation types and long-term changes in charcoal delivery mechanisms (e.g. Long et al. 1998), neither was modeled in this study. Second, background charcoal has been associated with a smoothing window that isolates high-frequency variations of CHAR in the decomposition processes. The simulations suggest that it is possible to select windows that maximize the accuracy of charcoal-record interpretations when sediments are sampled at fine intervals (e.g.  $< 0.1$  times the mFRI) but that accuracy is generally insensitive to smoothing windows when sampling intervals are larger (Fig. 2.7). Nevertheless, smoothing windows 2-5 times the

mFRI resulted in the highest accuracy at all sampling intervals. The smoothing window for decomposition can therefore be considered separately from the window used to estimate long-term trends in area burned.

We suggest distinguishing the ecological and functional interpretations of the term “background”. Ecologically, background charcoal may represent the total amount of charcoal in a sediment record and be controlled by several processes related to the fire regime. Functionally, the term applies to the analytical goal of removing variations not associated with "local" fire occurrence, which mainly originate from taphonomic processes of mixing and sampling. In this case, we suggest the term “low frequency variation”, which emphasizes the physical pattern of charcoal accumulation without implications about fire or ecological processes.

## **Conclusions**

Based on empirical data of Alaskan fire regimes and specific assumptions of charcoal transport and taphonomy, CharSim produces charcoal records that resemble sediment-charcoal records from boreal Alaska. In addition, CharSim simulations illustrate several connections between processes that affect sediment charcoal records and the decomposition approach used to interpret fire history from these records.

First, simulations indicate that charcoal records reflect area burned within the PCSA, but that secondary transport, sediment mixing, and sampling mute this relationship at short time scales (e.g.  $< \text{mFRI}$ ). As a result, simulated and empirical (Enache and Cumming 2006) records are only moderately correlated with area burned at short time scales, but these records are highly correlated with area burned within the PCSA at long time scales ( $> 10 \times \text{mFRI}$ ). These results lend support to the practice of using large smoothing windows to isolate “background” charcoal (as defined above) to infer regional area burned (e.g. Marlon 2003).

Second, the variability in charcoal peak heights in simulated records can largely be explained by relationships between fire sizes and the PCSA size (the source-area to fire-size ratio). As this ratio increases in CharSim simulations, the variability in charcoal

peak heights also increases because there is greater variability in fires sizes and locations within the PCSA. Comparisons of simulations with different source-area to fire-size ratios to Alaskan charcoal records suggest that large source areas, characterized by long-distance charcoal transport (10s of km), are required to obtain the basic patterns of variability in charcoal records from systems with large fire sizes (e.g. boreal forests). These dispersal distances are consistent with evidence of charcoal transport from wildland fires of tens of kilometers (Whitlock and Millspaugh 1996, Gardner and Whitlock 2001, Pisaric 2002, Hallett et al. 2003). However, long-distance transport per se does not erase the strong relationship between large charcoal peaks and local fires. In the simulations, the inferred fire occurrence using the decomposition approach is best related to fire occurrence with 500 m of the simulated lake. Interpreting “local” fires at this spatial scale is consistent with empirical studies comparing known fires to sediment charcoal stratigraphy (Clark 1990, Whitlock and Millspaugh 1996, Gavin et al. 2003, Lynch et al. 2004a).

Third, the charcoal-taphonomic processes of slope wash, mixing, and sampling bias sediment records against preserving small charcoal peaks associated with distance fires. By removing low-frequency variations, the decomposition approach further deemphasizes small peaks. The overall result of the decomposition method, therefore, is to enhance the signature of local fire occurrence, while simultaneously accounting for long-term variability in charcoal production rates.

**Table 2.1.** Components of the Charcoal Simulation Model (CharSim) include the major processes linking fires on a landscape to the creation of a sampled sediment charcoal record. Primary references provided quantitative values, while secondary references provided either additional support or qualitative information from which estimates were based.

<b>Component</b>	<b>Details and/or parameters</b>	<b>Primary References</b>	<b>Secondary References</b>
<b>1. Fire regime</b>	a) mean number of fires per year (Poisson probability) b) mean and variance of log-transformed fire-size distribution (e.g. log-normal probability)	a) Kasischke et al. (2002); Chapter 4 b) Alaska Fire Service (2004)	a) Lynch et al. (2002, 2004b)
<b>2. Charcoal production, dispersal, and primary deposition</b>	a) charcoal production b) charcoal dispersal c) mean fall speed d) mode and variation of injection heights e) wind speed f) wind direction	a) estimated b) Appendix A c) Lynch et al. (2004a) d) estimated, see Appendix A e) Taylor et al. (2004) f) instrumental wind data <sup>a</sup>	a) Clark et al. (1998)
<b>3. Secondary charcoal deposition</b>	a) proportion and temporal pattern of landscape-derived charcoal b) proportion and temporal pattern of within-lake redeposition	a) estimated b) estimated	a, b) Bradbury (1996), Whitlock and Millspaugh (1996), Clark and Patterson (1997)
<b>4. Sediment mixing</b>	a) mean mixing depth b) mixing distribution c) sediment accumulation rate	a) Chapter 4, estimated b) Chapter 4	
<b>5. Sediment sampling</b>	a) sampling resolution	a) Chapter 4 b) user defined	
<b>6. Fire history interpretation</b>	a) correlation between CHAR and area burned b) maximum accuracy	a) this paper b) this paper	

<sup>a</sup>Bettles, Alaska, 1971-2000: Alaska Climate Research Center, <http://climate.gi.alaska.edu/Climate/Wind/Direction/Bettles/BTT.html>

**Table 2.2.** Parameters used to generate the CharSim records in this paper.

CharSim component	Description	Parameter (units)	Value(s) used in this paper	
			variable fire size	constant fire size
<b>Fire regime</b>	probability of fire	? (fires yr <sup>-1</sup> )	1.00	1.00
	fire size	mean fire size (log ha)	6.813	8.971
		stdev. fire size (log ha)	2.078	0.00
	resulting mean fire-return interval <sup>1</sup>	yr	120	100
<b>Charcoal dispersal and primary deposition</b>	injection heights	$h_{mode}$ (m)	10, 100, 1000, mixed <sup>2</sup>	10, 100, 1000
	<b>Secondary charcoal deposition</b>	slope-wash redeposition	$P_{sw}$ (proportion)	0.01
sw time frame, $N_{sw}$ (yr)			100	100
sw mean, $\mu_{sw}$			10	10
within-lake redeposition		$P_{re}$ (proportion)	0.10	0.10
		redep. time frame, $N_{re}$ (yr)	50	50
		redep. mean, $\mu_{sw}$	5	5
	% of lake defined as center, $a$	10	10	
<b>Mixing</b>	mixing depth	$md$ (mm)	10	10
	sed. acc. rate	$s$ (cm yr <sup>-1</sup> )	0.0125	0.0125
<b>Sampling</b>	sampling interval	$d_{sample}$ (cm)	0.25	0.25
		temporal res. (yr sample <sup>-1</sup> )	20	20

<sup>1</sup> A "fire" is identified any time area burns within a 100 m radius from the edge of the lake, regardless of the number of ignitions that occurred in a year.

<sup>2</sup> The mixed scenario scaled injection heights proportionally to fire size, using  $h_{mode}$  values of 10, 50, 100, 500, and 1000.

**Table 2.3.** Parameters and description of the model runs used for comparison to Alaskan sediment-charcoal records, and results from a two-sample Kolmogorov-Smirnov (K-S) test.

	<b>prob. of fire</b>	<b>local-fire frequency</b>	<b>mixing depth</b>	<b>sed. acc. rate</b>	<b>sampling</b>		<b>K-S test result (<i>p</i>-value)</b>			
Comparison lake	?	mean fire- return interval <sup>1</sup>	<i>md</i> (mm)	<i>s</i> (cm yr <sup>-1</sup> )	<i>d<sub>sample</sub></i> (cm)	temp. res. (yr sample <sup>-1</sup> )	<i>h<sub>mode</sub></i> = 10 m	<i>h<sub>mode</sub></i> = 100 m	<i>h<sub>mode</sub></i> = 1000 m	<i>h<sub>mode</sub></i> = mixed <sup>2</sup>
<b>Ruppert</b>	1.0	120	20	0.0125	0.25	20	0.00	0.01	0.26	0.26
<b>Code</b>	1.0	120	10	0.0125	0.25	20	0.00	0.00	0.34	0.71
<b>Wild Tussock</b>	1.0	120	10	0.0125	0.25	20	0.00	0.01	0.25	0.59
<b>Last Chance</b>	1.0	120	5	0.025	0.50	20	0.00	0.00	0.60	0.77

<sup>1-2</sup> See Table 2.2.

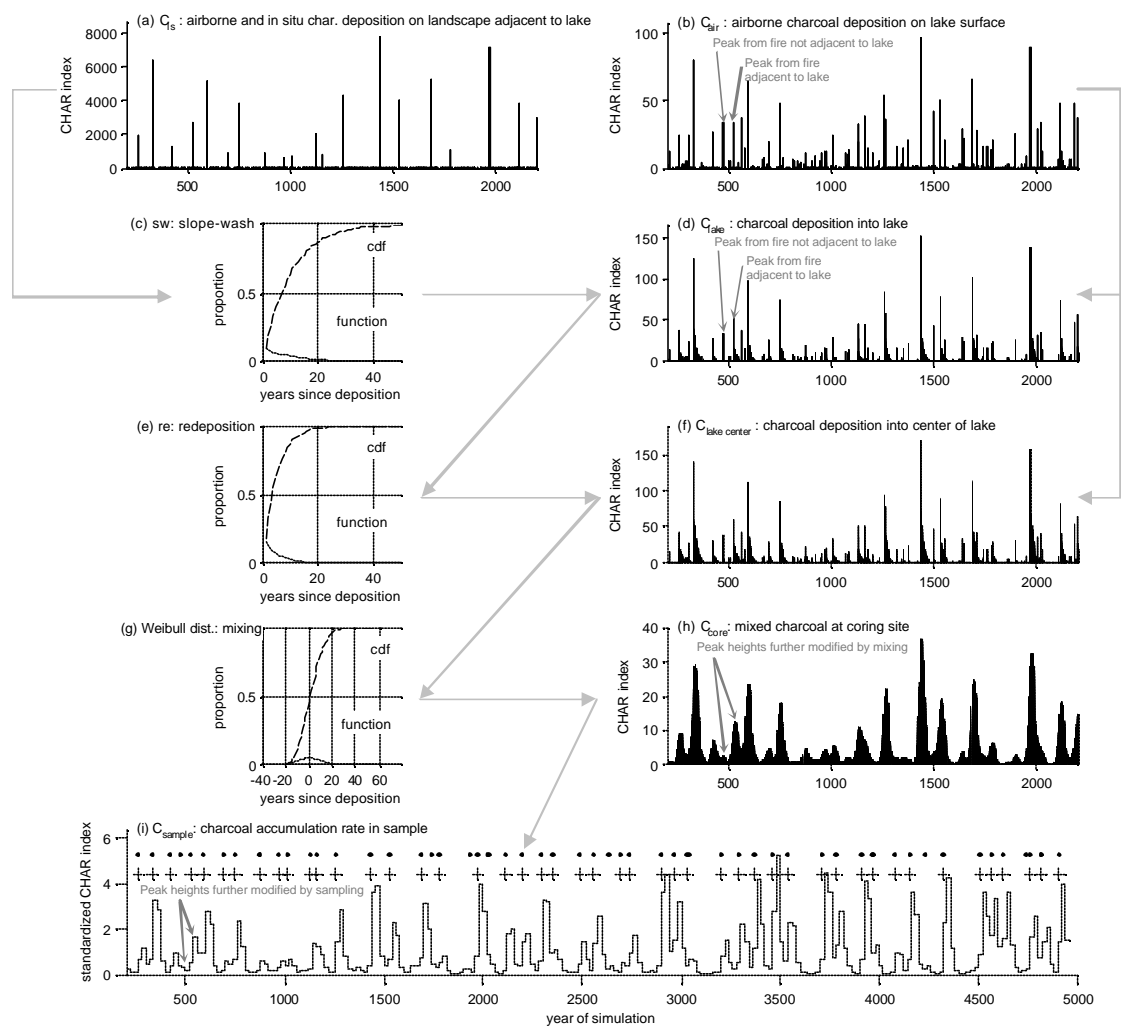


**Figure 2.1.** Pathway from airborne charcoal deposition to charcoal sampled in the simulated core, using a 1000-m modal injection height and parameters otherwise described in Table 2.2. One percent of the charcoal deposited on the landscape surrounding the lake ( $C_{ls}$ ; panel a) is distributed into the lake based on the slope-wash curve ( $sw$ ; panel c). Airborne charcoal deposited on the lake ( $C_{air}$ ; panel b) is added to charcoal input from slope wash to determine the amount of charcoal deposited on the lake sediment surface ( $C_{lake}$ ; panel d). One percent of the charcoal on the lake sediment surface is redeposited into the “center” of the lake (defined in the text) based on the redeposition curve ( $re$ ; panel e) to determine the amount of charcoal reaching the center of the lake ( $C_{lake\_center}$ ; panel f). Charcoal in the center of the lake is mixed according to a Weibull distribution (with shape parameter = 2.5, panel g) to determine the final charcoal stratigraphy within the core ( $C_{core}$ ; panel h). Finally, the simulated core is sectioned by depth to obtain the sampled values ( $C_{sample}$ ; panel i). Dots (.) and plus marks (+) indicate when fires burned within 1000 and 100 m of the lake, respectively.

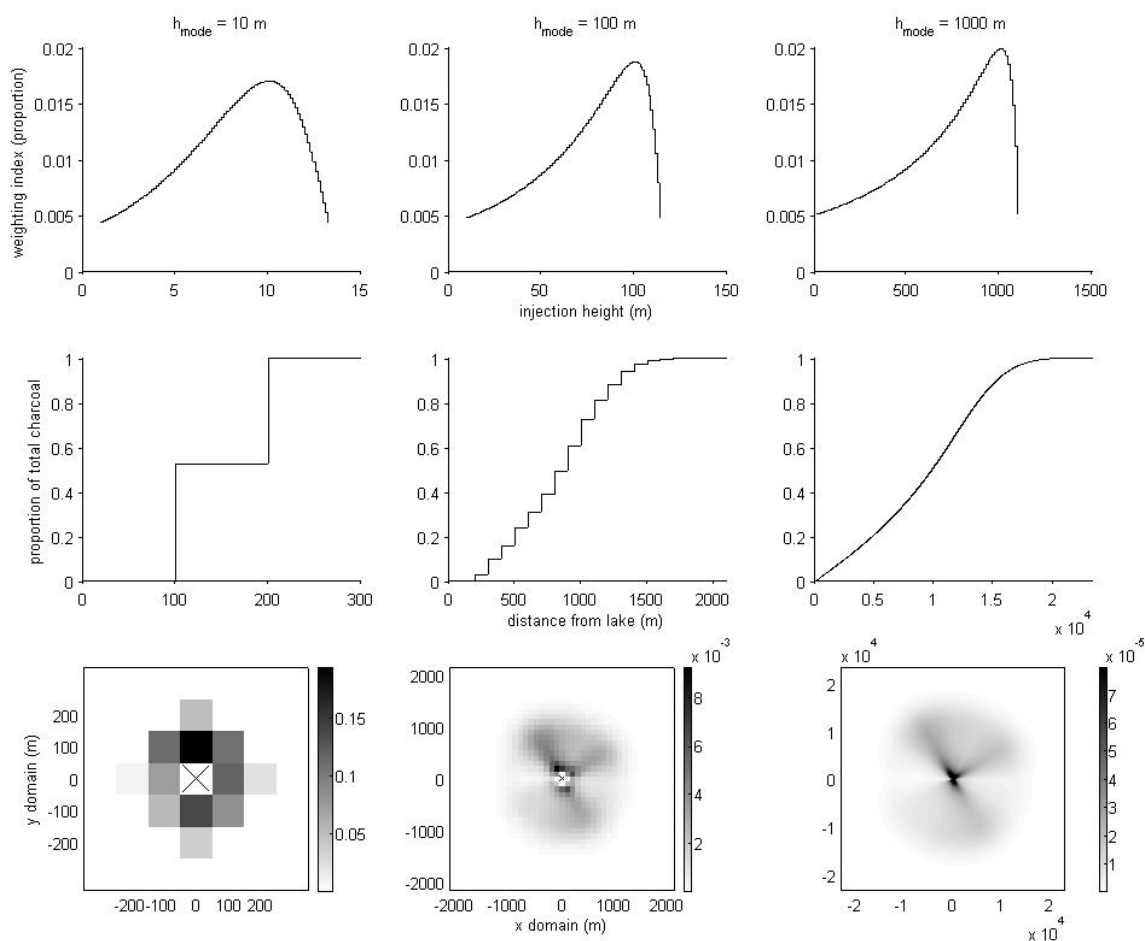


**Figure 2.2.** Potential charcoal source area (PCSA) for three modal injection height scenarios (columns), including distribution of injection heights (row one), cumulative charcoal deposited at different distances from the lake pixel (row two), and a visual representation of the PCSA, also termed a "charcoal dispersal table" (row three). Steps in row two are a function of the 100 x 100 m pixel size, and the color bars in row three represent proportional charcoal concentration.

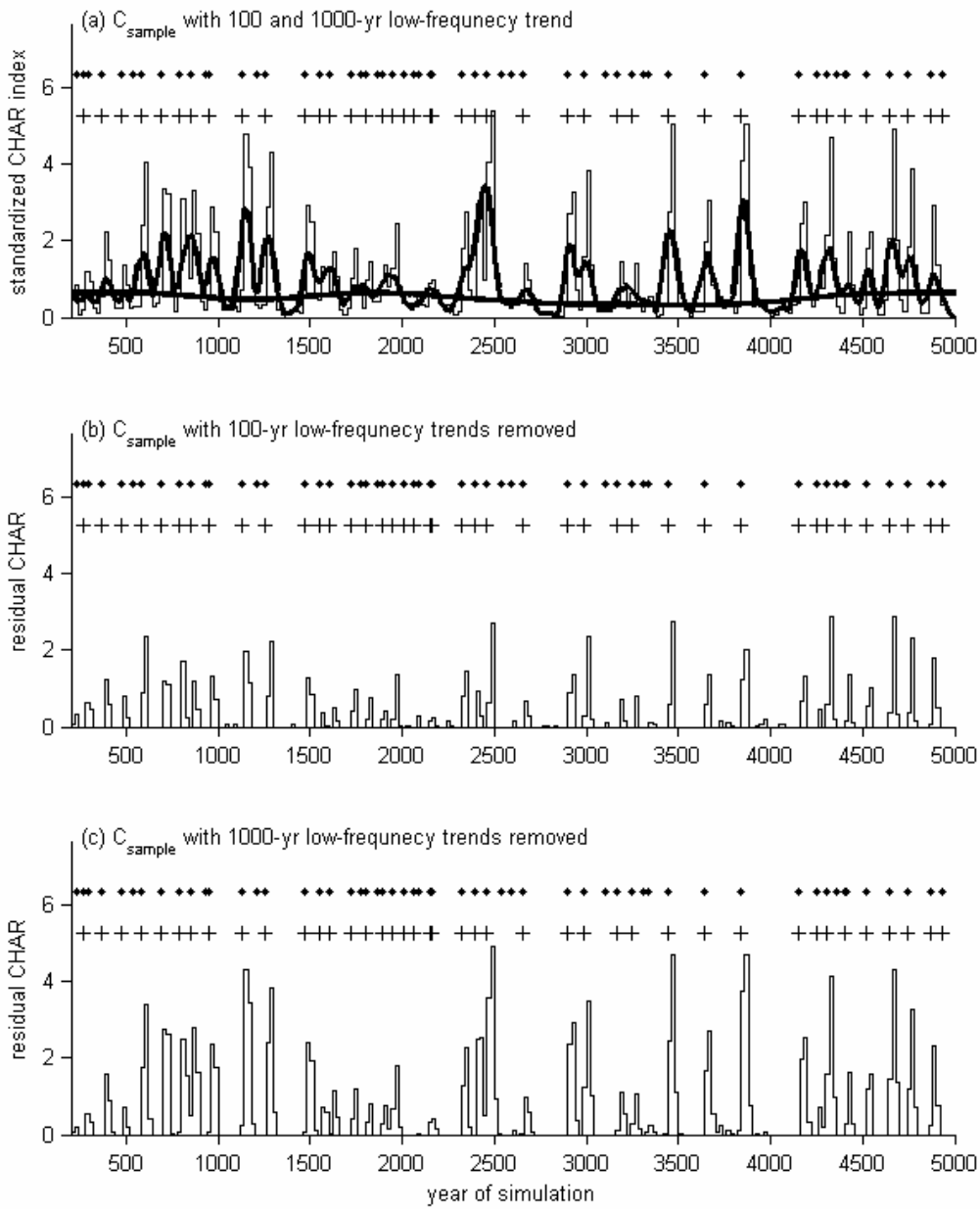


**Figure 2.3.** Two contrasting examples of low-frequency trends in CHARs (a), and the resulting positive residual series (“peak charcoal”) from which charcoal peaks are identified (b-c). Dots (.) and plus marks (+) indicate when fires burned within 1000 and 100 m of the lake, respectively.

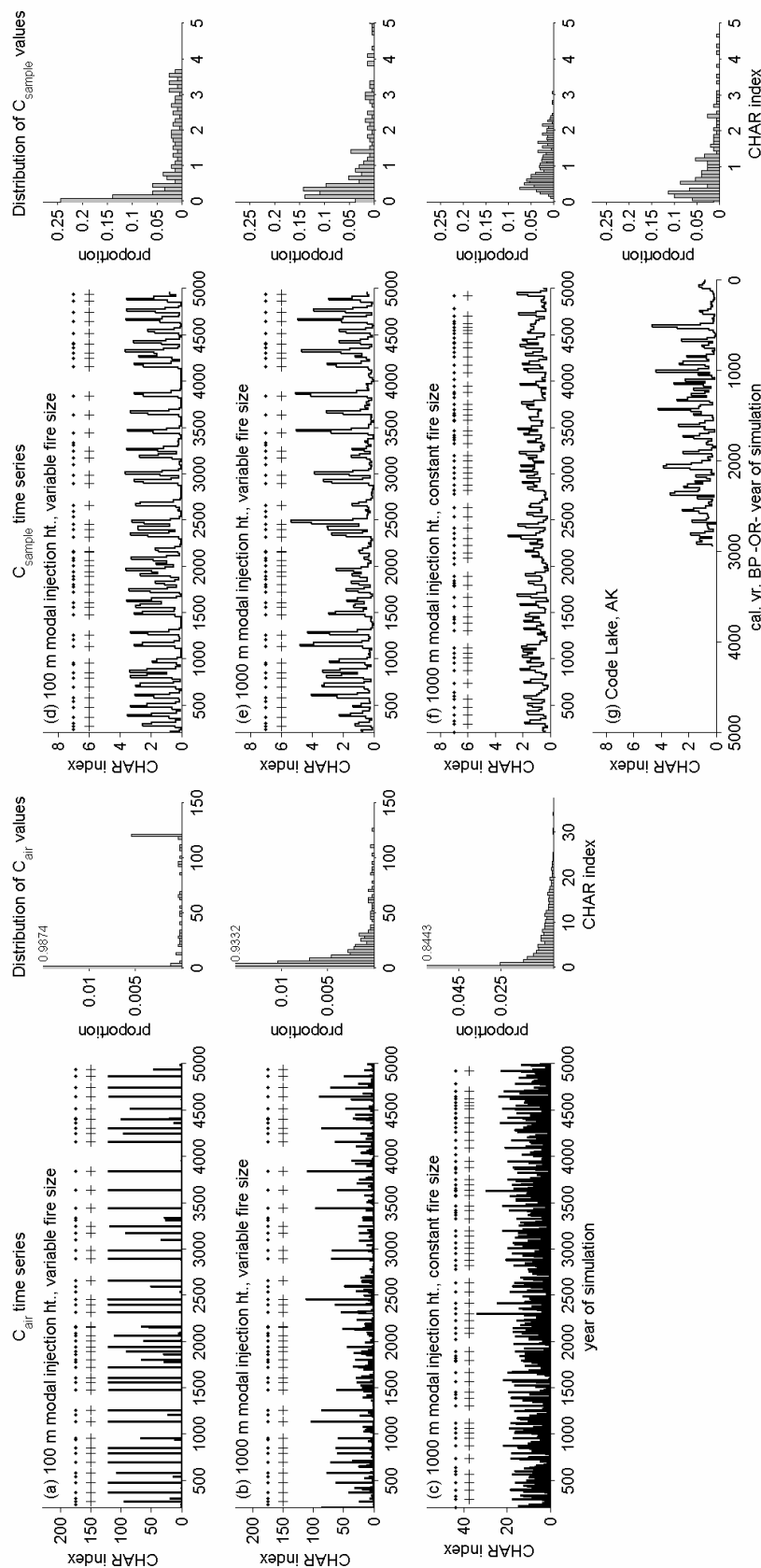


**Figure 2.4.** Variability in charcoal peak heights results from increased variability in modal injection heights,  $h_{\text{mode}}$ , variability in fire size, and secondary charcoal transport, mixing, and sampling. (a): 100-m  $h_{\text{mode}}$  scenario with variable fire sizes produces binary charcoal distributions significantly different than observed records from Alaskan lakes (g, Fig. 2.5). (b): Increasing injection heights to those characterized by 1000-m  $h_{\text{mode}}$  scenario increases variability in charcoal peak heights. (c): Keeping large injection heights (i.e. 1000-m  $h_{\text{mode}}$  scenario) but eliminating variability in fire size produces homogenous records with a narrow range of CHARs (i.e. b vs. c; note factor of four difference in the CHAR index). (d)-(f): Mixing and sampling homogenize records and produce more continuous CHAR distributions. (g): Only the mixed and sample record from the 1000-m  $h_{\text{mode}}$  scenario is similar to Alaskan records.

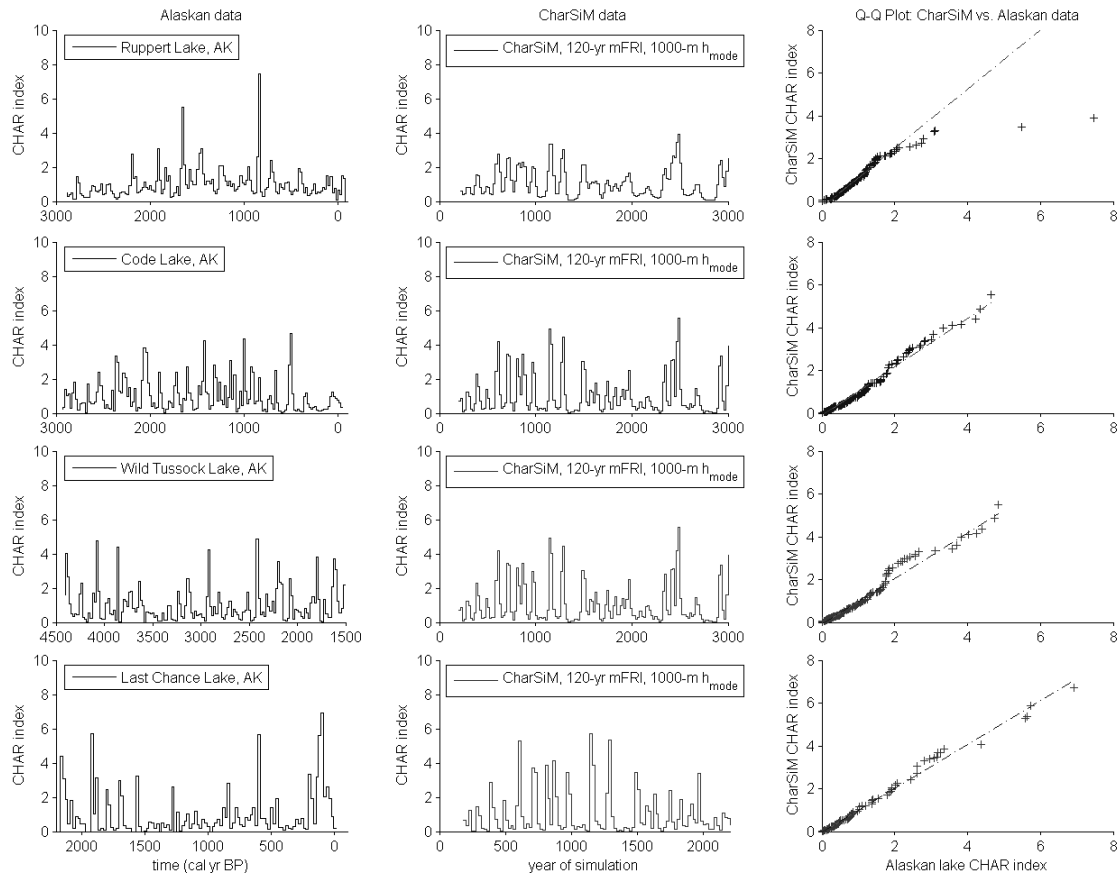


**Figure 2.5.** Comparison between charcoal accumulation from Alaskan lakes and simulated CharSim records using the 1000-m modal injection height scenario (columns 1-2), and a quantile-quantile (Q-Q) plot for each comparison (column three). Linear Q-Q plots suggest that the two samples come from the same distribution, while departures from linearity suggest otherwise. A two-sample K-S test comparing the distribution of charcoal from each Alaskan lake to the corresponding CharSim series fails to reject the null hypothesis of no difference ( $p \geq 0.25$ ; Table 2.3).

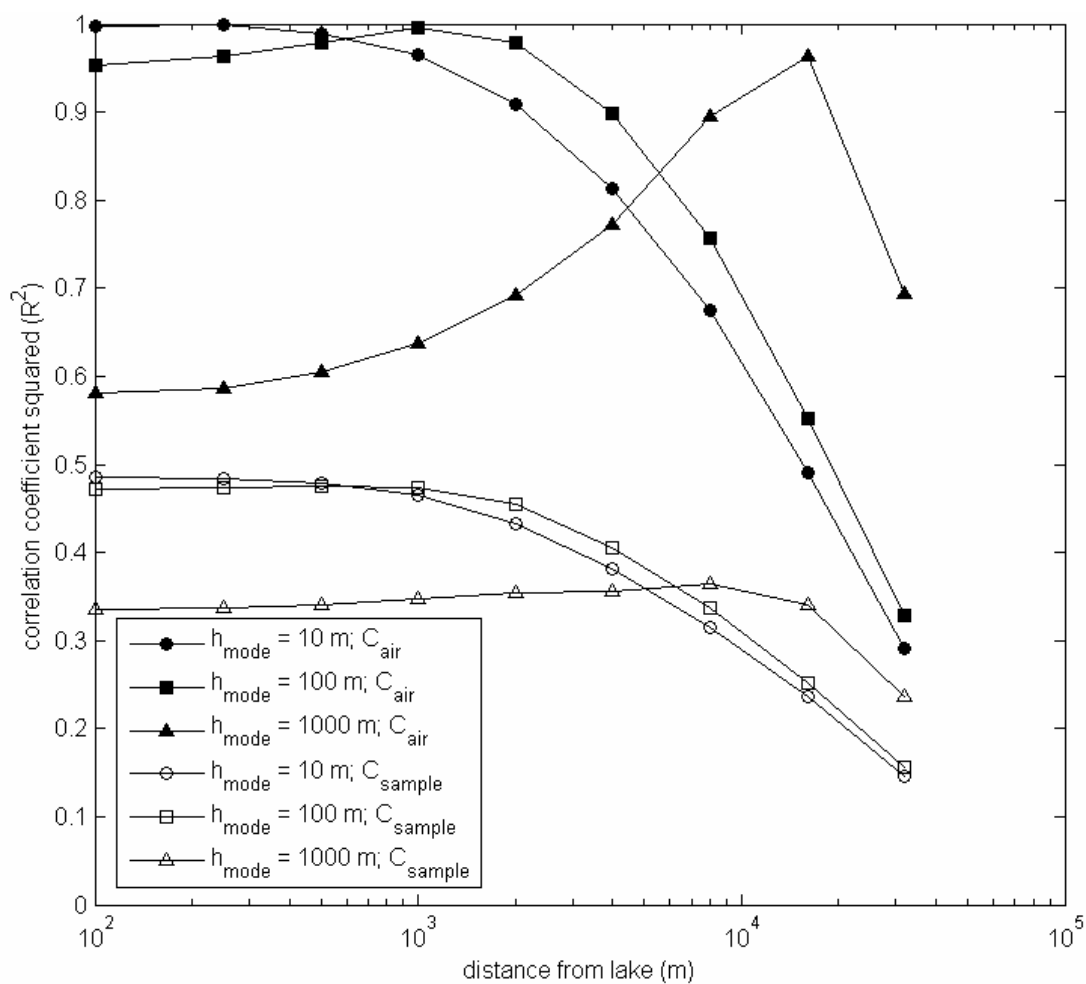


**Figure 2.6.** Correlation of airborne (filled symbols) and sampled (open symbols) charcoal accumulation and area burned as a function of spatial scale for 10- 100- and 1000-m  $h_{mode}$  scenarios. Resolution in sampled scenarios is 20-yr per sample.

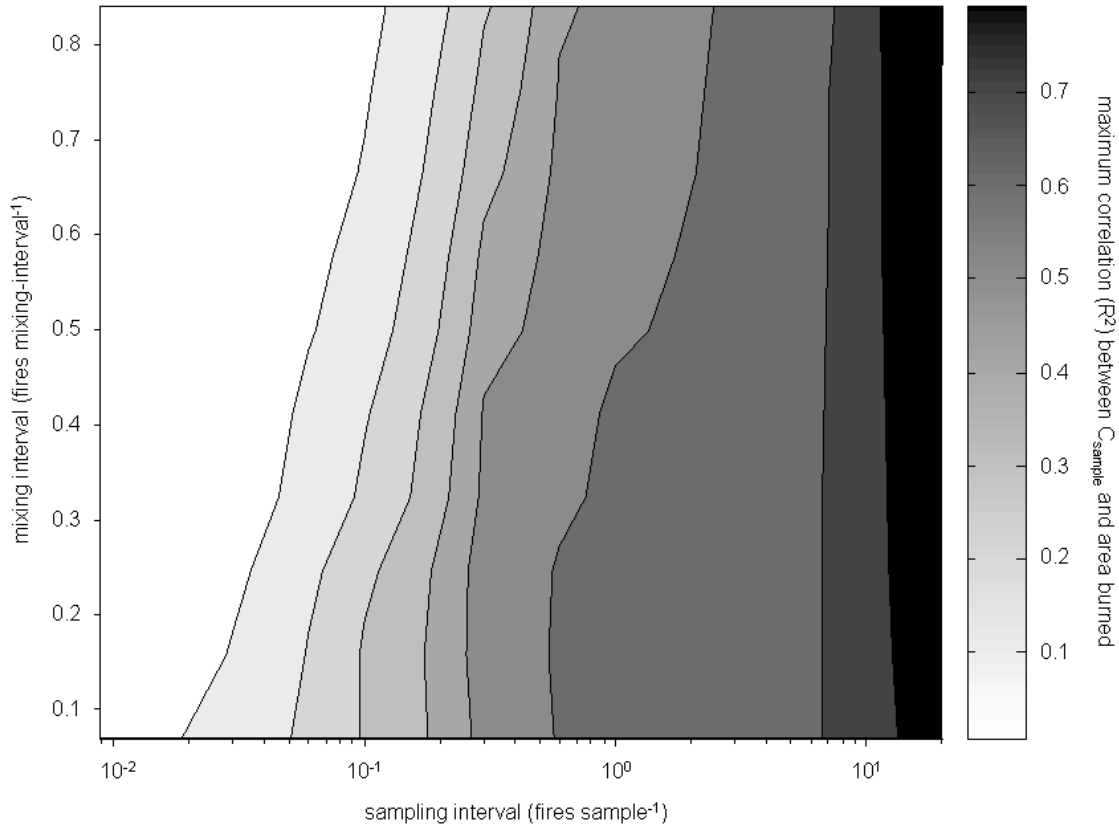


**Figure 2.7.** Maximum correlation (shaded values, color bar) between sampled charcoal accumulation,  $C_{sample}$ , and area burned as a function of sampling interval (x) and mixing interval (y). Correlations are based on 10 mixing and 12 sampling intervals, standardized to the mean fire return interval (120 yr), from a 20,000-year record using the 1000-m  $h_{mode}$  scenario and parameters otherwise described in Table 2.2. Correlations from all radii in Fig. 2.6 were considered, but only the maximum correlation is graphed. Optimum radii were either 8000 or 16,000 m, with an average of 11,000 m (stdev. 4000 m). Time scales are standardized to the mean fire return interval (120 yr in this case).

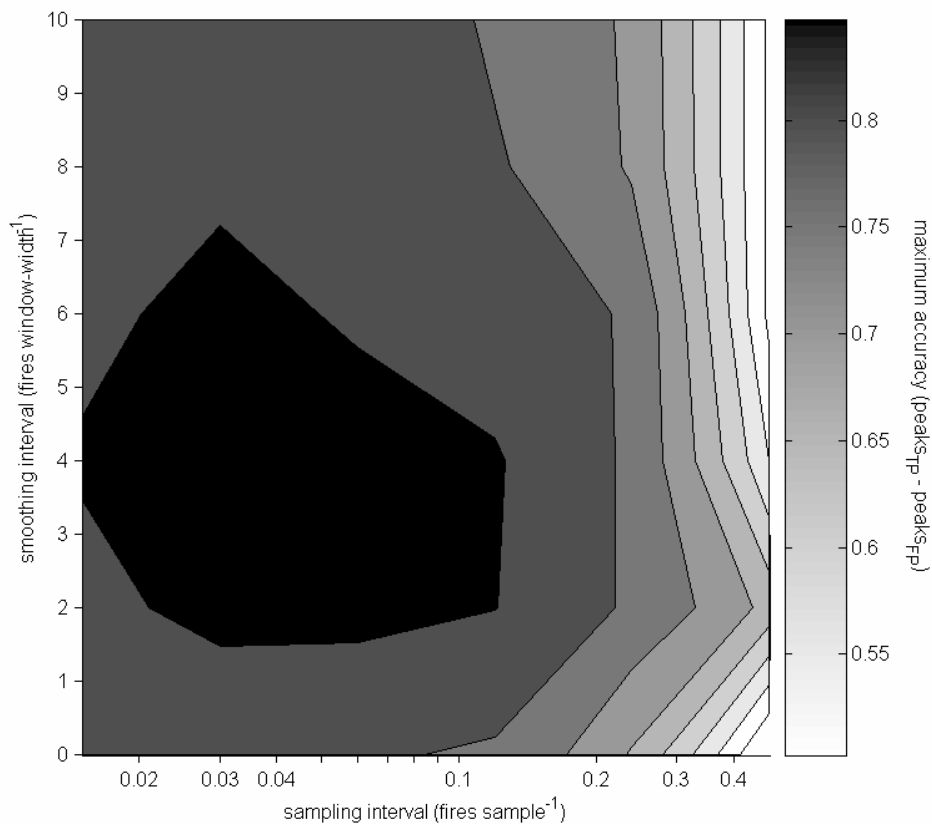


**Figure 2.8.** Maximum accuracy (shaded values, color bar) as a function of sampling times scales (x) and smoothing intervals (y) from interpreting charcoal peaks via the decomposition method. Accuracy values are based on 6 different sampling and smoothing intervals, normalized to the mean fire return interval (120 yr), from the same record used for Fig 6. Mixing is equivalent to 0.3 (fires mixing-interval<sup>-1</sup>) in Fig. 2.7 and a smoothing interval of zero corresponds to analyzing the raw record (i.e. no trends removed). Accuracy values range from 0.5-0.85 and were maximized across the spatial domains illustrated in Fig. 2.6 (see results).

**CHAPTER 3: VEGETATION-MEDIATED IMPACTS OF CLIMATIC CHANGE ON LATE  
GLACIAL AND HOLOCENE FIRE REGIMES IN THE SOUTHCENTRAL BROOKS RANGE,  
ALASKA**

Philip E. Higuera<sup>1</sup>, Linda B. Brubaker<sup>1</sup>, Patricia M. Anderson<sup>2</sup>, Feng Sheng Hu<sup>3</sup>, and  
Thomas Brown<sup>4</sup>

<sup>1</sup>College of Forest Resources, University of Washington, Seattle, WA

<sup>2</sup>Quaternary Research Center, University of Washington, Seattle, WA

<sup>3</sup>Department of Plant Biology, University of Illinois, Urbana, IL

<sup>4</sup>CAMS, Lawrence Livermore National Laboratory, Livermore, CA

**SUMMARY**

Direct and indirect impacts of millennial-scale climatic change on fire regimes are examined in the southcentral Brooks Range, Alaska, using four lake-sediment records and existing climatic interpretations. Charcoal accumulation rates (CHARs) provide estimates of fire return intervals (FRIs; the inverse of fire frequency) within each of five vegetation zones described with fossil pollen, stomata, and modern analog techniques at sites across a 120 km transect. During late glaciation and the early Holocene the region was dominated successively by herb tundra, shrub tundra, and deciduous woodland, all novel species assemblages relative to modern North American vegetation. Records from two sites span this interval. CHARs increased and FRIs decreased sharply with post-glacial climatic warming and the transition from herb to shrub tundra c. 13-14 k calendar years before present (AD 1950; ybp). FRIs were short in the shrub tundra period (means c. 140 yr) but increased considerably with the transition to deciduous woodland c. 10.5 k ybp (mean  $\gg$  250 yr), despite evidence of warmer- and drier-than-present summer conditions. All four records span the mid and late Holocene and document statistically similar changes in millennial-scale fire regimes across the study region. Despite evidence of climatic cooling and moistening through the mid and late Holocene, FRIs decreased significantly with the development of *Picea glauca* forest-tundra vegetation c. 8.0 k ybp (means c. 250-350 yr), and again with the development of the modern *Picea mariana* boreal forests c. 5.5 k ybp (means c. 150-170 yr). Overall these records show a greater correspondence between fire frequency and vegetation characteristics rather than with inferred climate, indicating that vegetation has played a strong role in mediating the

direct impacts of climatic change, primarily through modifying landscape flammability. In the context of recent and predicted warming in Alaska and the associated increase in shrub densities in tundra, the short FRIs in shrub tundra during late glaciation and the early Holocene imply that tundra can burn frequently under warmer climatic conditions.

## INTRODUCTION

Area burned in northern high-latitudes is predicted to increase with climatic warming over the next century (Rupp et al. 2000a, Calef et al. 2005), in some cases by more than 100% (Flannigan et al. 2005). Recent warming across these regions (Overpeck et al. 1997, Serreze et al. 2000) has already initiated vegetation changes at a variety of scales, including the advance and increased growth of conifers at treeline (MacDonald et al. 2000, Lloyd and Fastie 2002, Lloyd et al. 2003, Esper and Schweingruber 2004, Lloyd 2005) and increased growth and expansion of shrubs within tundra communities (Silipaswan et al. 2001, Sturm et al. 2001, Stow et al. 2004). The response of fire regimes to ongoing and predicted climatic change will ultimately depend upon interactions between climatic and vegetational variables that operate at multiple temporal and spatial scales. At short time scales, climate and weather directly influence ignition rates, fuel-moisture patterns, and fire spread, while vegetation determines the density and spatial pattern of fuels. At longer time scales, climate indirectly affects fire regimes by influencing vegetation composition and structure over large spatial scales. Together, interactions between climatic and vegetational variables determine overall landscape flammability and the characteristic patterns of fire in space and through time.

Numerous studies in North American boreal forests document the importance of direct climatic controls on fire occurrence and fire regimes. For example, over the past several decades, annual area burned has been tightly linked to warm, dry weather conditions and frequent lightning activity (Larsen and MacDonald 1995, Larsen 1996, Hess et al. 2001, Kasischke et al. 2002, Stocks et al. 2003, Duffy et al. 2005). Paleoecological studies support these climate-fire relationships and illustrate that fire frequencies have varied with millennial-scale changes in relative moisture throughout the

late Holocene (Carcaillet and Richard 2000, Carcaillet et al. 2001a, Lynch et al. 2002, Lynch et al. 2004b). However, the impacts of climatic change on fire regimes also depend upon indirect effects of climate on vegetation. Area burned across interior Alaska, for example, is positively correlated with tree cover (Kasischke et al. 2002), and modeling studies suggest the potential for increased burning in boreal Alaska in response to increased black spruce (*Picea mariana* Mill. BSP.) densities alone (Rupp et al. 2002).

The interactive effects of climate and vegetation on fire regimes are complex to study and predict, and the relative importance of either variable can change across space and through time. The complexity of these interactions is well illustrated in boreal forest systems. For example, while the probability of fire in boreal forests varies with stand age (i.e. vegetational control; Yarie 1981, Lynch et al. 2002), under extreme weather conditions these variations have little influence on the likelihood of a stand burning during a given fire (Bessie and Johnson 1995). Conversely, the impacts of long-term climatic change on fire regimes can be modified by vegetational changes that take place over decades to centuries, due to changes in landscape flammability (Lynch et al. 2002, Rupp et al. 2002, Lynch et al. 2004b).

Paleoecological reconstructions provide a long-term perspective necessary to understand the interactive effects of climatic and vegetational change on fire regimes (Hu et al. 2006). The paleoecological approach also has the unique ability to reveal evidence of climate-vegetation-fire relationships that are unobservable on the current landscape, thus expanding our view of potential future scenarios. When individual records are combined across broad spatial scales and compared to paleoclimatic records, strong inferences can be made into the climatic and vegetational mechanisms controlling fire regimes at multi centennial and millennial time scales (e.g. Clark 1990, Lynch et al. 2004b, Brunelle et al. 2005, Gavin et al. 2006).

We take a paleoecological approach to examine the interactions between climate, vegetation, and fire regimes in the southcentral Brooks Range, Alaska (Fig. 3.1), where millennial-scale climatic and vegetational history are well known based several decades of research in the region (Anderson and Brubaker 1994, Anderson et al. 2003; Table 3.1). Specifically, we wanted to understand how millennial-scale climatic changes have

interacted with arctic and boreal vegetation change to influence fire regimes in the southcentral Brooks Range. We add three new pollen and four new charcoal records to the existing database, which allows the first assessment of direct and indirect impacts of climatic change on past fire regimes. We use macroscopic charcoal from lake sediments to reconstruct fire return intervals (FRIs, the inverse of fire frequency) and statistically compare FRIs to detect changes between vegetation zones inferred from fossil pollen, stomata stratigraphy, and modern analog analysis. If climatic variations were the dominant control of fire regimes over the past 15,000 (15 k) years, we expect distinct, synchronous changes in fire occurrence that are consistent with direct climate-fire relationships and relatively independent of changes in vegetation (e.g. Carcaillet et al. 2001a). In contrast, if vegetational change was the dominant control of fire regimes, we expect distinct, synchronous changes in fire occurrence to be associated with shifts between vegetation zones and consistent with the role that fuels play in controlling long-term landscape flammability (e.g. Lynch et al. 2002). By documenting fire regimes in novel vegetation assemblages that covered the study region during late glacial and the early Holocene (c. 14.0-9.0 k ybp; e.g. Anderson et al. 1989, Edwards et al. 2005), our study also provides relevant examples of how direct and indirect impacts of climatic change may shape future fire regimes in arctic and boreal ecosystems.

### STUDY LAKES AND REGIONAL SETTING

We examined sediment cores from four lakes along a 120 km east-west transect in the foothills of the southcentral Brooks Range, within the Kobuk Ridges and Valleys Ecoregion (Nowacki et al. 2001; Fig. 3.1, Table 3.2). The region is underlain by alluvial and glacial sediments deposited most recently from the Walker Lake Glaciation, which terminated between 25-30 k ybp (Hamilton 1982). Modern climate is continental: January and July mean maximum temperatures in Bettles (Fig. 3.1) are -20°C and 21°C, respectively, and mean annual precipitation is 36 cm, with 55% falling between June and September (Western Regional Climate Center, AD 1951-2005 observations<sup>2</sup>). Forests and woodlands dominate lowlands and hill slopes, with *Picea mariana* in wet muskegs; *P.*

---

<sup>2</sup> Data available online: <http://www.wrcc.dri.edu/cgi-bin/cliMAIN.pl?akbett>

*glauca* (Moench) Voss. and *Populus balsamifera* Mill. along riparian areas; and *P. glauca*, *Betula papyrifera* Marsh. and *Populus tremuloides* Michx. on uplands and warm, south-facing slopes (Viereck et al. 1986, Nowacki et al. 2000). In non-forested areas, *Salix* spp., *Betula glandulosa* Michx., and *Alnus* spp. grow in shrub communities (Nowacki et al. 2000). Fire is the primary disturbance agent in the region, with estimated fire rotation periods in the Ecoregion of 175 years, based on observations from AD 1950-2001 (Kasischke et al. 2002).

We cored small (2-15 ha), relatively deep (7.0-11.6 m) lakes (Table 3.2) to maximize the probability of obtaining undisturbed charcoal and pollen records (Jacobson and Bradshaw 1981, Larsen and MacDonald 1993). Each lake is surrounded by discontinuous *P. mariana*-dominated forest and lies within a few tens of kilometers of the northern limit of *Picea* growth. Recent fires burned to the edge of Ruppert Lake in AD 1991 (15,357 ha; Fig. 3.1; Alaska Fire Service 2004) and within at least 4 and 6 km west/southwest of the lake in AD 1913 and AD 1891, respectively (Christiansen 1988). Fires burned to 10 km west and 13 km south of Xindi Lake in AD 1959 (5027 ha) and AD 1957 (34,424 ha), to 1 and 3 km east of Code Lake in AD 1959 (788 ha) and AD 1949 (2456 ha), and to 5 km west and 1 km southwest of Wild Tussock Lake in AD 1997 (9750 ha) and AD 1991 (6390 ha; Alaska Fire Service 2004; Fig. 3.1).

### LATE GLACIAL AND HOLOCENE CLIMATIC AND VEGETATIONAL HISTORY

A variety of paleoclimate indicators, including fossil floral and faunal assemblages, lake-level history, and glacial history, reveals the nature of millennial-scale climatic change in Alaska over the past 16 k yr (summarized by Anderson et al. 2003). These proxies indicate that the climate of the study region has shifted from cooler and drier than present during the late glacial period (16-13 k ybp), to warmer and drier (with some evidence suggesting wetter) than present by the early Holocene (11-8 k ybp). Temperatures cooled but remained warmer than present during the mid Holocene (7-4 k ybp), and present-day cool, moist conditions were established in the late Holocene (4-0 k ybp; Table 3.1).

Millennial-scale vegetation history of northcentral Alaska is well described by fossil pollen records covering the past 16 k yr (Anderson and Brubaker 1994), and provides a larger regional framework for evaluating the pollen records of this study. Over this period, five distinct vegetation types have been recognized (Anderson and Brubaker 1994, unless otherwise noted; Table 3.1): (1) herb tundra c. >16-15 k ybp, characterized by Poaceae, Cyperaceae, and *Artemisia*, with lesser amounts of forbs and *Salix*, similar in plant functional type to prostrate shrub tundra or Poaceae-forb tundra (Bigelow et al. 2003); (2) birch shrub tundra c. 15-13 k ybp, characterized by shrub *Betula glandulosa* or *B. nana* and *Salix*, with xeric herb species likely covering previously unvegetated areas; (3) deciduous forest or woodlands c. 13-9 k ybp, characterized by the presence of *Populus balsamifera* (and/or *P. tremuloides*), possibly arboreal *Betula*, and the continued presence of shrub *Betula* and *Salix* (Edwards et al. 2005); (4) forest-tundra c. 9-6 k ybp, with shrub *Betula* and *Alnus* (arriving c. 8 k ybp) and *P. glauca* forming gallery forests or treeline communities on upland sites; (5) modern boreal forests c. 6 k ybp to present, marked by an increase in conifer density, due mainly to the arrival of *P. mariana*.

## METHODS AND RATIONALE

### Lake sediments

Sediments below c. 25 cm of the mud-water interface were collected from the center of each lake with two parallel, overlapping 8-cm diameter cores in summer 2001 (Code, CO), 2002 (Ruppert, RP), or 2003 (Xindi, XI; Wild Tussock, WK) using a modified Livingston piston corer (Wright et al. 1984). Surface sediments (< c. 50 cm) were collected with a polycarbonate tube and the top 10-20 cm sliced at 0.5-1.0 cm in the field. The lower portions of the surface cores and all the deeper cores were split longitudinally in the lab to describe and photograph sediment stratigraphy. Two thirds of each core was sliced at 0.25-0.5 cm intervals and the other 1/3 was archived. All cores had intermittent laminae, and stratigraphic markers (visual laminae or charcoal peaks) were used to splice together overlapping segments of adjacent cores. Subsamples of 1 cm<sup>3</sup> were prepared at varying intervals for pollen and stomata analysis according to PALE (1994) protocols for arctic and subarctic sediments, except that samples were not

subjected to a coarse sieve (Carlson 2003, Pisaric et al. 2003). For charcoal identification, 3-5 cm<sup>3</sup> subsamples were taken from contiguous core slices, soaked in sodium metaphosphate for 72 hours, washed through a 150 μm sieve, and bleached with H<sub>2</sub>O<sub>2</sub> for 8 hours (Higuera et al. 2005b). Charcoal was identified at 10-40 x magnification based on color, morphology, and texture (Rhodes 1998). Pollen was counted at 400-1000 x magnification to a terrestrial pollen sum > 300 (mean = 398, stdev. = 107) and displayed as percentages of total terrestrial pollen. To estimate the transition from forest-tundra to boreal forest at RP and WK, stomata searches were conducted to an equivalent pollen sum of 2000 grains (Carlson 2003) in selected samples bracketing the *Picea* pollen rise c. 5.5 k ybp (Brubaker et al. 1983a). *Picea* stomata were identified based on comparisons with an Alaskan reference collection and Hansen (1994). Pollen and charcoal concentrations (# cm<sup>-3</sup>) were multiplied by the estimated sedimentation rate (cm yr<sup>-1</sup>) to obtain the pollen accumulation rate (PAR; grains cm<sup>-2</sup> yr<sup>-1</sup>) and charcoal accumulation rate (CHAR; pieces cm<sup>-2</sup> yr<sup>-1</sup>) of each sample.

## Chronologies

Sediment chronologies are based on <sup>210</sup>Pb dates for the upper 10-20 cm of each site and on AMS <sup>14</sup>C ages of concentrated charcoal from charcoal peaks, concentrated *Picea* pollen, or terrestrial macrofossils for deeper sediments (Table 3.3). <sup>210</sup>Pb ages were calculated using the Constant Rate of Supply model (Binford 1990) and <sup>14</sup>C ages were calibrated using CALIB 5.0 and the INTCAL 04 dataset (Reimer et al. 2004). All ages are reported as calibrated years before AD 1950 (ybp). Confidence intervals of calibrated <sup>14</sup>C ages represent the 2.5<sup>th</sup>, 50<sup>th</sup> and 97.5<sup>th</sup> percentiles of the weighted probability density function of calibrated ages (Telford et al. 2004a). Chronologies were developed individually for the <sup>210</sup>Pb and <sup>14</sup>C portions of each core using a weighted cubic smoothing spline in Matlab (The MathWorks, Inc.) with the smoothing parameter determined as a function of the average distance (cm) between dates, such that greater sampling of ages resulted in a more flexible spline. The inverse of the 95% confidence interval of the <sup>210</sup>Pb or calibrated <sup>14</sup>C date was used for weighting (cf. Telford et al. 2004b).

### **Pollen and stomata analysis**

Pollen zone boundaries, which correspond to vegetation types previously recognized in the region (Anderson and Brubaker 1994), were delineated primarily by visual inspection of pollen percentages of major tree, shrub, and herb taxa. *Picea* stomata presence/absence (RP and WK) and results from modern analog analysis further aided in delineating the boundary of the modern boreal forest.

We used squared-chord distances (SCD; Overpeck et al. 1985, Anderson et al. 1989) and receiver operating characteristic curves (ROC curves; Gavin et al. 2005) to quantify the probability that fossil pollen assemblages resembled modern pollen assemblages from North American Arctic Tundra, Boreal Forest, and Forest-tundra biomes (biomes defined by Federova et al. 1994, cited and mapped in Whitmore et al. 2005 and also mapped in Appendix C). Results are based on the average of the lowest 1% of SCD values and their probability-of-analog (ROC analysis) for comparisons to all samples in the three North American biomes. Further details of this technique are presented in Appendix C.

### **Charcoal analysis**

To assess whether CHARs differed between past vegetation biomes, we compared CHAR distributions between pollen zones in each lake using a two-sample Kolmogorov-Smirnov (K-S) test (e.g. Clark 1990, Lynch et al. 2002). We discuss differences in CHAR distributions only when the probability of Type I error,  $p$ ,  $< 0.05$ . Before charcoal peak identification, CHARs were interpolated to 15-yr time steps (e.g. Long et al. 1998), based on the mean sampling resolution at all sites (see Results), to account for variable sampling intervals. After this interpolation, we re-interpolated records to their original sampling intervals so changes in sampling intervals are visible in graphical displays.

We used a universal threshold criterion to identify charcoal peaks that we interpreted as evidence of “local” fire occurrence (e.g. Clark 1990). Consistent with recent literature (e.g. Clark 1990, Whitlock and Millspaugh 1996, Gavin et al. 2003,

Lynch et al. 2004a), we use “local” to refer to distances within approximately 500-1000 m of each lake, corresponding to an area of c. 100-300 ha (1-3 km<sup>2</sup>). Low-frequency (i.e. “background”) variations in CHARs,  $C_{background}$ , are assumed to reflect changing rates of charcoal production, secondary transport, sediment mixing, and/or sediment sampling (Long et al. 1998; Chapter 1). We subtracted  $C_{background}$  from raw charcoal series,  $C_{raw}$ , to obtain a residual “peak” series,  $C_{peak}$  (i.e.  $C_{peak} = C_{raw} - C_{background}$ ; Carcaillet et al. 2001a, Lynch et al. 2002, Gavin et al. 2006).<sup>3</sup> For each record, we selected a threshold value  $t$  that identifies charcoal peaks when  $C_{peak} > t$ .

Our threshold criterion assumes that fires create charcoal peaks that exceed  $C_{peak}$  variations related to sediment mixing, sediment sampling, and analytical noise. Thus we consider that the distribution of  $C_{peak}$  values contains two sub-populations,  $C_{noise}$  and  $C_{fire}$  (see Clark et al. 1996).  $C_{noise}$  is a normally distributed population centered at 0 (i.e.  $C_{background}$ );  $C_{fire}$  samples are the high CHARs caused by local fires (e.g. Clark et al. 1998, Ohlson and Tryterud 2000, Lynch et al. 2004a, Gavin et al. 2006) and consist of positive  $C_{peak}$  values exceeding the variation in  $C_{noise}$ . We modeled  $C_{noise}$  by estimating the variance in  $C_{peak}$  around the mean of 0, assuming that  $C_{peak} \leq 0$  captured the variation in the  $C_{noise}$  population<sup>4</sup>. Because the threshold separating these two populations should occur in the upper range of the  $C_{noise}$  population, we considered threshold values corresponding to the 95<sup>th</sup>, 99<sup>th</sup>, and 99.9<sup>th</sup> percentile of the  $C_{noise}$  population to identify  $C_{fire}$ . We evaluate results from all three thresholds but discuss results from the 99<sup>th</sup>-percentile criterion.

### Detecting difference in fire regimes

The visual patterns of charcoal peaks at each site indicated that changes in fire frequencies were primarily related to boundaries between pollen zones. We thus used the

---

<sup>3</sup> We estimated low-frequency trends with a locally-weighted regression robust to outliers using a 500-yr window (Cleveland 1979). For each site, we evaluated the impacts of smoothing windows by plotting the number of peaks identified as a function of a range of threshold value and smoothing windows of 100, 200...1000 years. In all cases the number of peaks identified with any given threshold was relatively insensitive to changes in smoothing windows > 300 years.

<sup>4</sup> Specifically, the variance of  $C_{noise}$  is estimated by calculating the variance of a population containing all  $C_{peak}$  values  $\leq 0$  and the absolute value of all  $C_{peak}$  values  $< 0$  (thus a symmetric population centered on 0).

distribution of FRIs within each pollen zone to characterize the frequency component of the fire regimes of each vegetation type. If a pollen zone had = 5 FRIs (= 6 fires), distributions were described using the mean FRI (mFRI) and a two-parameter Weibull model fit to FRIs using maximum likelihood techniques (in Matlab, The Mathworks Inc.; Clark 1989, Johnson and Gutsell 1994)<sup>5</sup>. Goodness-of-fit of each Weibull model was tested with a one-sample K-S test (Zar 1999) and Weibull models are not reported unless  $p > 0.10$  (i.e. there is > 10% chance that the empirical distribution is not different from the Weibull model; Johnson and Gutsell 1994). 95% confidence intervals for Weibull parameters and mFRIs were estimated based on 1000 boot-strap samples from each distribution. Using a likelihood-ratio test based on estimates of the Weibull  $b$  and  $c$  parameters (Thoman and Bain 1969, Johnson and Gutsell 1994; Appendix D), we tested two null hypotheses: (1) fire frequencies did not differ through time (i.e. between pollen zones of a given site), and (2) fire regimes did not differ across space (i.e. between sites for a given pollen zone). By utilizing both parameters of the Weibull distribution, this test provides a more powerful method for detecting difference in FRI distributions than possible by interpreting confidence intervals around mFRI and estimated Weibull parameters (e.g. Clark 1990, Lynch et al. 2002) or by using the non-parametric K-S test (e.g. Clark et al. 1996, Lynch et al. 2002, Gavin et al. 2006).

## RESULTS

### Chronologies and Sedimentation Rates

The RP and XI records start at 13.5 and 14.5 k ybp, respectively, while CO and WK records start c. 8 k ybp (Fig. 3.2). At all lakes, age models for the past 8 k yr are well constrained and generally pass through the 95% confidence interval of <sup>14</sup>C or <sup>210</sup>Pb dates (Fig. 3.2). At RP we rejected two <sup>14</sup>C dates on concentrated pollen at 19.02 and 29.5 cm because they are c. 500-1000 yr older than sediment ages defined by five other <sup>14</sup>C dates on charcoal between 10 and 60 cm (Fig. 3.2; Table 3.3). Age models = 8 k ybp are less

---

<sup>5</sup> The two-parameter Weibull distribution has a scale parameter,  $b$  (yr), and a shape parameter,  $c$  (unitless), and its probability density function, describing the probability of obtaining a given fire return interval,  $x$ , is defined as:  $f(x|b,c) = (cx^{c-1}/b^c)\exp(-[x/b]^c)$  (Johnson and Gutsell 1994).

well constrained by  $^{14}\text{C}$  dates, and predicted ages do not always intersect the uncertainty of sample ages (e.g. RP; Fig. 3.2).

Sedimentation rates at RP, XI, CO, and WK average (stdev.) 0.040 (0.023), 0.025 (0.016), 0.017 (0.003), and 0.019 (0.001)  $\text{cm yr}^{-1}$  (Fig. 3.2). While sedimentation rates vary little throughout the CO and WK records, they are higher prior to c. 8.0 and 11.0 k ybp at RP and XI, respectively (Fig. 3.2). The temporal resolution of charcoal samples ranges from  $< 5$  to  $> 50$  yrs  $\text{sample}^{-1}$  (Fig. 3.2), varying with sampling intervals and sedimentation rates (Fig. 3.2). The extremely slow sedimentation rates at XI from 5.5-0 k ybp preclude analysis of charcoal peaks during this period. The average (stdev.) time represented by charcoal samples at RP, XI, CO, and WK is 13 (6), 32 (24), 16 (4), 14 (5) yr, respectively. At RP, temporal resolution changes from c. 25 to 10 yr  $\text{sample}^{-1}$  at 2.2 k ybp because sampling intervals changes from 0.5 to 0.25 cm (Fig. 3.2). At XI, the mean (standard deviation) time represented by samples used for charcoal peak analysis (i.e. prior to 5.5 k ybp) is 26 (15) yr.

## **Pollen, Stomata, and Charcoal Records**

### 1. Herb Tundra Zone: 14.0-13.3 (RP), 15.5-14.3 (XI) k ybp

The Herb Tundra Zone is characterized by the dominance of Cyperaceae ( $>25\%$ ), Salix (c. 25%), Poaceae (c. 15%), and Artemisia (c. 10%) pollen, with relatively high percentages of Pediastrum algal cell nets ( $> 25\%$ ) (Fig. 3.3 a-b). SCDs are lowest for comparisons with modern tundra (c. 0.2), but the probability-of-analog ( $< 20\%$ ) indicates little similarity (Fig 3 a-b). CHARs are low at both RP and XI (medians = 0 pieces  $\text{cm}^{-2} \text{yr}^{-1}$ ; Fig. 3.4), and the lack of charcoal peaks in this zone precludes the analysis of FRIs (Fig. 3.5, 3.6).

### 2. Shrub Tundra Zone, 13.3-10.3 (RP), 14.3-10.3 (XI) k ybp

Increased *Betula* pollen (*B. glandulosa* and/or *B. nana*; Anderson and Brubaker, 1994) to  $> 60\%$  marks the transition from herb to shrub tundra (Fig. 3.3 a-b). SCDs (c.

0.2) continue to indicate a low similarity between fossil and modern pollen assemblages from all modern biomes (probability of analog < 20%; Fig. 3.3 a-b). The magnitude and variability in CHARs increase at the onset of this zone (medians = 0.02-0.05 pieces cm<sup>-2</sup> yr<sup>-1</sup>), with charcoal peaks exceeding 0.2 pieces cm<sup>-2</sup> yr<sup>-1</sup>, and CHAR distributions at both RP and XI are distinct from those in the Herb Tundra Zone ( $p \ll 0.01$ ; Fig. 3.4, 3.5). Fire regimes at RP and XI are characterized by mFRIs (95% CI) of 133 (99-171) and 139 (113-171) yrs, respectively (Fig. 3.6), with no difference in FRI distributions between sites (Table 3.4; Fig. 3.6).

### 3. Deciduous Woodland Zone, 10.3-8.8 (RP), 10.3-8.0 (XI) k ybp

This zone is characterized by increased *Populus* pollen percentages (10-20%) at RP and XI, and an increase in monolete (>10%, not plotted), *Lycopodium annotinum* (c. 10%, not plotted), and *Sphagnum* (> 5%; Fig. 3.3 a-b) spores at RP. Spore percentages also increase at XI, but remain below 5% of the pollen sum (not plotted). SCDs in this zone are the highest for the entire record at both sites (> 0.3), and no analogs are found within modern North America pollen spectra (probability of analog < 0.2; Fig. 3.3 a-b). CHARs at RP and XI decrease (medians = 0-0.01 pieces cm<sup>-2</sup> yr<sup>-1</sup>) and distributions are distinct from the Shrub Tundra Zone ( $p < 0.01$ ; Fig. 3.4). FRI distributions could not be characterized due to the lack of identified charcoal peaks, with only three fires inferred at RP and 1 at XI (Fig. 3.5, 3.6).

### 4. Forest-tundra Zone, 8.5-5.3 (RP), 8.0-5.5 (XI), 7.5-5.5 (CO), 8.0-5.5 (WK) k ybp

Decreases in *Populus* (< 10%) and increases in *Picea* ( $\geq 1\%$ ) pollen percentages mark the onset of the Forest-tundra Zone (Fig. 3.3 a-b). *Alnus* pollen percentages increase from trace amounts to > 50% at 7.50 and 7.25 k ybp (RP and XI, respectively). *Sphagnum* spore percentages increase to 15-20% at RP, but remain below 5% at XI (Fig. 3.3 a-b). Other spore types show little change until the addition of *Alnus* pollen, when all spore types decrease to < 10-15% at RP and  $\ll 5\%$  at XI (Fig. 3.3 a-b). The WK and CO records start during or shortly after the increase in *Alnus* pollen (WK and CO,

respectively; Fig. 3.3 c-d). Coincident with the rise in *Alnus* pollen, SCDs for comparisons with modern Boreal Forest and Forest Tundra decrease ( $< 0.1$ ), and probability-of-analog values for these biomes increase to  $> 30-40\%$  (Fig. 3.3). Previous interpretations of *Picea* pollen morphology from RP indicate the presence of *P. glauca* rather than *P. mariana* (Brubaker et al, 1983) during this zone.

CHARs at RP and XI are higher than in the Herb Tundra and Deciduous Woodland zones but lower than in the Shrub Tundra Zone (medians = 0-0.04 pieces  $\text{cm}^{-2} \text{yr}^{-1}$ ; Fig. 3.4). Charcoal peaks exceed 0.1 pieces  $\text{cm}^{-2} \text{yr}^{-1}$  and peak frequencies increase ( $\geq 2$  per 1000 yr; Fig. 3.5). Peaks at CO and WK also exceed 0.1 pieces  $\text{cm}^{-2} \text{yr}^{-1}$ , although CHARs at CO are notably lower than at other sites (Fig. 3.4). mFRIs (95% CI) for RP, XI, and WK are 330 (194-478), 353 (252-431), and 240 (146-333) yr, respectively, and FRI distributions do not differ among these sites (Table 3.4; Fig. 3.6). Comparisons with CO are not possible due to the small number of identifiable peaks (Fig. 3.5, 3.6). Inferences for CO are sensitive to the threshold criterion, and the lower (95<sup>th</sup> percentile) threshold yields mFRIs of 544 (350-774) yr, with 95% CIs overlapping those from RP and XI but not WK (Table 3.5, Fig. 3.6). Between-zone comparisons at RP and XI indicate that FRI distributions are distinct (longer) than those in the Shrub Tundra Zone (Table 3.4; Fig. 3.6). The distribution of FRIs at WK are distinct (longer) from Shrub Tundra regimes at XI, but not RP (although  $p = 0.09$  for this WK-RP comparison; Table 3.4; Fig. 3.6).

#### 5. Boreal Forest Zone, 5.2 k ybp - present (RP), 5.5 k ybp - present (XI, CO, WK)

*Picea* pollen percentages increase to  $> 10\%$  at all sites between 6 and 4 k ybp, and *Sphagnum* spore percentages increase throughout this zone to  $> 5-10\%$  (Fig. 3.3). Although the increase in *Picea* pollen is subtle at some sites (e.g. CO; Fig. 3.3 c), all sites show a sharp increase in the probability-of-analog with the modern Boreal Forest biome ( $> 75\%$ ) and lower probabilities for modern Forest-tundra ( $< c. 70\%$ ; Fig. 3.3 a, c-d). The first presence of *Picea* stomata c. 5.2 k (RP) and 5.4 k (WK) ybp also coincides with the

transition from Forest-tundra to Boreal Forest inferred from the modern analog analysis (Fig. 3.3 a, d).

CHARs and charcoal peak frequencies increase to their highest levels in all records (median CHARs = 0.05-0.11 pieces cm<sup>-2</sup> yr<sup>-1</sup>; Fig. 3.4-3.5), although the period of increase varies by c. 500 to 1000 yr (CO, WK vs. RP; Fig. 3.5). Charcoal peak analysis is not possible at XI, due to the low temporal resolution of samples (Fig. 3.3 b). mFRIs (95% CI) at RP, CO, and WK are 168 (133-208), 150 (125-175), and 151 (120-183) yr, respectively (Fig. 3.6), and FRI distributions do not differ among sites (Table 3.4). FRI distributions generally do not differ from the Shrub Tundra (all sites) but are distinct (shorter) from Forest-tundra (except at WK; Table 3.4; Fig. 3.6).

### **Charcoal Peak Identification and Sensitivity to Threshold Criteria**

The AD 1991 (-41 ybp) fire that burned to the edge of RP is represented by a peak starting at -20 ybp, and the AD 1913 (37 ybp) fire that burned within at least 4 km of RP is represented by a peak at 42 ybp. The most recent peaks identified peaks at CO (90 ybp) and WK (21 ybp) both occur before fire were documented starting in AD 1950 (0 ybp); thus the fires that burned to c. 1, 3, and 5 km from these lakes were undetected. Although not identified, the clear charcoal peak in the upper-most sediments of XI, starting c. 0 ybp with an apex c. -20 ybp does not correspond to any fires within 1 km; it may represent an unrecorded fire before AD 1950 (0 ybp), an unrecorded fire after 1950 (Kasischke et al. 2002), the 34,424 ha fire that burned south of XI in AD 1957 (-7 ybp), or the 5000 ha fire that burned to 10 km W of XI in AD 1959 (-9 ybp).

The sensitivity of charcoal peak identification to different threshold criteria varies between sites and between zones (Fig. 3.5). At XI and WK, for example, charcoal peak identification is generally robust to all three threshold criteria (Fig. 3.5). In contrast, peak identification at CO is sensitive to the threshold criterion selected (Fig. 3.5). Sensitivity at all sites is generally higher during periods with low CHARs (Fig. 3.5). Characterizations of the FRI distributions, however, are generally robust to all three threshold criteria at all sites (Table 3.5). For example, in the eight FRI distributions characterized with multiple

thresholds, the 95% CIs on the Weibull  $b$  parameter and mFRIs overlapped by at least 15 years between the lowest and highest threshold criteria (Table 3.5).

## DISCUSSION

### Limitations of the paleoecological records

Three limitations related to chronological control and charcoal peak identification restrict inferences about vegetation and fire history from our pollen and charcoal records. First, chronologies are poorly constrained prior to c. 9-10 k ybp, and different age-depth models affect the inferred timing of vegetation transitions during early portions of the record. Given that our sites span 120 km, we assume that regional climatic changes controlling major vegetation shifts were contemporaneous at all sites. Thus we interpret differences in the timing of vegetation-zone boundaries among sites (e.g. c. 1000 years for the onset of the Shrub Tundra Zone at Ruppert and Xindi Lakes) to represent chronological uncertainties rather than time-transgressive events. These temporal uncertainties prior to c. 9-10 k ybp also constrain our comparisons to paleoclimatic data (e.g. Anderson et al. 2003) to millennial time scales.

Second, chronological constraints affect CHAR records because of their dependence on sedimentation rates. When we considered multiple age-depth scenarios at Ruppert and Xindi Lakes prior to c. 10 k ybp, CHARs and inferred fire frequencies were sensitive within the Shrub Tundra Zone. However, no age-depth scenario eliminated the differences in CHAR distributions or inferred fire-frequency regimes among Herb Tundra, Shrub Tundra, and Deciduous Woodland zones.

Third, charcoal peak identification is sensitive to the threshold criteria considered, which affects inferences about past fire regimes. Inferences at short time intervals (e.g. < 500 yrs) differ because a given threshold did or did not identify some individual peaks (Fig. 3.5), implying that any single threshold fails to detect every fire that occurred and/or incorrectly identifies fires when they did not occur (i.e. false negative and false positives; as in Higuera et al. 2005b). The detection of the most recent fire at Ruppert Lake and the absence of charcoal peaks from recent fires > 1 km away at Code and Wild Tussock

lakes, however, indicate that these records detected only local fires over the past c. 50 years. In contrast to peak detection, the characterizations of FRI distributions at the millennial time-scales of pollen zones were generally robust to the threshold criteria. This gives us confidence that our reconstructions using the middle-ground criterion (99<sup>th</sup> percentile) reasonably reflect the fire regimes within past vegetation zones.

### **Refinements to previous vegetation interpretations**

Our pollen records are generally consistent with previous interpretations of vegetation history in the central Brooks Range region (Anderson and Brubaker 1994), but they refine current understanding in two ways. First, our records suggest pollen zones are 1-2 k yr younger than inferred in earlier studies. These age differences likely occur because we interpret AMS dates from terrestrial macrofossils compared to radiometric dates on bulk sediment in earlier studies. AMS dates on terrestrial macrofossils are thought to provide both more precise and accurate dates than radiocarbon dates on bulk aquatic and terrestrial organic matter (e.g. 1000-2000 years; Oswald et al. 1999, Abbott et al. 2000). Second, though our SCD results are consistent with previous results (Anderson et al. 1989), the additional consideration of probability-of-analog estimates reinforce the no-analog nature of vegetation prior to the arrival of *Picea* and *Alnus*. They also identify the transition to modern boreal forest more distinctly than do SCD values alone.

### **Post-glacial fire regimes: temporal patterns and inferred controls**

#### Fire regimes in no-analog ecosystems: Herb Tundra, Shrub Tundra, and Deciduous Woodland zones

Although our records span only a brief period of late-glacial herb tundra, they suggest that fire was rare in this vegetation type. Both climatic and vegetational factors likely reduced the probability of fire in this period. Summer climate was both colder and drier than present (Table 3.1), with chironomid-based estimates suggesting that summer water temperatures were 4° C below present (Higuera et al. 2005a). Cold temperatures

imply limited opportunity for convection needed for lightning ignition. Interpretations of pollen spectra argue for an herb-dominated tundra that varied spatially between relatively productive lowland communities and discontinuous vegetation on upland sites (Anderson and Brubaker 1994, Anderson et al. 2003). A discontinuous vegetation cover would have limited fire spread if/when ignitions did occur. This scenario is similar to conditions influencing fire occurrence in modern high-arctic tundra, where the climate is cold and dry, net primary productivity is low, and vascular plant cover is discontinuous (Walker et al. 2005).

Fire became relatively common with the transition from herb to shrub tundra c. 13-14 k ybp (mFRI c. 140 years; Fig. 3.6). Fire in the shrub tundra was more common than in most modern Alaskan tundra (Kasischke et al. 2002) but similar to fire occurrence in Alaskan boreal forests (Kasischke et al. 2002, Lynch et al. 2002; this study), implying that both climatic and vegetational factors favored burning. Both the increase in temperature and drier-than-present conditions of past shrub tundra period (Table 3.1) would have favored ignition and fire spread. In addition, previous vegetation interpretations of this zone suggest a fuel type and density conducive to fire, with tall (> 3 m) *Betula glandulosa* shrubs forming extensive thickets across the landscape (Brubaker et al. 1983a, Anderson and Brubaker 1994, Anderson et al. 2003). The growth form, small stem diameters, and highly resinous twigs of *Betula glandulosa* (Dugle 1966) make it susceptible to fire on the modern landscape (de Groot and Wein 2004) and would have provided the flammable fuels necessary for fire spread when ignitions occurred during the Shrub Tundra Zone. Further, both experimental burning and warming stimulate the growth of *Betula glandulosa* (de Groot and Wein 1999), making short FRI possible due to rapid revegetation. Although the FRIs in the Shrub Tundra Zone were similar to those in the Boreal Forest Zone, the overall lower CHARs (Fig. 3.4) suggests less biomass burning per fire in the late-glacial shrub tundra compared to modern boreal forests. Inferring a modern system analogous in vegetation structure and fire regime to the late-glacial Shrub Tundra Zone is difficult, due to the novel vegetation assemblage and short FRIs. The most flammable modern tundra communities in Alaska are on the Seward Peninsula and along the lower reaches of the Noatak River drainage (Fig. 3.1), where

vegetation is dominated by both graminoid and shrub tundra (Walker et al. 2005) and estimated fire rotation periods (analogous to mFRI) are c. 150-350 yr (Noatak; Racine et al. 1985) and c. 275 (Seward; Kasischke et al. 2002).

Fire frequency decreased sharply with the development of a deciduous woodland c. 10.5 k ybp, implying that climatic and/or vegetational conditions inhibited burning. Given evidence that summers were  $> 2^{\circ}$  C warmer and 25-40% drier than present (Elias 2000, Kaufman et al. 2004; Table 3.1), climatic conditions should have been favorable for burning. We thus infer that the decline in fire occurrence was primarily influenced by vegetation. Specifically, the low flammability of deciduous trees in this period (both *Populus* and *Betula*; Edwards et al. 2005) would have reduced fire spread across the landscape, as *P. tremuloides* and other deciduous species do in the modern boreal forest (Johnson 1992, Cumming 2001, Hely et al. 2001). Thus, one scenario for reduced fire occurrence is that deciduous trees acted as fire breaks in an otherwise flammable landscape. While fires may have started at similar rates as in the Shrub Tundra Zone, the widespread occurrence of deciduous stands could have reduced fire spread and overall area burned. On the other hand, some climatic interpretations, based primarily on the presence of *Populus* (e.g. Anderson and Brubaker 1993), infer moist conditions during the early Holocene, suggesting an alternative scenario that both climatic and vegetational variables lowered the probability of fire.

#### Fire regimes in Forest-tundra and Boreal Forest zones

Fires became somewhat more common with establishment of *P. glauca* within shrub tundra in the mid-Holocene (mFRI c. 250-350 years; Fig. 3.5-3.6). The single charcoal peak at Code Lake (based on the 99<sup>th</sup> percentile threshold) is inconsistent with records from the other lakes, which show several charcoal peaks. The lack of peaks at Code Lake may represent undetected fires (i.e. false negatives) or the chance absence of fires near this lake. Our interpretation of fire occurrences during this period contrasts with those of Lynch et al. (2002), who inferred fire was unimportant at Dune Lake (Fig. 3.1). We suggest that methodological differences may explain this contrast, as sediment

samples in the Lynch et al. study during the Forest-tundra Zone were 1/5 those in this study (1 vs. 5 cm<sup>3</sup>). Pollen assemblages in the Forest-tundra zone suggest a treeline-like vegetation, with *P. glauca* trees or stands dispersed within a landscape matrix of *Betula* and/or *Alnus* shrubs (Brubaker et al. 1983a, Anderson and Brubaker 1994). The lack of *Picea stomata* at the end of this zone and the similarity of fossil pollen assemblages to modern Forest-tundra (Fig. 3.3 a, d) is also evidence for treeline-like vegetation (Carlson 2003). Climatic conditions within this zone were characterized by cooling summer temperatures, but remaining warmer than present, and increasing moisture (Table 3.1). Neither climatic trend is consistent with an increase in fire compared to the previous period. Thus we suggest that the most likely cause for increased burning in the Forest-tundra Zone was the replacement of deciduous with coniferous trees, which increased the overall flammability of the landscape. The change to cooler and moister climatic conditions between the Deciduous Woodland and Forest-tundra zones may explain why fire frequencies did not return to levels similar to those in the Shrub Tundra Zone. Overall, the infrequent, but persistent, occurrence of fire in the Forest-tundra zone is consistent with the wide range of estimated fire rotation periods in modern forest-tundra (180-1000+ yr; Payette et al. 1989, Kasischke et al. 2002).

The development of *P. mariana*-dominated forests 5-5.5 k ybp was accompanied by an increase in fire frequency (Fig. 3.5), with mFRIs (151-174 years; Fig. 3.6) broadly consistent with estimated fire rotation period in our study region (i.e. 175 yr in the Kobuk Ridges and Valley Ecoregion; Kasischke et al. 2002). The increased CHARs in this period (Fig. 3.4) likely reflect increased fuel loads associated with the dominance of *P. mariana*, which is well known for its dense fine fuels (Viereck 1973). Several lines of evidence indicate that climate continued to cool in the late Holocene, and effective moisture increased to near-modern levels by c. 5 k ybp (Table 3.1). Since these climatic changes are not conducive to ignition or fire spread, the increased fire occurrence in the late Holocene was likely due to the addition of *P. mariana* and the development of a more flammable landscape. Our interpretations are consistent with inferences from several other Holocene sediment records from boreal Alaska (Dune, Low, Moose and Chokosna lakes, Fig. 3.1; Lynch et al. 2002, Lynch et al. 2004b, Hu et al. 2006), and with

modeling studies that simulate increased fire frequencies with increased *P. mariana* (Rupp et al. 2002). Fire frequencies varied slightly within the Boreal Forest Zone (Fig. 3.5, Chapter 3), but these changes are minor compared to differences between zones.

### **Direct and indirect impacts of climatic change on fire regimes**

Late glacial and Holocene fire regimes across the study area changed with millennial-scale vegetation shifts. While climate likely caused these major vegetation shifts (Anderson and Brubaker 1993, 1994, Anderson et al. 2003), the fire-regime changes are difficult to reconcile with direct effects of climate on fire. For example, inferences of cooler, wetter climate in the mid to late Holocene (Boreal Forest Zone) are inconsistent with the increased fire frequencies during this period. Similarly, the decrease in fire in the early Holocene (Deciduous Woodland Zone) is inconsistent with inferences of warmer-than-present climatic conditions. However, the inferred changes in vegetation flammability associated with these vegetation transitions are consistent with observed fire-regime shifts. Thus we suggest that changes in flammability associated with different vegetation were likely more important in determining past fire regimes than the direct impacts of millennial-scale climatic change.

Other studies have inferred that vegetation characteristics have modified the impact of Holocene climatic change on fire regimes. For example, Lynch et al. (2002, Lynch et al. 2004b) also found increases in charcoal accumulation and inferred fire frequencies with the development of the boreal forest and a cooling and moistening of the climate in the mid- to late-Holocene in interior Alaska. In addition, a shift from coniferous to deciduous vegetation during the early Holocene at Devil's Bathtub in upper New York State, associated with rising temperatures and moisture (Shuman et al. 2004), was associated with decreased fire frequencies (Clark et al. 1996). Both studies inferred that climatically-induced changes in vegetation altered the flammability of the landscape in ways that were more influential than the direct impacts of climate on fire regimes.

These examples stand in contrast to an extensive body of literature documenting direct effects of climate on fire occurrence at a variety of temporal scales. In the eastern

boreal forest of North America, Carcaillet et al. (2001a) inferred that climate rather than vegetation was the primary control of fire regimes since the mid Holocene. In their study, changes in fire frequencies were not associated with vegetation changes in coniferous species. In subalpine forests in the Rocky Mountains, fire frequencies changed over the past 16 k years within a single vegetation type, presumably in response to changes in relative moisture (Millspaugh et al. 2000). On the modern landscape, area burned in boreal forest is well correlated with a variety of climatic variables at sub- and inter-annual time scales, including growing season temperature and precipitation (Kasischke et al. 2002) and synoptic-scale atmospheric circulation patterns (Hess et al. 2001, Duffy et al. 2005).

Differences between the above studies and our findings are likely related to the nature of changing flammability associated with past vegetation shifts. For example, in the Carcaillet et al. (2001a) study, the impacts of climate led to changes in conifer species (*Picea*, *Pinus*, *Thuja* / *Juniperus*) assemblages that apparently did not affect vegetation flammability enough to modify the direct influence of climate on fire regimes. On the other hand, if climatic changes cause vegetation shifts that greatly impact the flammability and/or continuity of fuels, vegetation may play a larger role than climate in controlling fire regimes. Our Alaskan records for the Deciduous Woodland and Boreal Forest Zones suggest that when climate and vegetation shift in opposite direction with respect to their direct effects on the probability of fire, vegetation can mediate climate change in counter-intuitive ways. However, our records also show that climatic and vegetational change can have the same directional influence on the probability of fire. For example, climatic warming between the late glacial period (Herb Tundra) and early Holocene (Shrub Tundra) likely increased the probability of fire directly, by changing ignition rates, and indirectly, by the facilitating the development of the birch shrub tundra with more continuous and flammable fuels.

### **Implications for global change in arctic and subarctic ecosystems**

Our inferences about the interactive effects of climate and vegetation on fire regimes have two main implications for anticipating the responses of arctic and subarctic fire regimes to future climatic warming. First, climatic change will likely have both direct and indirect effects on future fire regimes, and climate-fire relationships operating at annual to multi-decadal time scales may not scale up to centennial and multi-centennial time scales. Specifically, at centennial and longer time scales, changes in the flammability of the dominant vegetation cover may be more important in determining fire regimes than direct climatic controls. Most modeling efforts predict that warmer temperatures will increase area burned within boreal forests which in turn will result in the replacement of conifer with deciduous forest types (Rupp et al. 2000a, Flannigan et al. 2005), with increases in deciduous forest > 500% in some scenarios (Calef et al. 2005). A recent experimental study also found that short FRIs favored the replacement of conifers with *Populus tremuloides* (Johnstone and Chapin 2006). The lack of fire under warmer-than-present climates of the early Holocene (i.e. Deciduous Woodland Zone) implies that a major shift to deciduous vegetation could create negative feedbacks with fire occurrence, via a shift to an overall less-flammable fuel type. The absence of conifers in the Deciduous Woodland Zone is a key difference between paleo and modern (and future) vegetation, eliminating a dominant successional trajectory from the early Holocene landscape (i.e. deciduous to conifer post-fire development). However, with distant conifer seed sources, deciduous stands can be maintained in modern boreal landscape by gap-phase replacement, making a negative feedback with fire possible (Cumming et al. 2000, Johnstone and Chapin 2006).

Second, the high fire frequencies in shrub tundra of the early Holocene provide important evidence of the potential for tundra fire regimes to radically differ from those on the modern landscape. Considering the predicted and ongoing increases in shrub growth, shrub density (Chapin et al. 1995, Silipaswan et al. 2001, Stow et al. 2004, Wahren et al. 2005), and temperatures (Serreze et al. 2000) across northern Alaska, our records suggest that fire could become more common in northern Alaskan shrub tussock tundra. Increased fire occurrence in tundra is particularly relevant, given the potential for

positive feedbacks with increasing atmospheric CO<sub>2</sub> concentrations and widespread concern over the fate of terrestrial carbon in tundra and other high-latitude ecosystems (Zimov et al. 1999, Chapin et al. 2000, Mack et al. 2004, Weintraub and Schimel 2005).

**Table 3.1.** Summary of late glacial and Holocene climatic and vegetational change in the study region.

Period	k ybp (cal.)	Temperature	Relative Moisture	Vegetation	
		relative to present	relative to present	vegetation type <sup>2,4</sup>	key taxa <sup>2,4</sup>
Late glacial	15 - 16			Herb Tundra	<i>Salix</i> , <i>Artemisia</i> , Cyperaceae, Poaceae
	14 - 15	much cooler <sup>4-6,8-9</sup>	much drier <sup>2,4,6</sup>		
	13 - 14			Shrub Tundra	<i>Betula</i> , <i>Salix</i> , Cyperaceae, Poaceae
	12 - 13				
	11 - 12	warmer <sup>2,4-6,8-9,12</sup>			
Early Holocene	10 - 11		drier <sup>1,6</sup> or moister <sup>2</sup> (?)	Deciduous Woodland <sup>7</sup>	<i>Betula</i> , <i>Salix</i> , <i>Populus</i> , Cyperaceae Poaceae
	9 - 10	much warmer <sup>2,4-6,12</sup>			
	8 - 9				
Mid Holocene	7 - 8	warmer <sup>2,4-6</sup>	drier than present, but moister than before <sup>1,3,6</sup>	Forest-tundra	<i>Picea glauca</i> , <i>Betula</i> , <i>Alnus</i> , Cyperaceae
	6 - 7				
	5 - 6				
	4 - 5				
Late Holocene	3 - 4			Boreal Forest	<i>Picea glauca</i> , <i>Picea mariana</i> , <i>Betula</i> , <i>Alnus</i>
	2 - 3	near present <sup>4-6,10-11</sup>	near present <sup>1,3,6</sup>		
	1 - 2				
	0 - 1				

<sup>1</sup>Abbott et al. (2000); <sup>2</sup>Anderson and Brubaker (1993); <sup>3</sup>Anderson et al. (2001); <sup>4</sup>Anderson et al. (2003);  
<sup>5</sup>Bartlein et al. (1991); <sup>6</sup>Edwards et al. (2001); <sup>7</sup>Edwards et al. (2001); <sup>8</sup>Elias (2000); <sup>9</sup>Elias (2001); <sup>10</sup>Ellis  
and Calkin (1984); <sup>11</sup>Evison et al. (1998); <sup>12</sup>Kaufman et al. (2004).

**Table 3.2.** Lake locations, characteristics, and record quality.

Lake Name (unofficial)	N Latitude	W Longitude	Elevation (m asl)	Surface Area (ha)	Depth at Corring Site (m)	Mean sample resolution +/-stdev. (yr sample <sup>-1</sup> )	Age of record (k ybp)
Ruppert	67°04'16"	154°14'45"	230	3	7.0	13 ± 6	14,000
Xindi	67°06'42"	152°29'30"	240	7	10.6	32† ± 24	15,500
Code	67°09'29"	151°51'40"	250	2	7.0	16 ± 4	7500
Wild Tussock	67°07'40"	151°22'55"	290	15	11.6	14 ± 5	8000

† mean (stdev.) for section of core used for charocal peak identification was 26 (15) yrs.

**Table 3.3.** AMS  $^{14}\text{C}$  and calibrated dates from Ruppert, Xindi, Code, and Wild Tussock lakes.

Sample depth (cm)	Material Dated	Laboratory ID <sup>1</sup>	$^{14}\text{C}$ date <sup>2</sup> (yr BP)	Calibrated date <sup>3</sup>	95% CI
<b>Ruppert Lake</b>					
16.60 - 17.60	concentrated charcoal	CAMS 106161	600 ± 100	594	475 - 743
19.02 - 19.98	concentrated <i>Picea</i> pollen	CAMS 104482	1620 ± 40	1507	1400 - 1598*
26.48 - 27.20	concentrated charcoal	CAMS 110400	1170 ± 35	1088	1002 - 1190
29.5 - 30.5	concentrated <i>Picea</i> pollen	CAMS 100062	2445 ± 50	2520	2329 - 2677*
30.5 - 31.5	concentrated charcoal	CAMS 106160	1150 ± 60	1065	904 - 1175
41.17 - 42.13	concentrated charcoal	CAMS 111400	1505 ± 40	1388	1266 - 1461
45.98 - 46.71	concentrated charcoal	CAMS 110401	1740 ± 35	1648	1542 - 1739
57.78 - 58.75	con. charcoal & <i>Picea</i> needle	CAMS 111401	2185 ± 40	2210	2104 - 2352
78.5 - 79.5	concentrated charcoal	CAMS 110948	3000 ± 60	3185	3029 - 3379
86.5 - 87.0	concentrated charcoal	CAMS 111402	3145 ± 35	3369	3285 - 3466
99.0 - 100.0	concentrated <i>Picea</i> pollen	CAMS 100063	3860 ± 45	4281	4155 - 4429
100.0 - 101.0	con. charcoal & <i>Picea</i> needle	CAMS 110949	3770 ± 40	4137	4004 - 4275
115.2 - 115.6	concentrated charcoal	CAMS 110402	5050 ± 45	5812	5720 - 5952
160.5 - 161.0	concentrated charcoal	CAMS 110950	6350 ± 110	7266	7077 - 7556
206.5 - 207.5	concentrated charcoal	CAMS 113762	7460 ± 110	8256	8082 - 8478
298.0 - 300.5	con. charcoal & <i>Betula</i> leafs	CAMS 122361	8710 ± 40	9654	9446 - 9750
324.5 - 326.5	concentrated charcoal	CAMS 111403	10220 ± 160	11939	11159 - 12549
380.5 - 381.5	concentrated charcoal	CAMS 110951	10740 ± 80	12820	12610 - 13239
423.9 - 427.4	concentrated charcoal	CAMS 122362	10870 ± 80	12860	12749 - 12952
<b>Xindi Lake</b>					
10.5 - 12.0	concentrated charcoal	CAMS 113558	1240 ± 70	1159	1036 - 1323
24.0 - 25.5	concentrated charcoal	CAMS 116226	3490 ± 35	3956	3940 - 3963
31.0 - 32.0	concentrated <i>Picea</i> pollen	CAMS 105876	4930 ± 90	5679	5472 - 5877
32.0 - 33.0	concentrated charcoal	CAMS 112145	4560 ± 120	5208	4860 - 5527
43.0 - 43.5	concentrated charcoal	CAMS 113559	4760 ± 70	5493	5377 - 5656
51.0 - 52.0	concentrated charcoal	CAMS 116227	5960 ± 60	7153	7144 - 7156
85.5 - 87.5	wood macrofossil	CAMS 106159	9585 ± 40	10907	10685 - 11083
127.0 - 127.5	concentrated charcoal	CAMS 114331	10180 ± 120	11844	11332 - 12330
167.5 - 168.5	concentrated charcoal	CAMS 114332	11800 ± 120	13648	13391 - 13903
183.5 - 184.5	concentrated charcoal	CAMS 114333	11570 ± 300	13456	12833 - 13961
<b>Code Lake</b>					
8.50 - 9.00	concentrated charcoal	CAMS 116841	405 ± 40	534	513 - 537
31.00 - 31.50	concentrated charcoal	CAMS 114723	1295 ± 35	1235	1182 - 1325
49.00 - 49.50	concentrated charcoal	CAMS 114724	2275 ± 30	2305	2266 - 2443
59.25 - 60.00	concentrated charcoal	CAMS 116840	2805 ± 40	3154	3104 - 3167
86.25 - 87.00	wood macrofossil	CAMS 80792	4155 ± 40	4691	4560 - 4833
96.50 - 97.50	concentrated charcoal	CAMS 116839	4875 ± 35	5742	5630 - 5746
123.00 - 123.50	wood macrofossil	CAMS 80794	6555 ± 40	7462	7367 - 7552
<b>Wild Tussock Lake</b>					
31.00 - 31.25	concentrated charcoal	CAMS 112143	1895 ± 45	1845	1737 - 1955
53.25 - 53.75	concentrated charcoal	CAMS 113763	2880 ± 60	3012	2820 - 3167
69.25 - 70.75	concentrated charcoal	CAMS 122363	3360 ± 35	3601	3516 - 3714
116.00 - 116.50	concentrated charcoal	CAMS 112144	4920 ± 70	5671	5461 - 5831
111.75 - 113.75	concentrated charcoal	CAMS 116228	4590 ± 50	5578	5572 - 5580
132.75 - 133.50	concentrated charcoal	CAMS 116229	5660 ± 120	6991	6833 - 7013

<sup>1</sup>CAMS: Center for Accelerator Mass Spectrometry, Lawrence Livermore National Laboratory, Livermore, CA. <sup>2</sup> Conventional radiocarbon years before present (AD 1950). <sup>3</sup> Calibrated using CALIB 5.0 and the INTCAL04 calibration dataset (Reimer et al., 2004); weighted median of the probability distribution function with 95% confidence interval (Telford et al., 2004). \* Date not used in chronology; see Results for explanation.



**Table 3.5.** Sensitivity of FRI distributions to threshold criteria used for peak identification. For each zone, within each site, fire-history parameters are given for each of the three threshold criteria considered.

Lake Zone	Fire-history parameter (95% CI) and threshold criterion <sup>1</sup>								
	Weibull <i>b</i> parameter (yr)			Weibull <i>c</i> parameter (unitless)			mean fire return interval (yr)		
	0.95	<b>0.99</b>	0.999	0.95	<b>0.99</b>	0.999	0.95	<b>0.99</b>	0.999
<b>Ruppert Lake</b>									
Shrub Tundra	132 (109-155)	<b>149</b> <b>(110-193)</b>	196 (127-275)	2.63 (2.17-3.48)	<b>1.68</b> <b>(1.35-2.95)</b>	1.38 (1.13-2.22)	115 (97-136)	<b>133</b> <b>(99-171)</b>	177 (115-248)
Deciduous Woodland	-	-	-	-	-	-	284 (207-393)	<b>246</b> <b>(235-258)</b>	-
Forest-tundra	225 (154-324)	<b>365</b> <b>(215-529)</b>	492 (231-822)	1.29 (1.11-1.77)	<b>1.42</b> <b>(1.11-2.47)</b>	1.25 (1.01-2.72)	206 (138-290)	<b>330</b> <b>(194-478)</b>	457 (203-746)
Boreal Forest	177 (141-215)	<b>189</b> <b>(150-235)</b>	255 (195-312)	1.75 (1.50-2.46)	<b>1.68</b> <b>(1.40-2.33)</b>	1.99 (1.53-2.97)	157 (125-192)	<b>168</b> <b>(133-208)</b>	227 (175-279)
<b>Xindi Lake</b>									
Shrub Tundra	151 (121-186)	<b>157</b> <b>(127-192)</b>	157 (123-192)	1.89 (1.60-2.46)	<b>2.08</b> <b>(1.74-2.87)</b>	2.03 (1.67-2.80)	132 (106-162)	<b>139</b> <b>(113-171)</b>	139 (111-172)
Deciduous Woodland	-	-	-	-	-	-	416 (380-452)	-	-
Forest-tundra	372 (292-428)	<b>388</b> <b>(282-446)</b>	388 (291-446)	4.30 (2.61-13.22)	<b>4.36</b> <b>(2.25-25.53)</b>	4.36 (2.25-21.09)	338 (262-406)	<b>353</b> <b>(252-431)</b>	353 (261-431)
<b>Code Lake</b>									
Forest-tundra	-	-	-	-	-	-	544 (350-774)	-	-
Boreal Forest	154 (130-180)	<b>169</b> <b>(142-197)</b>	213 (153-286)	2.02 (1.72-2.79)	<b>2.10</b> <b>(1.75-2.87)</b>	1.33 (1.05-3.13)	135 (114-158)	<b>150</b> <b>(125-175)</b>	202 (137-296)
<b>Wild Tussock Lake</b>									
Forest-tundra	183 (133-241)	<b>269</b> <b>(158-370)</b>	344 (204-456)	1.82 (1.43-3.41)	<b>1.68</b> <b>(1.1-4.85)</b>	1.96 (1.10-5.99)	161 (115-214)	<b>240</b> <b>(146-333)</b>	308 (190-418)
Boreal Forest	166 (131-203)	<b>172</b> <b>(138-209)</b>	168 (139-201)	1.69 (1.42-2.45)	<b>1.73</b> <b>(1.45-2.77)</b>	1.96 (1.53-3.38)	146 (116-179)	<b>151</b> <b>(120-183)</b>	148 (123-178)

<sup>1</sup> Percentile of the  $C_{noise}$  distribution used to select the threshold value; see Methods for details.

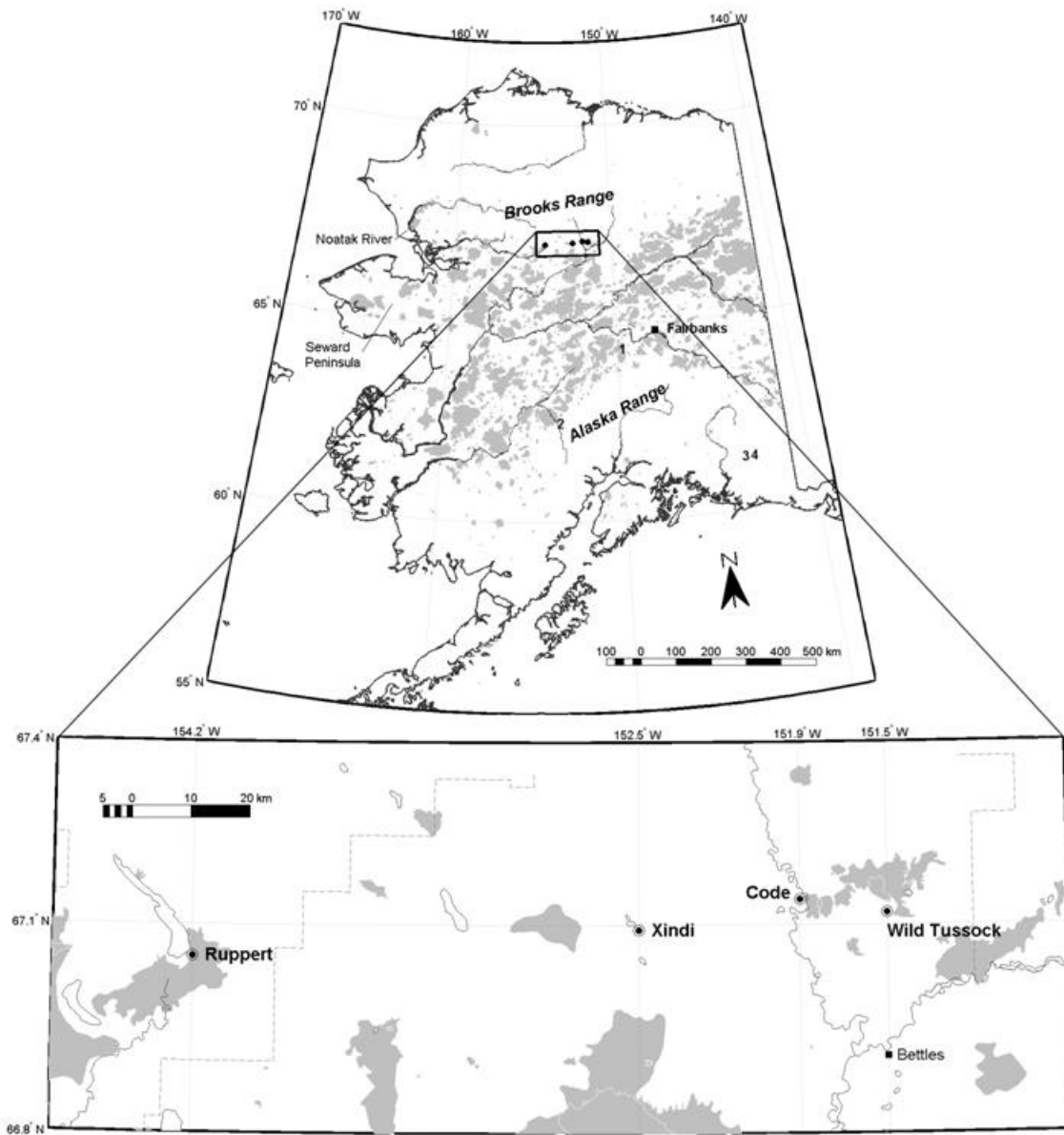


**Figure 3.1.** Location of lakes in this study and others discussed in the text (1, Dune Lake; 2, Low Lake; 3, Moose Lake; 4, Chokosna Lake). Grey polygons are areas that have burned within between AD 1950-2003 (Alaska Fire Service 2004), and the dashed line on the lower map is the southern border of Gates of the Arctic National Park. The black dots and larger circles identifying each lake on the bottom map are 2 and 4 km in diameter, representing the approximate spatial scale of each fire history record (i.e. 500-1000 m radius from lake).

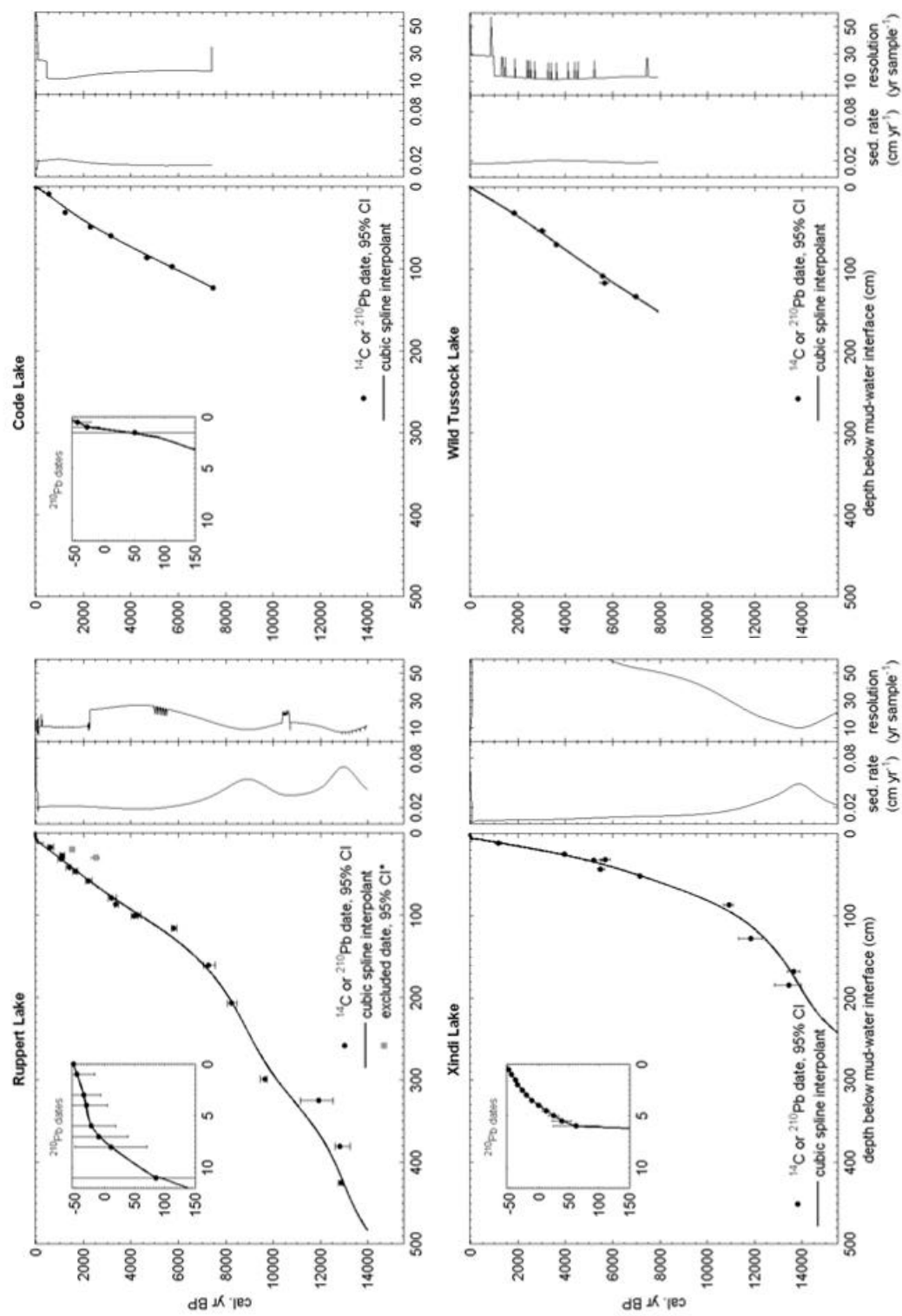


**Figure 3.2.** Age-depth models for each site with the resulting sedimentation rates and sample resolution. \*see Results for explanation.

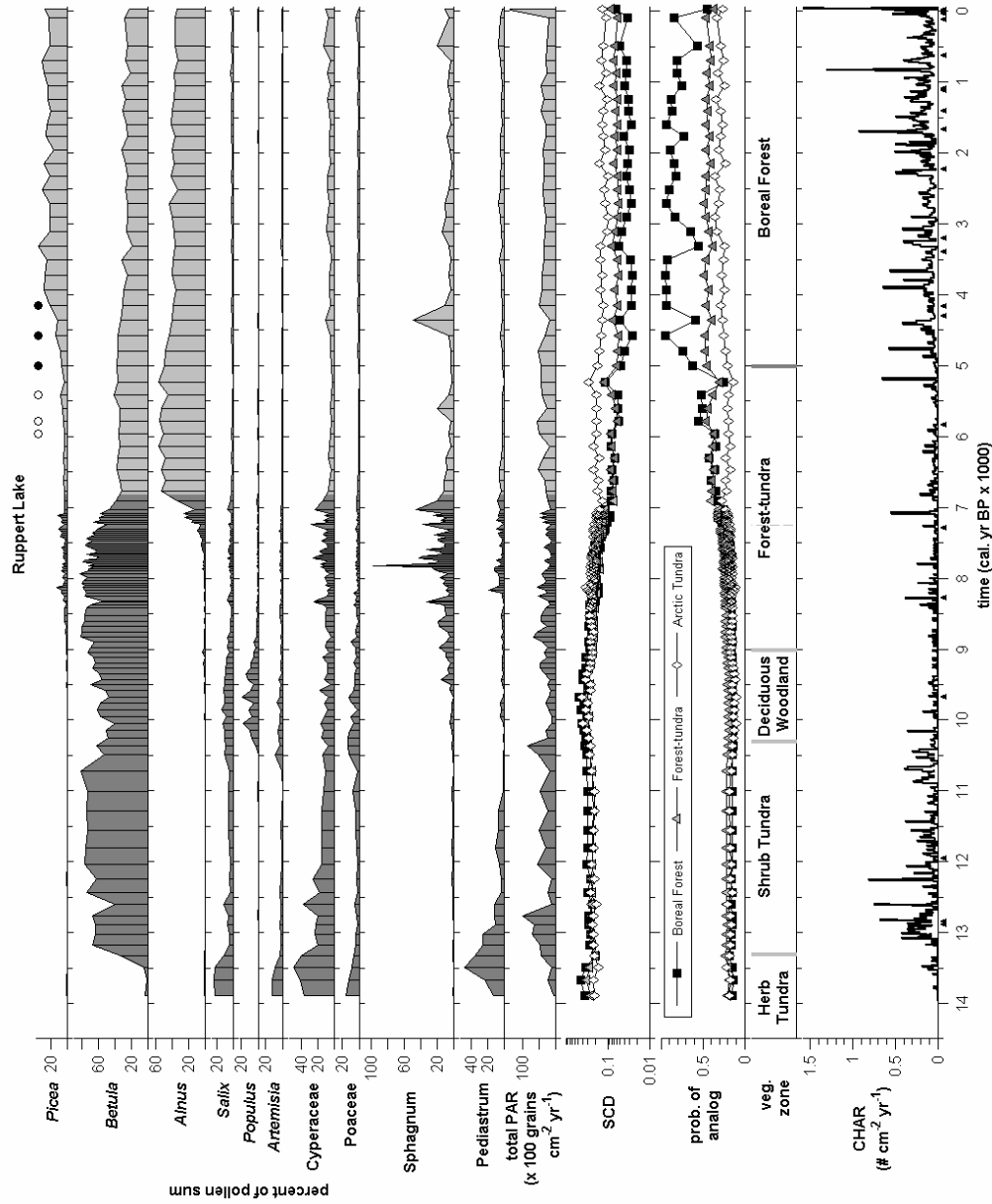


**Figure 3.3 (a).** Pollen percentages of selected taxa; total pollen accumulation rate (PAR); squared chord distance (SCD) and probability of analog values for comparisons between fossil samples and those from modern Boreal Forest, Forest-tundra, and Arctic Tundra; vegetation zones; and charcoal accumulation rate (CHAR) for Ruppert (a), Xindi (b), Code (c), and Wild Tussock (d) lakes. Filled (empty) circles on *Picea* panel for Ruppert and Wild Tussock represent *Picea* stomata presence (absence). Triangles below lower x axis represent the location of  $^{14}\text{C}$  or  $^{210}\text{Pb}$  dates.

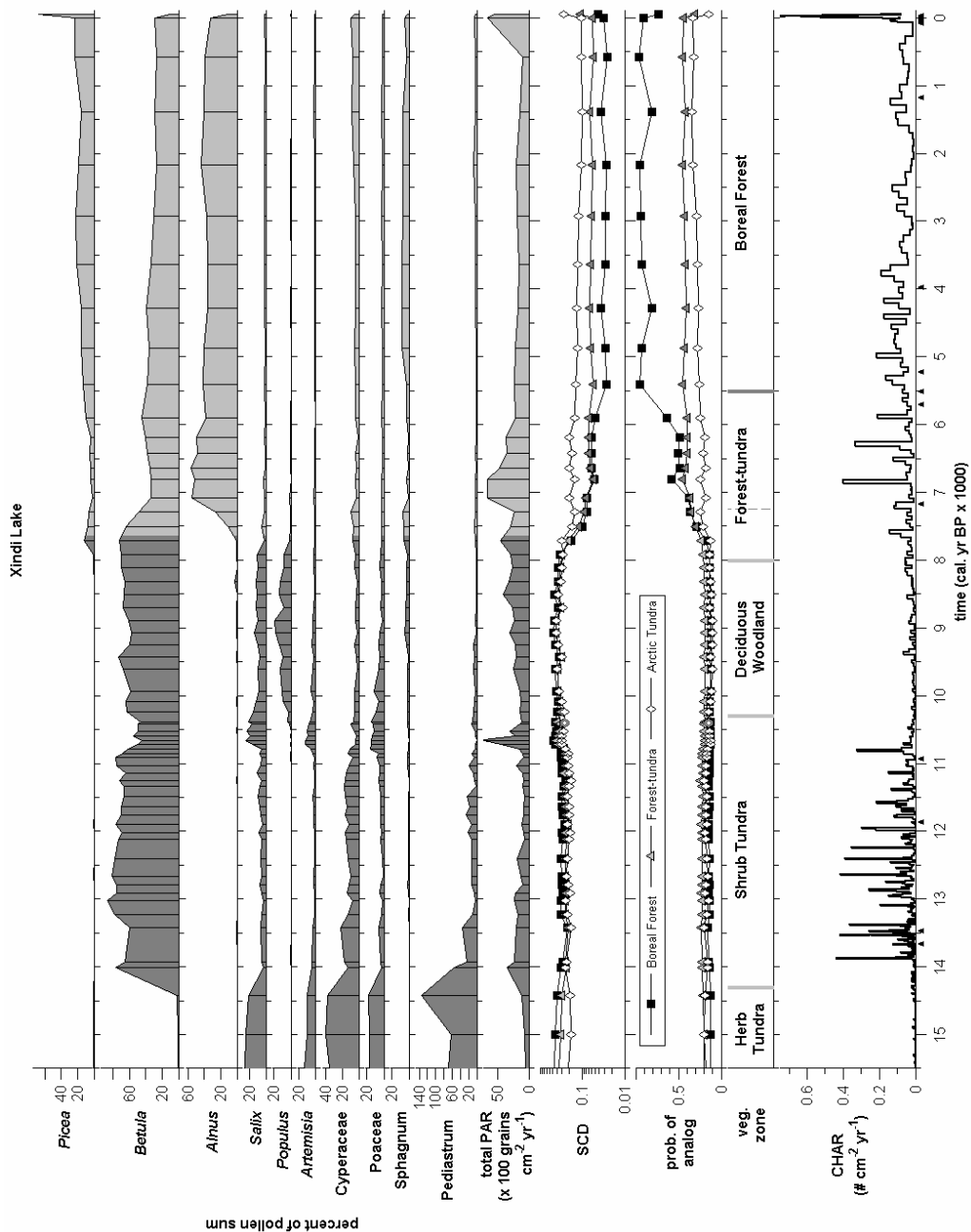


Figure 3.3 (b).

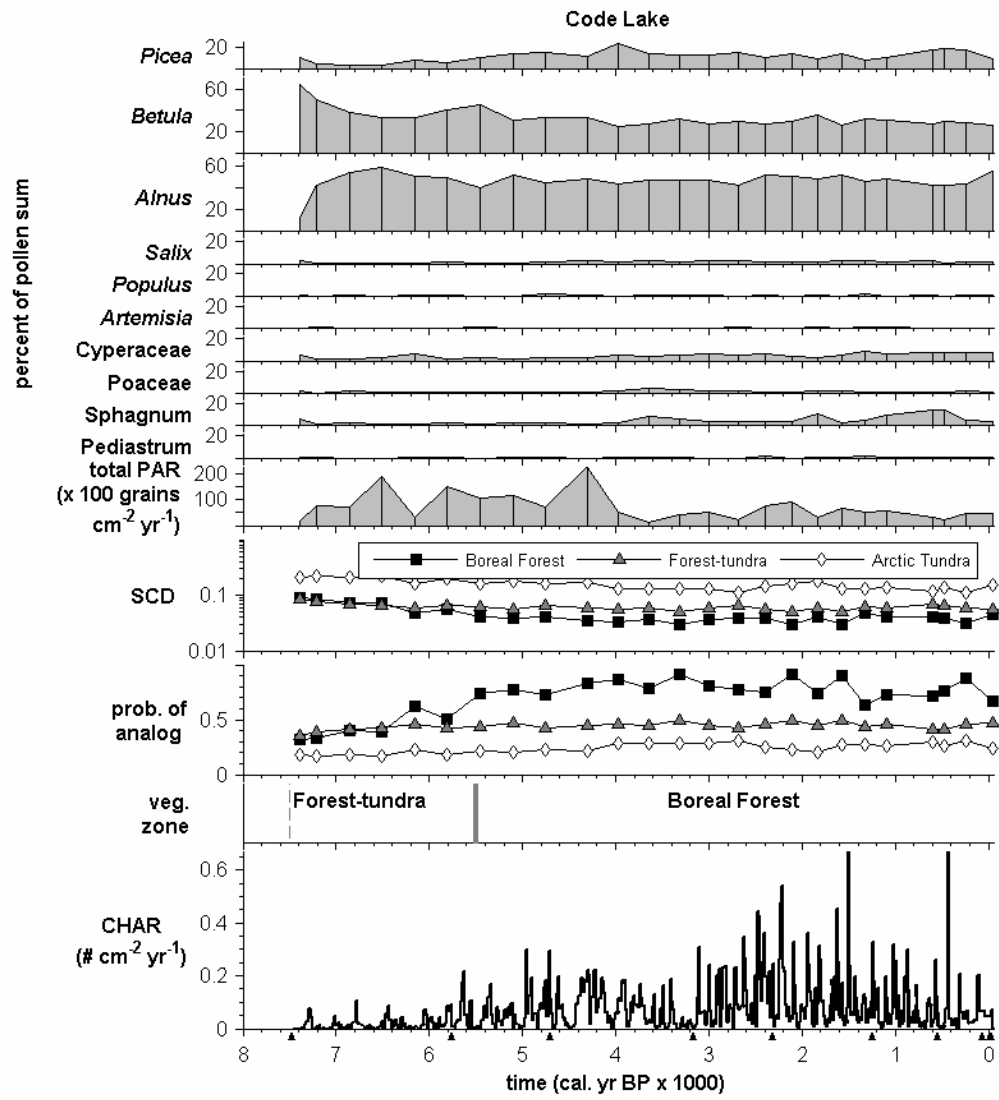


Figure 3.3 (c).

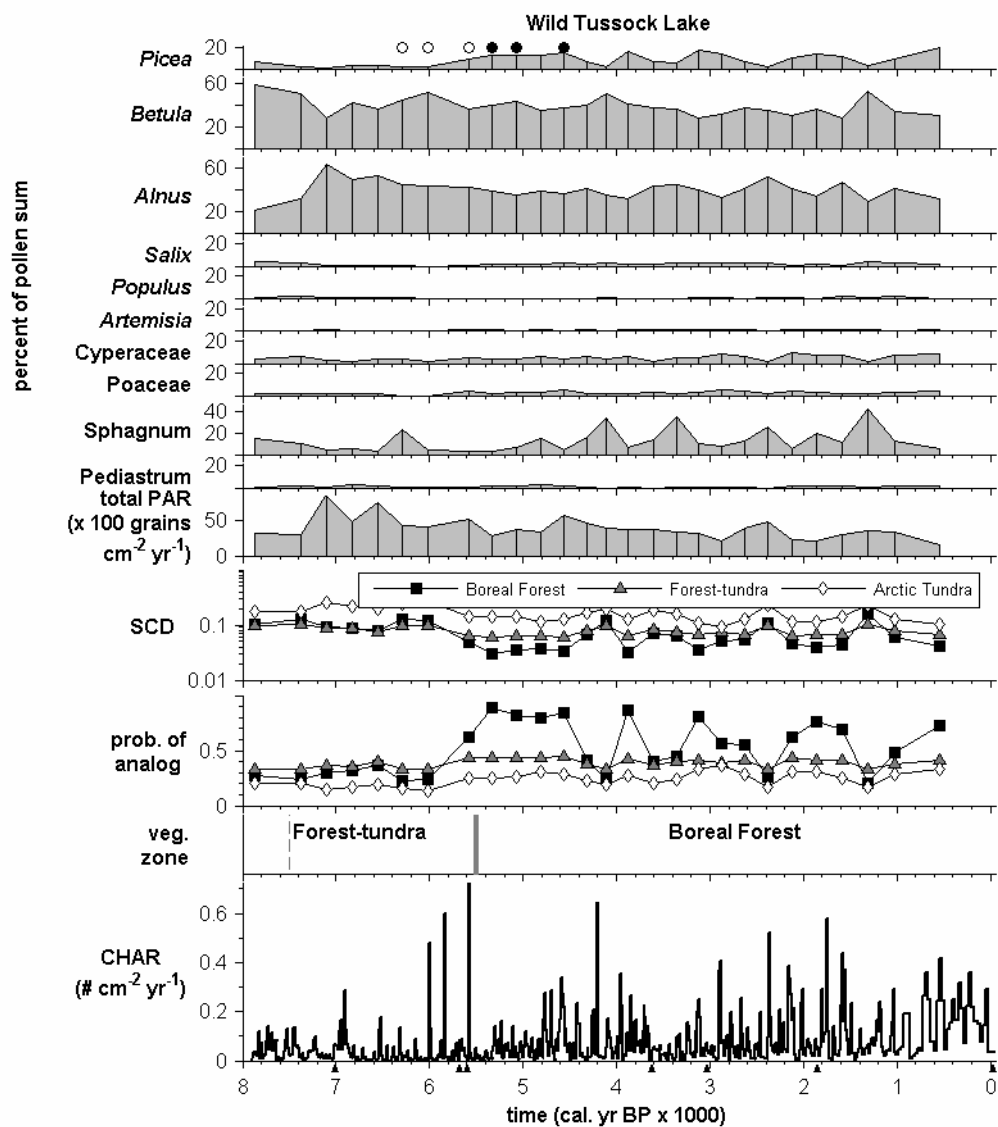
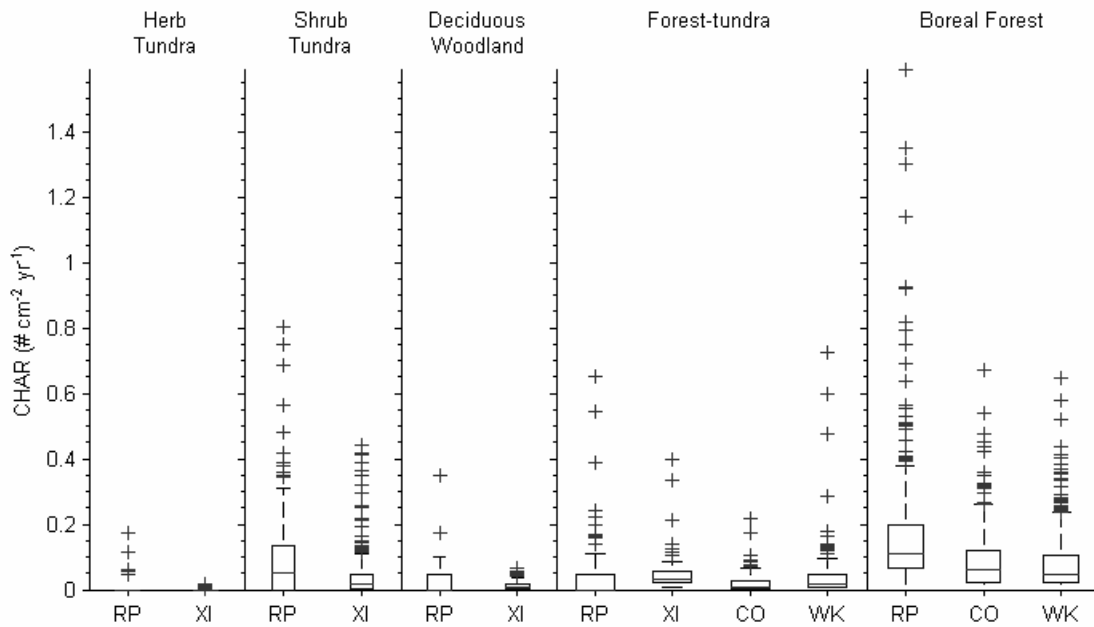
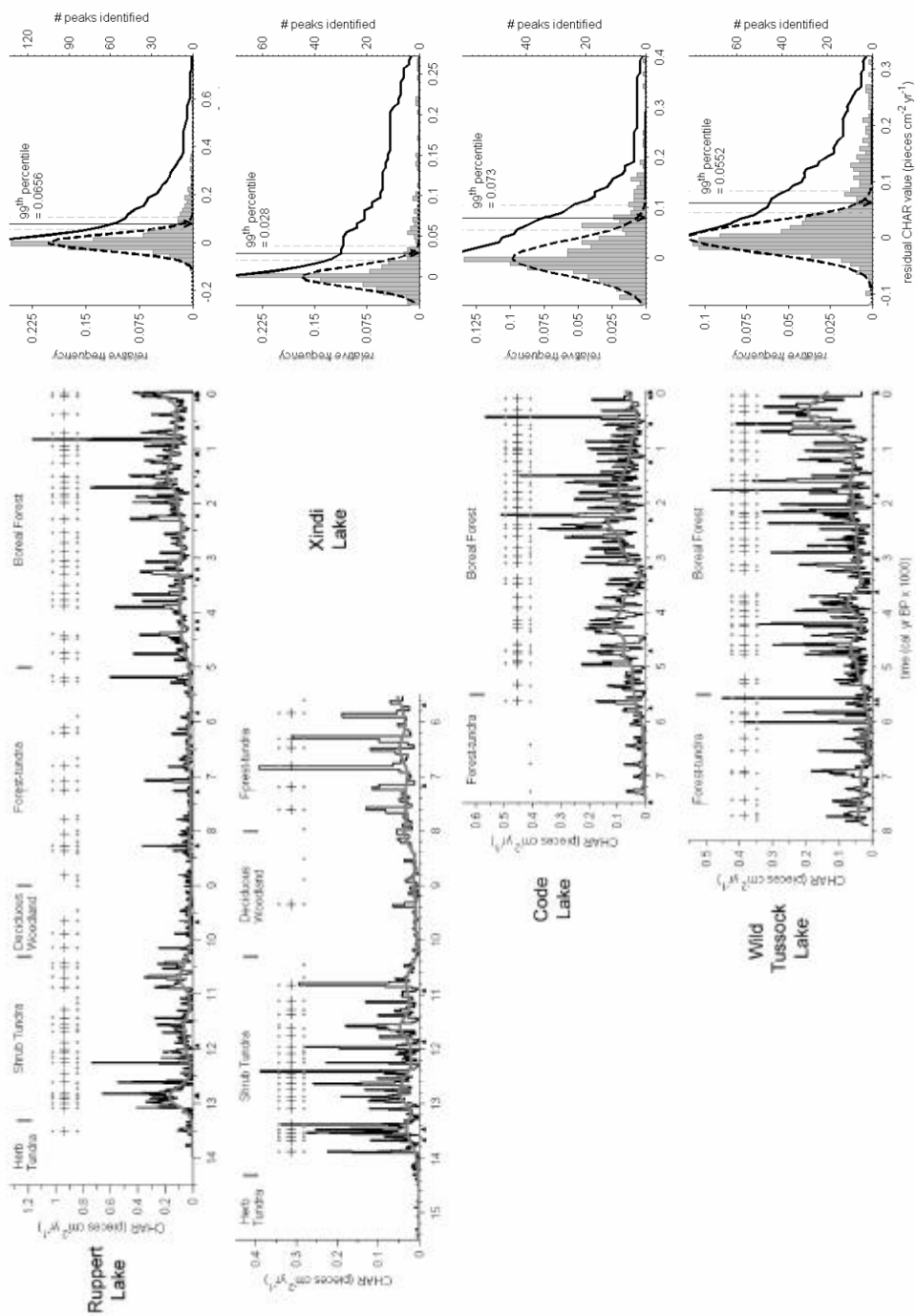


Figure 3.3 (d).



**Figure 3.4.** Distribution of raw CHARs at Ruppert (RP), Xindi (XI), Code (CO) and Wild Tussock (WK) lakes, within each vegetation zone. Boxes define the lower and upper quartile values, with a horizontal line at the median; “+” represents outliers.



**Figure 3.5.** Column 1: Interpolated CHAR records, low-frequency (500 yr) trends, and peaks identified with each threshold criterion (99th percentile criterion used for interpretation represented with '+') for each site (rows). Column 2: Histogram of  $C_{peak}$  values, modeled distribution of the  $C_{noise}$  component (normal curve, thick dashed line), the number of peaks identified as a function of threshold value (thick solid line), and the three threshold values considered (vertical lines; dashed, solid, dashed corresponds to the 95<sup>th</sup>, 99<sup>th</sup> and 99.9<sup>th</sup> percentile of the  $C_{noise}$  distribution, respectively).

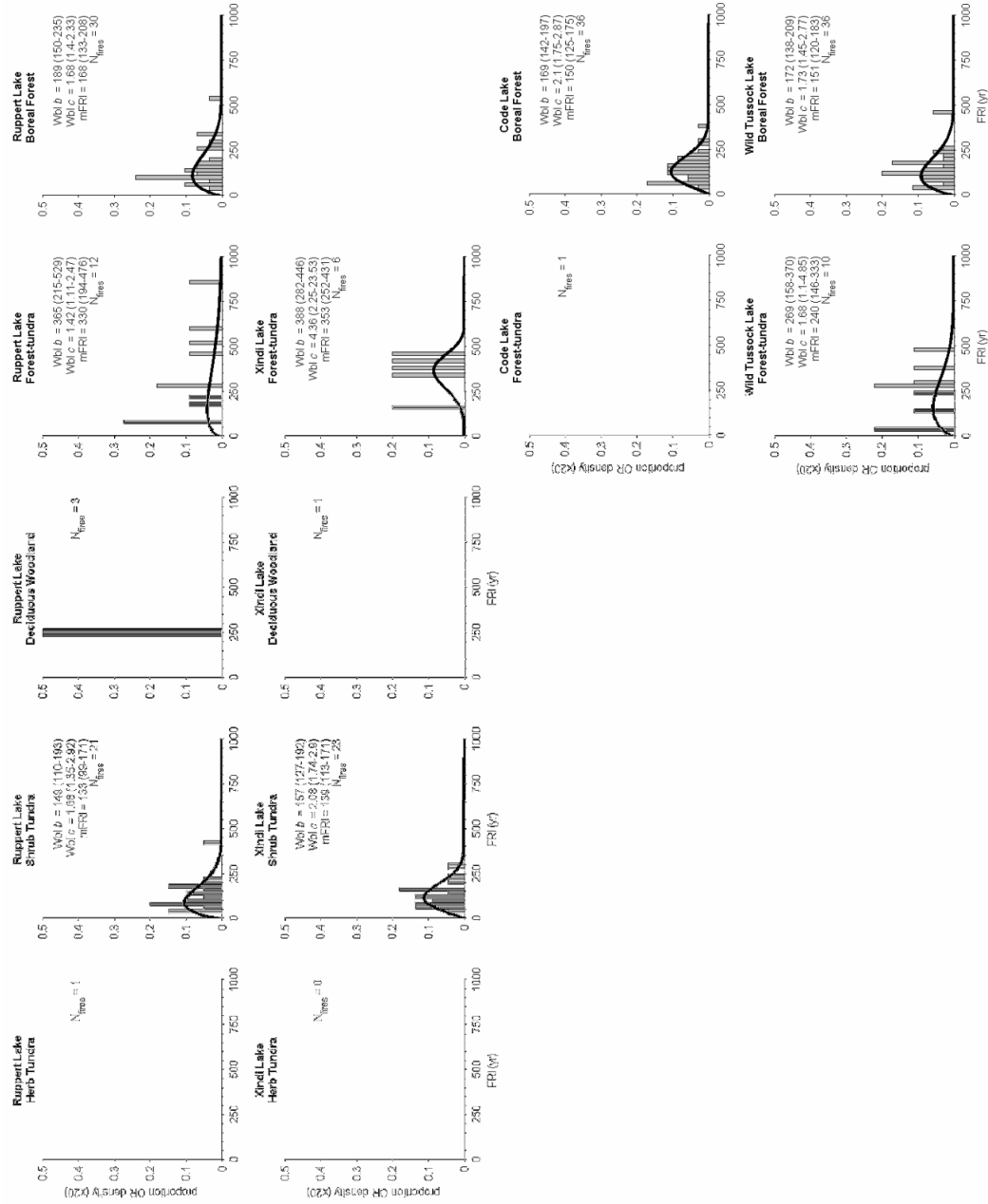


**Figure 3.6.** Distribution of FRIs, fitted Weibull models with  $b$  and  $c$  parameter estimates (95% CI), mFRIs (95% CI), and number of fires ( $N_{\text{fires}}$ ) identified within each vegetation zone (columns) at each site (rows).

#### **CHAPTER 4: IMPACTS OF CENTENNIAL AND MILLENNIAL-SCALE CLIMATIC CHANGE ON BOREAL FOREST FIRE REGIMES IN THE SOUTHCENTRAL BROOKS RANGE, ALASKA**

Philip E. Higuera<sup>1</sup>, Linda B. Brubaker<sup>1</sup>, Patricia M. Anderson<sup>2</sup>, Feng Sheng Hu<sup>3</sup>, and Ben C. Clegg<sup>3</sup>, Thomas Brown<sup>4</sup>

<sup>1</sup>College of Forest Resources, University of Washington, Seattle, WA

<sup>2</sup>Quaternary Research Center, University of Washington, Seattle, WA

<sup>3</sup>Department of Plant Biology, University of Illinois, Urbana, IL

<sup>4</sup>CAMS, Lawrence Livermore National Laboratory, Livermore, CA

#### **SUMMARY**

Lake sediments from the southcentral Brooks Range, Alaska, are used to infer the influence of climatic change on boreal forest fire regimes (defined by fire return intervals, FRIs). Macroscopic charcoal and fossil pollen provide estimates of FRIs and past vegetation at 3 sites since 5.5 k calendar years before present (AD 1950; ybp) and a fourth site since 2.2 k ybp. FRIs from each site, representing c. 1-3 km<sup>2</sup> (local scale), and from a composite record, representing the 150-km wide study area (landscape scale), are statistically compared between climatic zones, which in turn are inferred from an existing centennial-scale carbon- and oxygen-isotope record from the study area. In general, FRIs did not differ between climatic zones at the local scale. At the landscape scale, significantly different FRIs were distinguished between three climatic zones. The mean FRI (mFRI; 95% CI) was 173 yr (140-209) between 5.0 and 2.7 k ybp, when conditions were as dry or drier than present. The mFRI decreased to 127 yr (112-142) after 2.7 k ybp, even though climatic conditions were apparently moister, with no apparent change in vegetation. This pattern is consistent with previous studies from Alaska and Canada and suggests that moisture variability and the frequency of fire-conducive weather may have increased c. 2.7 k ybp due to a shift in atmospheric circulation in the North Pacific. FRIs were insensitive to a moisture increase c. 1.2 k ybp, but the mFRI increased by 50% to 190 (134-244) yr with the onset of the Little Ice Age cooling (400 ybp). The varying responses of fire regimes to late Holocene climatic change emphasize the need for a rigorous understanding of climatic and non-climatic variables to both infer past climatic conditions from fire records and anticipate future fire regimes.

## INTRODUCTION

Current and future warming across the boreal biome has motivated concerns over changing fire regimes, their impacts on ecosystems and society, and their potential feedbacks with the climate system (Serreze et al. 2000, IPCC 2001, AICI 2004, Hinzman et al. 2005). Climate influences the fire regimes<sup>6</sup> of boreal forests at a variety of spatial and temporal scales through its effects on fuels, moisture levels, ignition rates, and fire weather (Johnson 1992, Hess et al. 2001, Duffy et al. 2005, Hu et al. 2006). Across the North American boreal forest, fire is favored by warm, dry weather conditions (Flannigan and Harrington 1988, Larsen and MacDonald 1995, Larsen 1996, 1997, Flannigan et al. 2005), typically associated with persistent high-pressure systems that develop during summer months ("blocking highs"; Nash and Johnson 1996). The development of blocking highs, in turn, is linked to synoptic-scale circulation patterns that vary at inter-annual to decadal time scales (e.g. El Nino, Pacific Decadal Oscillation; Hess et al. 2001, Duffy et al. 2005). Modern records also reveal that fire regimes vary spatially across Alaskan boreal forests as a function of growing season temperatures, precipitation, and lighting-strike densities (Kasischke et al. 2002, Dissing and Verbyla 2003).

The impacts of climate on boreal fire regimes are less well understood at millennial time scales (Hu et al. 2006). Intuitively, one might think that long-term and short-term climatic variations should have similar effects, with increased temperatures, ignitions and/or decreased moisture leading to increased fire occurrence. However, millennial-scale records of fire history in boreal forests point to more complicated interactions between climatic variables, vegetation and fire. In southern Alaska and eastern Canada, for example, charcoal records from lake sediments indicate that fire frequencies increased during periods of increased moisture in the late Holocene (Carcaillet and Richard 2000, Carcaillet et al. 2001a, Lynch et al. 2004b). Interpretations

---

<sup>6</sup> In this paper we use the term "fire regime" to refer to the pattern of fire occurrence within an ecologically relevant spatial or temporal domain: e.g. within an Ecoregion (Kasischke et al. 2002), or within a specific climatic period. Across a region, fire occurrence can be measured by annual area burned ( $\text{ha yr}^{-1}$ ), and through time, fire occurrence can be measured by fire frequency ( $\text{fire yr}^{-1}$ ) or its inverse, fire return intervals ( $\text{yr fire}^{-1}$ ).

from both regions emphasize that increased seasonal to inter-annual climatic variability (including summer droughts and/or ignition rates) could have modified the direct effect of greater mean annual moisture on fire regimes. Furthermore, when climatic change affects vegetation assemblages it can result in counterintuitive changes in fire regimes by modifying landscape flammability (Rupp et al. 2002, Lynch et al. 2004b, Chapter 3).

The response of boreal fire regimes to climatic change at intermediate (multi-century) time scales is even less well understood. There are two main reasons for this poor understanding. First, few centennial-scale climatic records exist in boreal regions. Second, detecting multi-century changes in stand-replacing fire regimes is difficult based on a charcoal record at a single site, due to the limited number of fires that occur over these time periods and the high temporal variability in fire occurrence at local spatial scales (Hu et al. 2006). Obtaining an adequate sample size to characterize multi-century changes in fire regimes is a main methodological challenge to fire history studies in forests with long fire return intervals. As highlighted by Gavin et al. (2006), the solution to this problem requires a greater sampling density than typically employed in fire history studies using sediment charcoal records.

In this study, we use macroscopic charcoal in lake sediment cores to reconstruct boreal-forest fire histories at local and landscape spatial scales in northcentral Alaska (Fig. 4.1). We compare these fire histories to an oxygen- and carbon-isotope record of multi-century variations in effective moisture (the ratio of precipitation to evaporation) developed specifically for the study region from sediments of Takahula Lake (Fig. 4.1, Clegg and Hu, in prep.). Statistical comparisons of fire return intervals (FRIs) are used to test the null hypothesis that fire regimes did not change between periods of different effective moisture over the past 5.0 k years. Pollen assemblages from the same records provide a vegetational context for inferring the causes of past changes in fire regimes. The fire histories presented here represent the first opportunity to evaluate the impacts of multi-century to millennial climatic changes on boreal-forest fire regimes within the region.

## STUDY LAKES AND REGIONAL VEGETATION, FIRE, AND CLIMATE HISTORY

The four study lakes are located along a 150 km E-W transect near the southern border of Gates of the Arctic National Park, within the Kobuk Ridges and Valleys Ecoregion (Nowacki et al. 2001; Fig. 4.1). Current climate is continental, and vegetation is a mosaic of *Picea mariana* Mill. BSP., *P. glauca* (Moench) Voss., *Populus balsamifera* Mill., *P. tremuloides* Michx., *Betula papyrifera* Marsh. trees, and *Salix*, *B. glandulosa* Michx., and *Alnus* shrubs (climate and vegetation described in detail in Chapter 3). Fire is the primary disturbance agent, with an estimated fire rotation period for the ecoregion of 175 yr, based on observations from 1950-2001 (Kasischke et al. 2002; Fig. 4.1).

Sediment cores were collected from small (2-15 ha), relatively deep (7-15 m) basins to maximize the probability of obtaining undisturbed charcoal and pollen records (Jacobson and Bradshaw 1981, Larsen and MacDonald 1993; Table 4.1). The core from Last Chance Lake (LC, unofficial name; 67°04'45" N, 150°45'08" W; 250 m asl) comes from a 8.5 m deep, 7 ha sub-basin within the 34 ha lake; the characteristics of Ruppert (RP), Code (CO), and Wild Tussock (WK) lakes are described in Chapter 3. Each lake is surrounded by discontinuous *P. mariana* forest. Recent fires at RP, CO, and WK are described in Chapter 3. Fires at LC burned to 6 km west, 7 km east and 3 km west of the lake in 1997 (9750 ha), 1994 (2475 ha), and 1984 (742 ha), respectively (Alaska Fire Service 2004; Fig. 4.1).

The vegetation and fire history of this region has been described with sediment records covering the last 10-15 k yr (Anderson and Brubaker 1994; Chapter 3). Immediately prior to the development of boreal forest vegetation c. 5.5 k ybp (years before present, AD 1950), the region was covered by *Betula* and *Alnus* shrubs with scattered *P. glauca*. Fires were infrequent, with mean fire return intervals (mFRI) c. 250-350 years (Chapter 3). The arrival of *P. mariana* c. 5.0-5.5 k ybp marked the transition from forest-tundra to boreal forests similar to current forests of this region. mFRIs for the entire boreal forest period were c. 150-175 yr (Chapter 3).

To evaluate relationships between fire history and past climatic changes, we rely on a carbon- and oxygen-isotope record from Takahula Lake (c. 45 km northeast of

Ruppert Lake; Clegg and Hu in prep.; Fig. 4.1), supplemented by several temperature and moisture proxy records from Alaska (referred to below). The Takahula Lake record is divided into five periods suggesting different effective moisture and/or temperature regimes since 5.0 k ybp. The period 5.0-2.7 k ybp is inferred to have been as dry or drier than present, in agreement with interpretations of increased dune activity at the Great Kobuk Sand Dunes c. 250 km west of the study area (Mann et al. 2002). From c. 2.7-1.2 k ybp, the Takahula Lake record suggests considerably wetter conditions than present (Clegg and Hu in prep.) and dune activity decreased (Mann et al. 2002). Effective moisture reached modern levels at Takahula c. 1.2 k ybp. Temperatures in the study region since 5 k ybp are less well constrained, but glacial (Ellis and Calkin 1984, Evison et al. 1998) and oxygen isotopes from the Brooks Range (Anderson et al. 2001) suggest cooler temperatures than before with some periods possibly cooler than present. The isotope record from Takahula also shows evidence of a pronounced cold period 400-100 ybp (AD 1550-1850), which coincides with other evidence of a Little Ice Age (LIA) cooling (Clegg and Hu in prep.). For example, glaciers advanced or stabilized in the Brooks Range 800-390 ybp (AD 1410-1600; Ellis and Calkin 1984, Evison et al. 1998); tree-ring records near Ruppert Lake (Fig. 4.1) suggest c. 3-4 °C cooler spring-summer temperatures from at least 120 ybp to 70 ybp (AD 1830-1880) relative to present (Garfinkel and Brubaker 1980), and tree-ring records in the Brooks Range and across the Arctic suggest mean annual temperatures c. 1.5° C cooler than present over a similar period (D'Arrigo and Jacoby 1993). In addition, geochemical and isotope evidence from southcentral Alaska suggests that summers were c. 1.7° C cooler and likely moister than periods before and after 550-150 ybp (AD 1400-1800; Hu et al. 2001), and glacial records from the Alaskan coastal ranges indicate advances or stand stills c. 550-150 ybp (AD 1400-1800; e.g. Wiles et al. 1999, Calkin et al. 2001, Wiles et al. 2002). The fifth climatic zone (100 to -50 ybp) represents current conditions after the end of the LIA.

## METHODS AND RATIONALE

### Sediment Records

Sediment cores were sampled and analyzed for pollen and charcoal using methods described in Chapter 3. Briefly, cores were continuously sliced at 0.25-0.5 cm intervals and macroscopic charcoal from continuous subsamples (LC mean = 6 cm<sup>3</sup>) was counted at 10-40 x. Pollen was counted at 400-1000 x in 1 cm<sup>3</sup> subsamples from selected levels (LC terrestrial pollen sum  $\mu = 333$  grains,  $s = 28$ ). Sediment ages were estimated by interpolating between <sup>210</sup>Pb dates in the upper 10-20 cm and AMS <sup>14</sup>C dates on charcoal in deeper sediments (Table 4. 1) using a cubic smoothing spline (Fig. 4.2). The influence of each date on the age-depth relationship was inversely weighted by its 95% confidence interval, such that dates with larger errors had less influence on the age model (e.g. Telford et al. 2004b; Fig. 4.2). Sediment accumulation rates (cm yr<sup>-1</sup>) were used to convert pollen and charcoal concentration (# cm<sup>-3</sup>) to pollen and charcoal accumulation rate (PAR, grains cm<sup>-2</sup> yr<sup>-1</sup> and CHAR, pieces cm<sup>-2</sup> yr<sup>-1</sup>, respectively). The mean resolution of continuous samples from LC is 11 yr sample<sup>-1</sup> ( $s = 5$ ). Before charcoal peak identification CHARs were interpolated to 15-years time steps (e.g. Long et al. 1998), based on the mean sampling resolution at all sites (Chapter 3), to account for variable sampling intervals within and between sites.

The dominant vegetation near each lake was interpreted based on pollen percentages, stomata presence/absence, and modern analog analysis using squared-chord distances (SCD; Overpeck et al. 1985, Anderson et al. 1989) and receiver operating characteristic curves (ROC curves; Gavin et al. 2005) as described in Chapter 3. In the analog analyses, fossil pollen assemblages were compared to modern assemblages from North American Arctic Tundra, Boreal Forest, and Forest-tundra biomes (biomes described by Whitmore et al. 2005; see Chapter 3).

Charcoal records were analyzed using a decomposition approach to estimate local fire occurrence and fire return intervals (FRIs) as described in Chapter 3. Briefly, CHARs were smoothed with a locally-weighted regression robust to outliers using a 500-yr window (Cleveland 1979) and subtracted from the interpolated record to obtain a residual series,  $C_{peak}$ , with the 500-yr trend removed. A threshold was selected for the  $C_{peak}$  series

to identify charcoal peaks associated with “local” fire occurrence. Consistent with recent literature (e.g. Clark 1990, Whitlock and Millspaugh 1996, Gavin et al. 2003, Lynch et al. 2004a), “local” is defined as c. 500-1000 m of each lake, corresponding to an area of c. 100-300 ha (1-3 km<sup>2</sup>). Threshold selection assumes that residual CHAR series contain two sub-populations, a normally-distributed “noise” population,  $C_{noise}$ , caused by sediment mixing, sediment sampling, and analytical noise, and a population of high CHARs,  $C_{fire}$ , caused by local fire occurrence (see Clark et al. 1996, Gavin et al. 2006; Chapter 3). As in Chapter 3, we considered threshold values corresponding to the 95<sup>th</sup>, 99<sup>th</sup>, and 99.9<sup>th</sup> percentile of the estimated  $C_{noise}$  population to identify charcoal peaks but report results for the 99<sup>th</sup> criterion.

### **Statistical Treatment of Fire Return Intervals**

Fire history records were analyzed to test the null hypothesis that fire regimes, defined by distributions of FRIs, were insensitive to the climatic changes inferred from the Takahula Lake record. The analyses addressed two spatial scales: “local”, corresponding to the record of an individual site (c. 1-3 km<sup>2</sup>) and “landscape”, represented by a composite record including all sites (c. 4-12 km<sup>2</sup> from the c. 150 km<sup>2</sup> study area). Given the larger area represented by the composite as compared to the single site record(s), the composite record includes a larger number of FRIs per time period and enhances the ability to detect small or short-term changes in fire regimes. For example, consider fire regimes for two 900 year periods. If mFRIs change from 100 yr to 150 yr (a 50% increase) between periods, an average of 9 fires (900/100) would represent the first regime and an average of 6 fires (900/150) would represent the second. Detecting this change with > c. 30% power (i.e. probability of correctly rejecting the null hypothesis of no difference) requires at least 10 FRIs (Appendix D). The only way to increase the sample size of FRIs within a given time period is to sample more area by pooling FRIs from individual sites. Three steps were used to reach this goal: (1) partitioning FRIs at each site into different time periods (“zones”); (2) testing for between-site differences in fire regimes within each zone; and (3) testing for between-zone differences in fire regimes in individual and composite records (Fig. 4.3).

For the first step, we used both *a priori* and *a posteriori* methods (Fig. 4.3, box 1). *A priori* zones were based on the five climatic periods of the Takahula Lake record (Clegg and Hu in prep.), and *a posteriori* zones were based on the patterns observed in the FRI series. Since the timing of *a priori* and *a posteriori* zones was similar (c. 300 yr difference), only *a priori* zones are presented. FRIs in zones with  $\geq 5$  FRIs were described by a Weibull model fit by maximum likelihood techniques (e.g. Chapter 3; Clark 1989, Johnson and Gutsell 1994). The goodness of fit was evaluated with a one-sample Kolmogorov-Smirnov test (Zar 1999), and models are reported only if the probability of a Type I error,  $p$ , was  $> 0.10$  (i.e.  $> 10\%$  chance that the empirical distribution is not different from the Weibull model; Johnson and Gutsell 1994). For all zones, 95% confidence intervals for Weibull parameters and mFRIs were estimated from 1000 boot-strapped samples from each distribution.

The second step (Fig. 4.3, box 2) used a likelihood ratio test to compare FRI distributions between sites for each zone (Thoman and Bain 1969, Johnson and Gutsell 1994; Chapter 3). This test is more powerful than techniques previously used for this purpose (Appendix D). For each comparison, the null hypothesis of no difference was rejected when  $p \leq 0.05$ . If between-site comparisons for a given period showed no differences, then fire regimes were considered similar and FRIs were pooled to form a composite record (Johnson and Gutsell 1994). Forming a composite record assumes that each site represents an independent, random sample from the same fire regime. Samples here represent the fire regime surrounding small lakes, and although lakes were not selected randomly, selection was based on factors unrelated to fire occurrence (e.g. lake depth).

The final step tested for differences between zones in the individual and composite record(s) using the likelihood ratio test described above (Fig. 4.3, box 3). If FRI distributions were similar between adjacent zones, data from the two periods were merged into one zone and the analysis was repeated until only distinct zones were identified (Fig. 4.3).

## RESULTS

### Sediment Records

Sedimentation rates at LC are stable over the 2.2 k yr record (0.013-0.124 cm yr<sup>-1</sup>;  $\mu = 0.041$ ;  $s = 0.010$ ). The lowest two dates at 90 and 110 cm, both from wood macrofossils, are in reverse order (Table 4.1; Fig. 4.2), but the 90 cm date has a minor effect on the age model due to its large 95% CI (Fig. 4.2). Pollen assemblages at all sites are dominated by *Picea* (*P. glauca* and *P. mariana*; Brubaker et al. 1983a, Anderson and Brubaker 1994), *Betula*, and *Alnus*, and show minor long-term variations (Fig. 4.4). All assemblages have a high probability of analog with modern Boreal Forest (RP, CO, WK) and/or Forest-tundra (LC) (Fig. 4.4). At RP *Picea* pollen increases gradually from < 5% to > 20% 5.5 -4.0 k ybp, and stomata first occur c. 5.0 k ybp (Fig. 4.4 a). In contrast, CO and WK *Picea* pollen percentages are  $\geq 10\%$  by 5.5 ybp but rarely exceed 20%. *Picea* stomata are present at WK by c. 5.4 k ybp (Fig. 4.4). CHARs vary from < 0.1 to c. 0.6 pieces cm<sup>-2</sup> yr<sup>-1</sup> across sites, with three peaks exceeding this limit at RP (Fig. 4.4). Mean CHARs generally increase between 5.5 and 4.0 k ybp at RP, CO, and WK and fluctuate inconsistently thereafter (Chapter 3). At LC mean CHARs are relatively constant until an increase at c. 300 ybp (Fig. 4.5).

### Fire History

The intermediate threshold criterion identifies 21 charcoal peaks since 2.2 k ybp at LC, (Fig. 4.5) and 31, 36, and 35 peaks since 5.5 k ybp at RP, CO, and WK, respectively. Peak identification is relatively insensitive to threshold criteria at RP, WK, and LC, but varies somewhat with threshold at CO (see Chapter 3). The fire that burned to the edge of RP in AD 1991 (-41 ybp) is detected by a charcoal peak starting at -20 ybp. Recent fires that burned to c. 1, 3, 5 and 7 km of CO, WK, and LC are not detected in the charcoal record. The most recent peak at LC at -7 ybp does not correspond to a nearby fire and may represent an unrecorded small fire at that time (Kasischke et al. 2002).

Initial partitioning: Zone I (5.0 – 2.7), Zone II (2.7-1.2), Zone III (1.2-0.4), Zone IV (0.4-0.1) Zone V (0.1-0.0 k ybp)

Zone I-III FRI distributions were similar between sites ( $n = 5-15$ ,  $p > 0.10$ ), with the exception of CO and LC in Zone II ( $n = 11, 10$ ;  $p = 0.01$ ). Between-site comparisons were not possible in zones IV-V due to small sample sizes ( $< 5$  FRIs), and we assume these distributions were similar. Given the general absence of between-site differences, FRIs from all sites were pooled into a composite record for all zones. In the composite record, FRIs decreased between zones I and II ( $n = 43, 42$ ;  $p = 0.04$ ) and increased between zones III and IV ( $n = 23, 6$ ;  $p = 0.03$ ). In contrast, FRI distributions were similar between zones II and III ( $n = 43, 23$ ;  $p = 0.14$ ) and zones IV and V ( $n = 6, 5$   $p = 0.84$ ). Thus data for zones II-III and zones IV-V were combined and the analysis was repeated, starting at the site level for each of the three zones.

Final partitioning: Zone I (5.0 – 2.7), Zone II-III ( 2.7-0.4), Zone IV-V (0.4-0.0 k ybp)

At individual sites, mFRIs decrease from Zone I to Zone II-III (by 25, 20 and 15% for RP, CO, and WK, respectively) and increase from Zone II-III to Zone IV-V (by 70, 32, 26, and 66% for RP, CO, WK, and LC, respectively; Fig. 4.6). However, the only statistically significant shift is between zones I and II-III at CO ( $n = 15, 18$ ;  $p = 0.04$ ; Table 4.2; Fig. 4.6). Within Zone I and Zone II-III, FRIs distributions are similar between sites ( $n = 13-18$ ,  $p = 0.09-0.89$ ; Table 4.2, Fig. 4.6). Between-site comparisons were not possible from Zone IV-V due to small sample sizes ( $< 5$  FRIs), and again, we assume these distributions are similar. Given the similarity among sites, FRIs from each zone were pooled to form a composite record, resulting in 42, 65, and 11 FRIs in zones I, II-III, and IV-V, respectively (Fig. 4.7).

In the composite record, Zone I is characterized by a mFRI (95% CI) of 173 yr (140-209; Fig. 4.7). The Zone II-III FRI distribution differs from Zone I ( $n = 65, 43$ ;  $p < 0.01$ ), representing a 27% decrease (mFRI 127 yr [112-142]; Fig. 4.7). The Zone IV-V FRI distribution differs from Zone II-III ( $n = 11, 65$ ;  $p = 0.03$ ), with a 50% higher mFRI of 190 yr (134-244) yr (Fig. 4.7), but is similar to Zone I ( $n = 11, 43$ ;  $p = 0.52$ ).

## DISCUSSION

### **Fire regimes at local spatial scales**

The climatic changes documented at Takahula Lake had minor impacts on fire regimes which were generally undetectable at the local scale (Table 4.2; Fig. 4.6). Although all lake records showed the same directional changes in mFRI, these changes were small (< c. 25%) or persisted for short periods (< 1000 yr; Fig. 4.6). The relatively stable fire regimes documented since c. 5 k ybp contrast sharply with the distinct changes in fire regimes recorded at the same sites (RP, CO, and WK) during the late glacial period and early to mid-Holocene (c. 14-5 k ybp; Chapter 3). Climatic changes were much larger prior to 5 k ybp (e.g. Bartlein et al. 1991, Anderson et al. 2003) and influenced vegetation at broad spatial scales, resulting in measurable changes in the fire regimes at the scale of individual lakes (Chapter 3). The results of this study also contrast with charcoal records from sites in central Alaska (Dune and Low lakes; Fig. 4.1; Lynch et al. 2002, Hu et al. 2006) and eastern Canada (Carcaillet et al. 2001a), which show one or more distinct change(s) in fire regimes within the boreal forest vegetation zone. The differences with other sites imply that (1) local fire regimes in the study area were less sensitive to late Holocene climatic changes and/or (2) climatic changes in the study area were less extreme than in other regions. Overall, the results of this study add to an emerging pattern of spatial and temporal complexity in late-Holocene fire regimes between southern, central, and northcentral Alaska (Hu et al. 2006).

### **Fire regimes at landscape spatial scales**

The composite record of FRIs documents changes in fire regimes that were not detected at the individual site level. Fire regimes at this larger scale shifted twice, with mean FRIs decreasing at 2.7 k ybp with the transition to increased effective moisture, and increasing at 400 ybp with the transition to cooler Little Ice Age conditions.

### Fire regime shift at 2.7 k ybp

The 30% decrease in mFRI with the transition from dry to moist conditions 2.7 k ybp is unexpected given recent data showing greater area burned in dry than in wet summers in Alaska and Canada (Flannigan and Van Wagner 1991, Hess et al. 2001, Kasischke et al. 2002, Duffy et al. 2005, Flannigan et al. 2005). However, charcoal studies in southern Alaska and eastern Canada have also identified decreasing FRIs with increasing moisture in the late Holocene (Carcaillet and Richard 2000, Carcaillet et al. 2001a, Lynch et al. 2004b). This pattern is also consistent with the higher fire occurrence documented in tree-ring records from southern and eastern Canada during the cool, moist Little Ice Age (Bergeron and Archambault 1993, Weir et al. 2000). In general, the shift to shorter FRIs at 2.7 k ybp implies that the factors directly controlling past fire regimes were not reconstructed in the Takahula Lake record and/or non-climatic variables exerted strong influences over past fire regimes.

One possible explanation for shorter FRIs after 2.7 k ybp is that short-term climatic variations, not registered in the Takahula record, were the major controls of past fire ignition and spread (Carcaillet and Richard 2000, Carcaillet et al. 2001a, Lynch et al. 2004b). In eastern Canada, a network of paleofire and paleoclimatic records suggests that a late Holocene shift in the polar front led to increased winter precipitation but more frequent summer drought and thus to more frequent fire weather (Carcaillet and Richard 2000, Carcaillet et al. 2001a). Unfortunately, existing Alaskan climatic reconstructions have not addressed variability in seasonal moisture. A recent paleoclimatic record suggesting a weakening or western displacement of the Aleutian Low (AL) c. 2.7 k ybp (Anderson et al. 2005; Fig. 4.8) may help explain the decrease in mFRI after this time. First, weak ALs are currently associated with increased winter precipitation in interior Alaska (Mock et al. 1998), suggesting that at least some of the increased moisture after 2.7 k ybp came outside of the fire season (Fig. 4.8). Second, weak ALs are correlated with atmospheric and oceanic circulation patterns that increase the probability of fire in interior Alaska (Duffy et al. 2005). In particular, weak ALs are common during (1) the cool phase of the Pacific Decadal Oscillation (Trenberth and Hurrell 1994, Duffy et al. 2005), and (2) the positive phase of the East Pacific index (Barnston and Livezey 1987).

Both patterns favor meridional airflow and the development of blocking highs during the summer. Thus the correspondence of decreased FRIs with reconstructions of increased moisture at Tukuhula and a weakened AL in the North Pacific (Anderson et al. 2005; Fig. 4.8) is consistent with current evidence of annual to decadal climatic patterns influencing Alaskan fire regimes (Duffy et al. 2005). Although the degree to which modern data from Alaska (Duffy et al. 2005) apply to understanding millennial-scale fire-climate relationships is unclear, the combination of modern data and the reconstructed AL pattern suggest that atmospheric circulation affecting the development of blocking highs may have altered past fire regimes through impacts on fire weather.

An alternative explanation for decreased FRIs after 2.7 k ybp is that non-climatic factors, such as vegetational change, led to an overall increase in landscape flammability (e.g. Lynch et al. 2002, Rupp et al. 2002, Lynch et al. 2004b, Chapter 3). Because *P. mariana* has abundant fine fuels but occupies moist sites (Dyrness et al. 1986, Viereck et al. 1986), interpretations of Alaskan sediment records have recently argued that a shift to moister climate could indirectly result in higher fire frequencies (see summary by Hu et al. 2006; Chapter 3). Unfortunately, pollen data offer limited insights into this hypothesis. The slowly increasing *Picea* pollen percentages at Ruppert Lake 5.5-4.0 k ybp are consistent with the gradual development of *P. mariana* boreal forests, but neither Code nor Wild Tussock pollen records show this pattern (Fig. 4.4). While our stomata data and previous studies suggest that *P. mariana* was present near Ruppert Lake by 5.0 k ybp (Fig. 4.4; Brubaker et al. 1983a, Anderson and Brubaker 1994), there is little evidence for changes in the proportions of either species over the past 5.0 k (Brubaker et al. 1983a, Anderson and Brubaker 1994).

#### Inensitivity to the climatic shift at 1.2 k ybp

The decline in effective moisture c. 1.2 k ybp had no detectable impact on FRIs in the study area. This insensitivity may reflect the small magnitude of the climatic shift or the effect of complicated interactions among climatic variables. For example, drier conditions could have favored fire spread, but the overall probability of fire might not have

changed if ignition rates declined. This possibility is consistent with the hypothesis that a weaker AL increased the frequency of severe fire weather c. 2.7 k ybp. The AL reconstruction suggests that the strength of the AL increased c. 1.0 k ybp, with much greater variability from 1.0 k ybp to present compared to 3.0-1.0 k ybp (Anderson et al. 2005; Fig. 4.8). Following the same logic outlined above, this change could have led to a decrease in the frequency of severe fire weather, counteracting the impacts of lower effective moisture.

### Did the Little Ice Age (LIA) affect the fire regime?

The correspondence of a 50% increase in FRIs in the composite record with LIA cooling at Takahula Lake, and the correspondence of cool summers with reduced fire ignitions and spread in Alaska (Hess et al. 2001, Kasischke et al. 2002, Duffy et al. 2005) suggest that cool temperatures directly influenced fire regimes in the study area. LIA moisture conditions are unclear at Takahula Lake (Clegg and Hu in prep.), but evidence from southcentral Alaska suggests an increased moisture during the LIA (Hu et al. 2001). Increased FRIs under a moister climatic conditions are also consistent with a direct influence of climate on the fire regime (Kasischke et al. 2002). Although Clark (1989, 1990) detected decreased fire frequencies during the presumably cool/moist LIA in northwestern Minnesota, few other sediment-charcoal studies have found changes in fire-regime during the LIA (e.g. Gavin et al. 2003). The absence of LIA effects may reflect a general insensitivity of boreal fire regimes to short-term climatic oscillations, or the difficulty of detecting short-term changes with individual sediment-charcoal records.

### **Detecting short-term or subtle changes in fire regimes**

The ability of the composite record to distinguish fire regimes between climatic periods highlights the importance of pooling fire history data from multiple sites (Gavin et al. 2006). Due to the long return intervals and high temporal variability of fires in stand-replacing fire regimes, individual lake records can detect only relatively large or long-lasting changes in a fire occurrence (e.g. > 30-50% over millennial time scales), for

example those between major Holocene climatic periods (Chapter 3). Detecting sub-millennial changes in stand-replacing fire regimes will almost certainly require pooling data from several sites, an approach used in tree-ring (e.g. Johnson and Gutsell 1994) but not sediment-charcoal studies of fire history (but see Gavin et al. 2006). The compositing approach used here allows the statistical assessment of large numbers of FRIs but comes with several assumptions that are difficult to assess over short time periods and/or in the absence of independent climatic and vegetational records.

First, fire regimes are homogenous across sites and within time periods. At millennial time scales, this assumption can be tested using between-site comparisons and independent climate and vegetation records. However, this assumption is difficult or impossible to evaluate at short time periods because individual records document few FRIs. For example, in this study the limited number of fires since 400 ybp prevented statistical comparisons between sites (Fig. 4.6). Second, zone boundaries represent climatic changes that could affect fire regimes (Johnson and Gutsell 1994). Ideally zone boundaries are based on *a priori* hypotheses, for example that fire regimes changed with known climatic and/or vegetational shifts (Chapter 3). With *a posteriori* hypotheses, the probability of Type I error,  $p$ , in statistical comparisons should be adjusted accordingly. Within a 5000-yr record representing the same fire regime, one would expect one 250-yr period to yield a  $p$  of 0.05. In this case, interpreting this period as “statistically significant” is misleading. Finally, FRIs at each site are independent samples of the fire regime. If two sites are burned by the same fire(s), then pooling FRIs would artificially increase statistical power (i.e. pseudo-sampling). This assumption is particularly important when fire sizes are large, as in boreal forests. In this study, the timing of fire occurrence does not suggest that individual fires burned multiple sites (data not shown), but this inference is limited by the temporal resolution of sediment charcoal records.

## Conclusions

This study has several implications for describing and inferring the cause of fire histories with sediment charcoal records. In boreal and other stand-replacing fire regimes,

detecting subtle or multi-century changes in fire occurrence will require pooling data from multiple sites (Gavin et al. 2006, Hu et al. 2006). The compositing method employed here provides sample sizes sufficient to detect a 30% decrease in mFRI over the late Holocene and a 50% increase in mFRI since 400 ybp. However, inferring the causes of past fire-regime change requires additional information about variables controlling fire occurrence (e.g. climate and vegetation). The results of this and other studies demonstrate the potential complexity of this process. For example, increased FRIs since 400 ybp are consistent with Little-Ice-Age cooling (Hu et al. 2001, Clegg and Hu in prep.). In contrast, the increase in FRIs with moister conditions 2.7 k ybp is inconsistent with the general interpretation of fire-climate relationships. Finally, the lack of change at 1.2 k ybp implies no response to climate. Ultimately, an understanding of the patterns and causes of boreal fire history depends on a variety of studies that (1) reconstruct fire regimes at sub-regional scales, (2) reconstruct climatic and vegetational variables most relevant to fire ignition and spread (e.g. summer moisture levels), and (3) test hypotheses about the causes of fire-regimes changes using conceptual or numerical models linking climate, vegetation, and fire at a variety of scales (e.g. Rupp et al. 2000b). Thus this study emphasizes the need for a rigorous understanding of climatic and non-climatic controls of boreal fire regimes to infer past climate based on fire history or anticipate the consequences of future climate change in boreal ecosystems (e.g. Calef et al. 2005, Flannigan et al. 2005).

**Table 4.1.** AMS radiocarbon dates for the Last Chance Lake sediment core.

<b>Sample depth (cm)</b>	<b>Material Dated</b>	<b>Laboratory ID<sup>1</sup></b>	<b><sup>14</sup>C date<sup>2</sup> (yr BP)</b>	<b>Calibrated date<sup>3</sup></b>	<b>95% CI</b>
Last Chance Lake					
25.75 - 26.75	concentrated charcoal	CAMS 116842	510 ± 35	643	631 - 646
50.75 - 51.30	concentrated charcoal	CAMS 114334	1230 ± 60	1158	1040 - 1313
74.25 - 75.25	concentrated charcoal	CAMS 116843	1480 ± 35	1520	1506 - 1522
89.5 - 90.0	wood macrofossil	CAMS 113766	2310 ± 45	2322	2212 - 2477
110.3 - 111.3	wood macrofossil	CAMS 113765	2115 ± 35	2084	1881 - 2168

<sup>1</sup>CAMS: Center for Accelerator Mass Spectrometry, Lawrence Livermore National Laboratory, Livermore, CA.

<sup>2</sup> Conventional radiocarbon years before present (AD 1950). <sup>3</sup> Calibrated using CALIB 5.0 and the INTCAL04 calibration dataset (Reimer et al., 2004); weighted median of the probability distribution function with 95% confidence interval (Telford et al., 2004).

**Table 4.2.** Probability of Type-I error for within-zone, between-site (shaded values), between-zone, within-site (boxed values), and between-zone, between-site (non-shaded, non-boxed) comparisons of FRI distributions using the likelihood ratio test. Values  $\leq 0.05$  are in bold.

Zone	Site	n	I	I	II	II	II	II
			CO	WK	RP	CO	WK	LC
			15	15	14	18	16	17
I	RP	13	0.885	0.745	0.513	0.121	0.344	<b>0.036</b>
I	CO	15	--	0.706	0.567	<b>0.043</b>	0.276	<b>0.018</b>
I	WK	15	--	--	0.45	0.133	0.322	0.128
II	RP	14	--	--	--	0.241	0.763	0.184
II	CO	18	--	--	--	--	0.578	0.101
II	WK	16	--	--	--	--	--	0.091

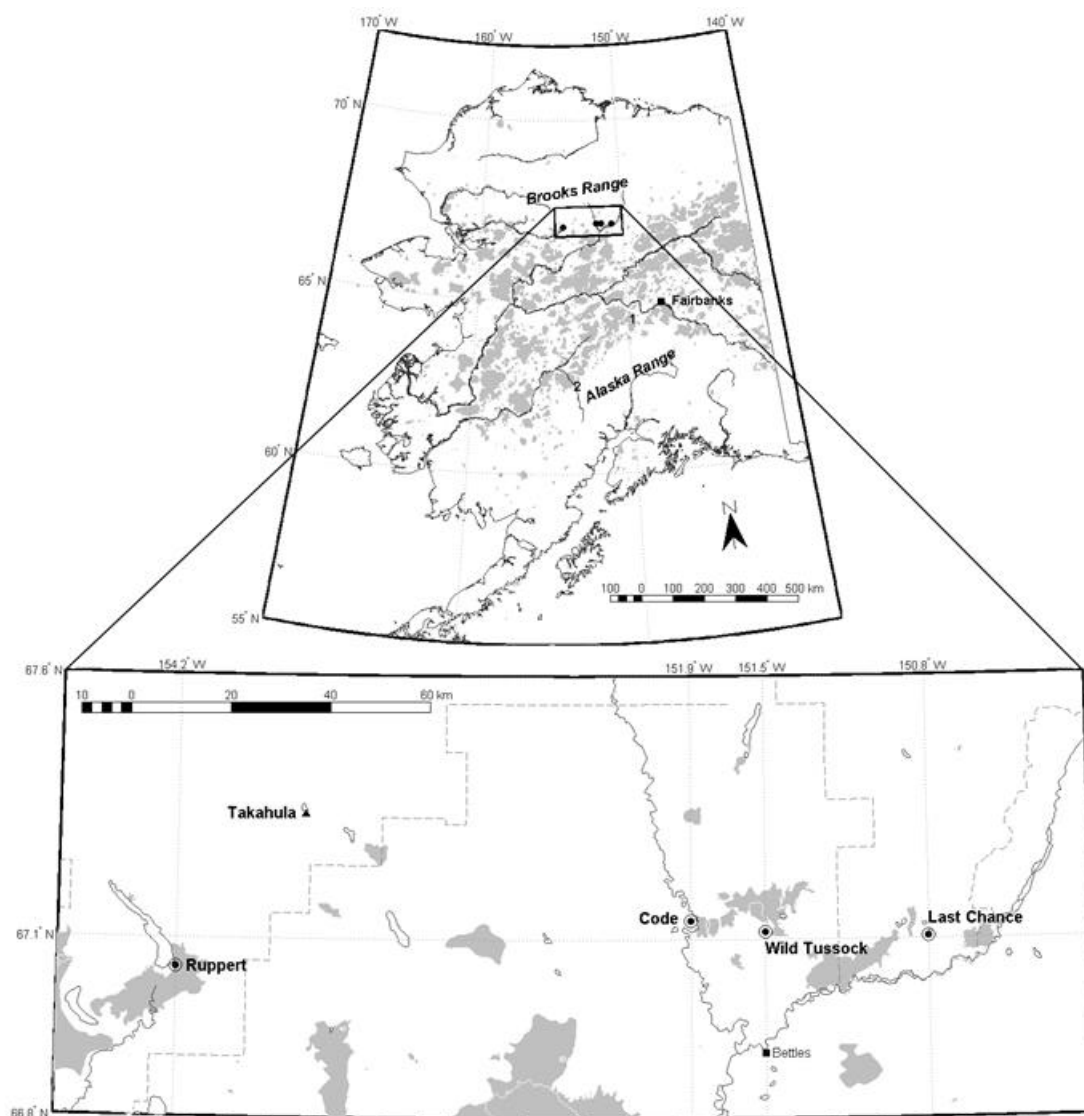


**Figure 4.1.** Location of lakes used in this study and others discussed in the text (1, Dune Lake; 2, Low Lake). Grey polygons are areas that have burned between AD 1950-2003 (Alaska Fire Service 2004), and the dashed line on the lower map is the southern border of Gates of the Arctic National Park. The black dots and larger circles identifying each lake on the bottom map are 2 and 4 km in diameter, representing the approximate spatial scale of each fire history record (i.e. 500-1000 m radius from lake). Climatic interpretations are based primarily on a sediment core from Takahula Lake (triangle in lower map; Clegg and Hu in prep.)

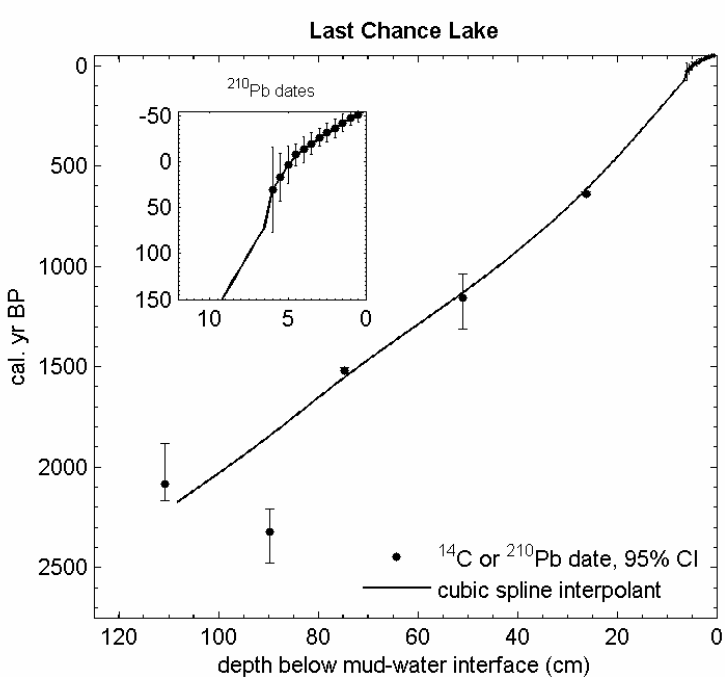


**Figure 4.2.** Age-depth model for Last Chance Lake based on a cubic spline interpolant between <sup>210</sup>Pb and AMS <sup>14</sup>C dates from terrestrial macrofossils. Error bars represent 95% confidence intervals (CI).

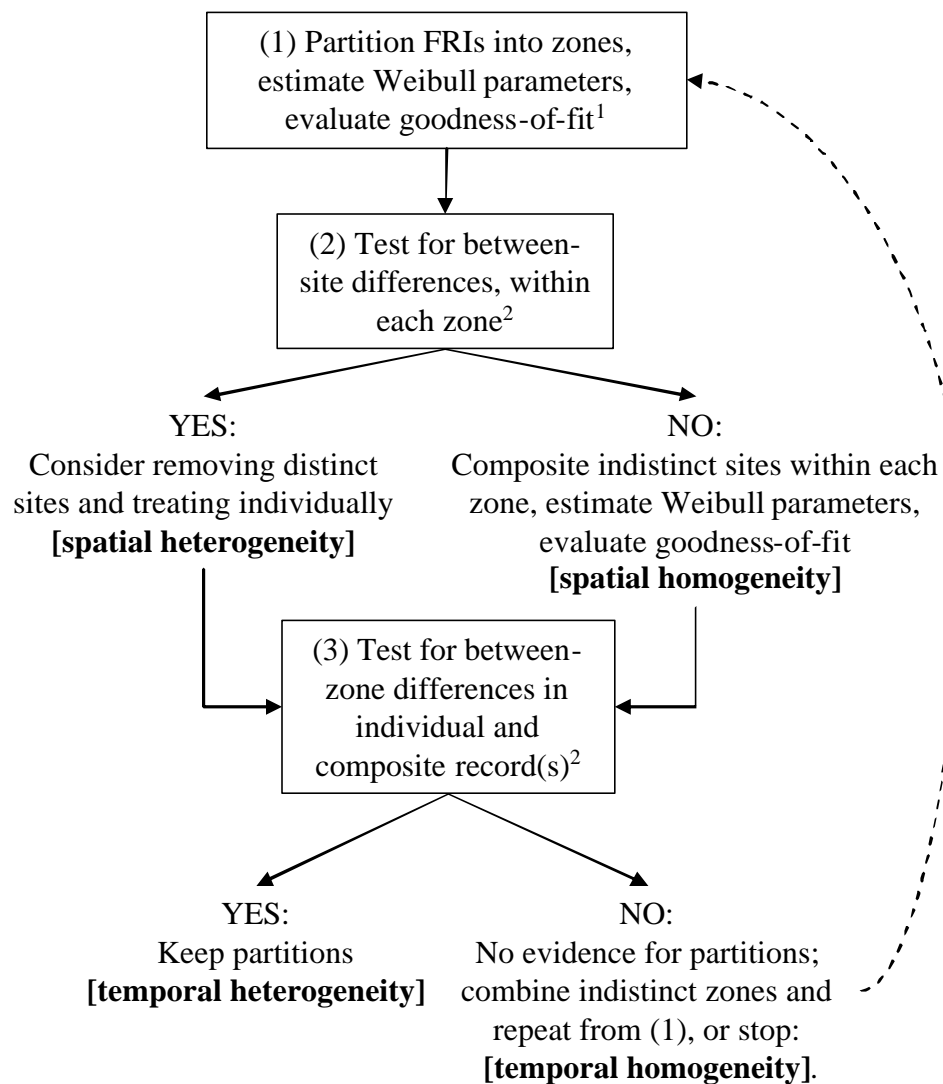


**Figure 4.3.** Framework for inferring impacts of climatic change on historic fire regimes. See methods for the details involved in each step. <sup>1</sup>Using a K-S test; <sup>2</sup> using a likelihood ratio test, as described in “Methods...”.

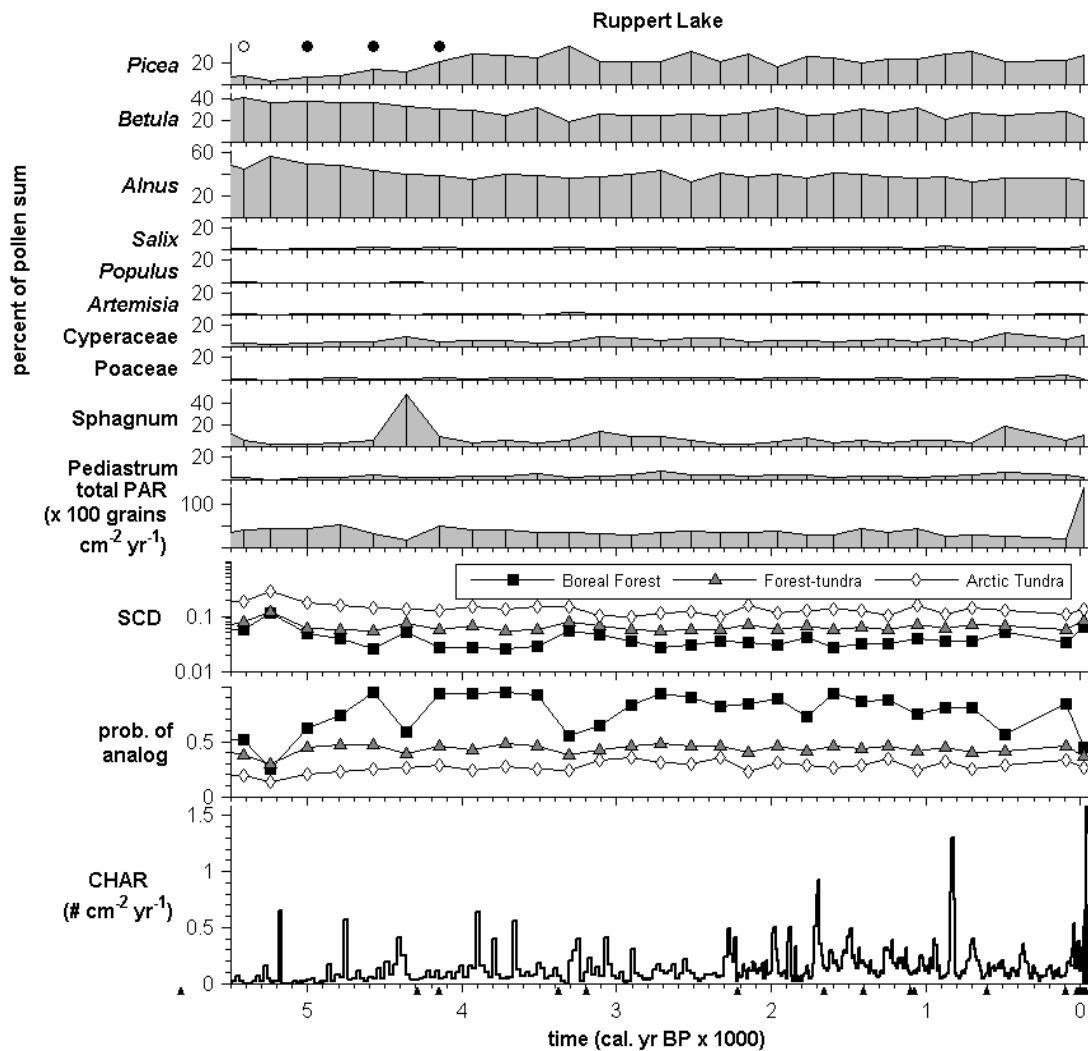


**Figure 4.4 (a).** Pollen percentages of selected taxa; total pollen accumulation rate (PAR); squared chord distance (SCD) and probability of analog values for comparisons between fossil samples and those from modern Boreal Forest, Forest-tundra, and Arctic Tundra; vegetation zones; and charcoal accumulation rate (CHAR) for Ruppert (a), Code (b), Wild Tussock (c), and Last Chance (d) lakes. Filled (empty) circles on *Picea* panel for Ruppert and Wild Tussock represent *Picea* stomata presence (absence). Triangles below lower x axis represent the location of <sup>14</sup>C or <sup>210</sup>Pb dates.

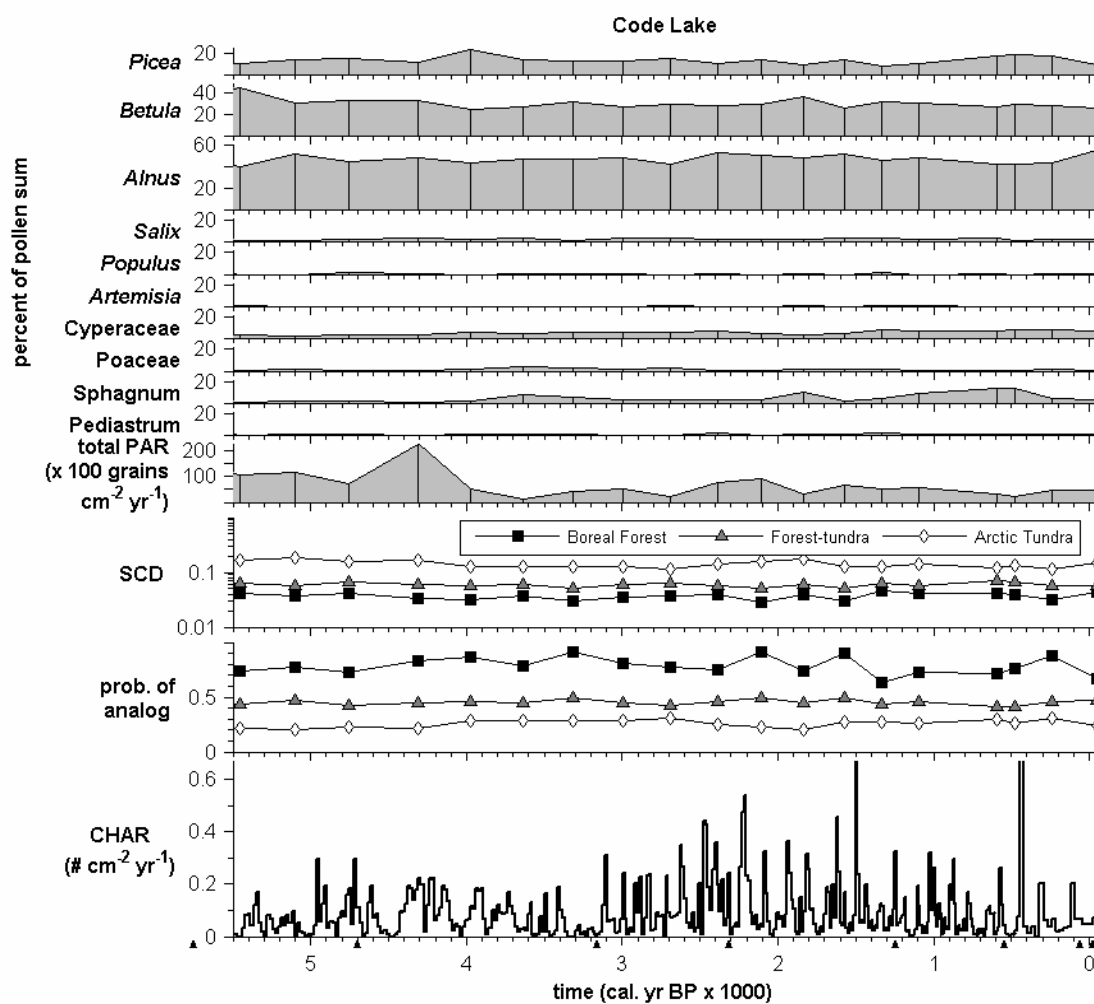


Figure 4.4 (b).

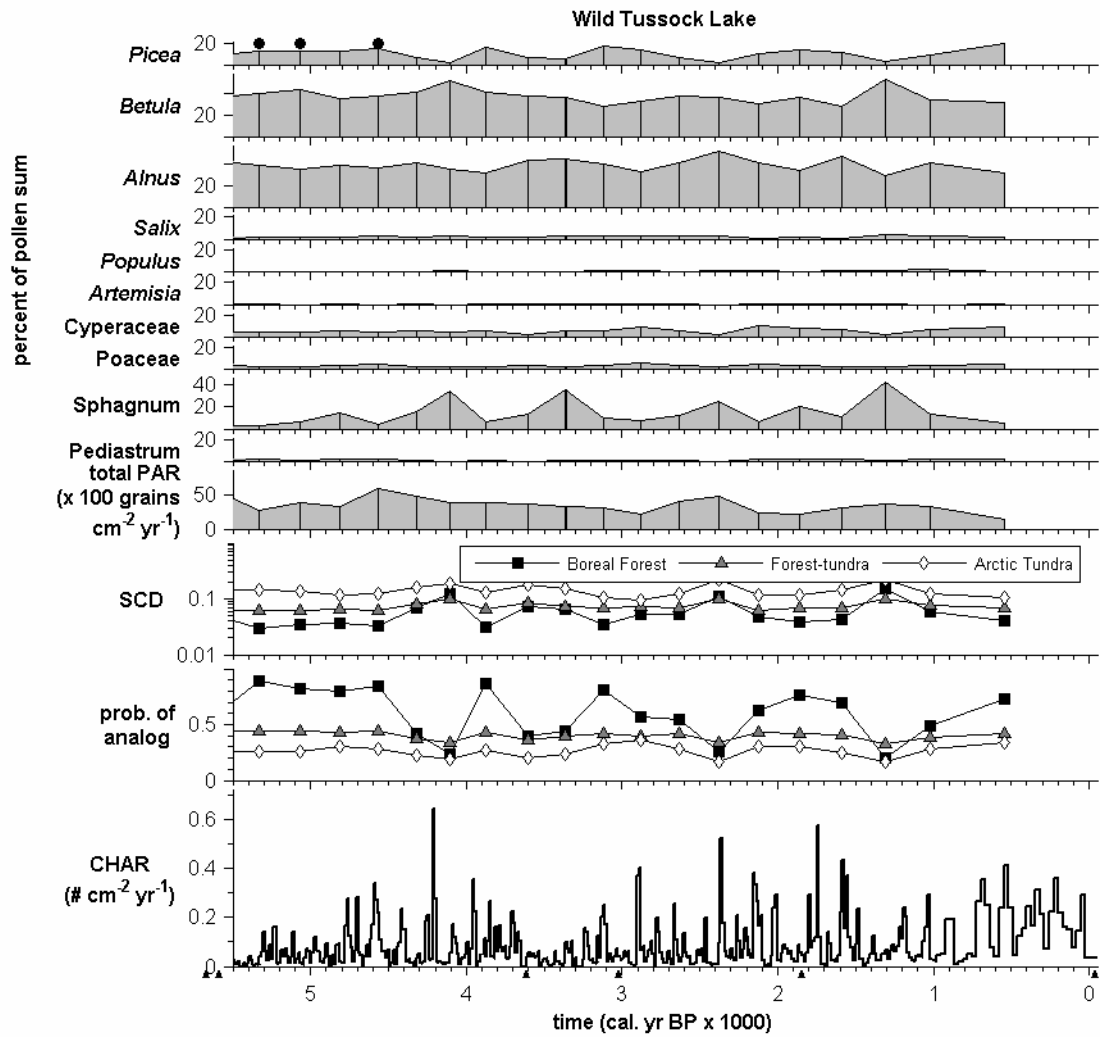


Figure 4.4 (c).

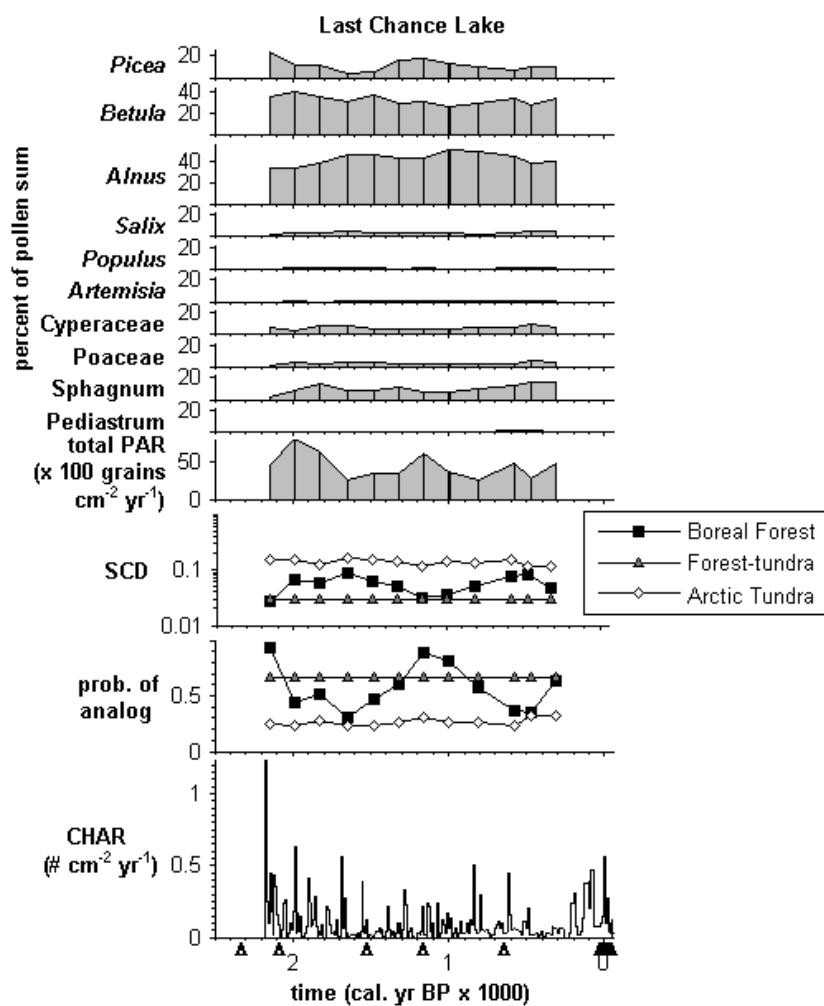
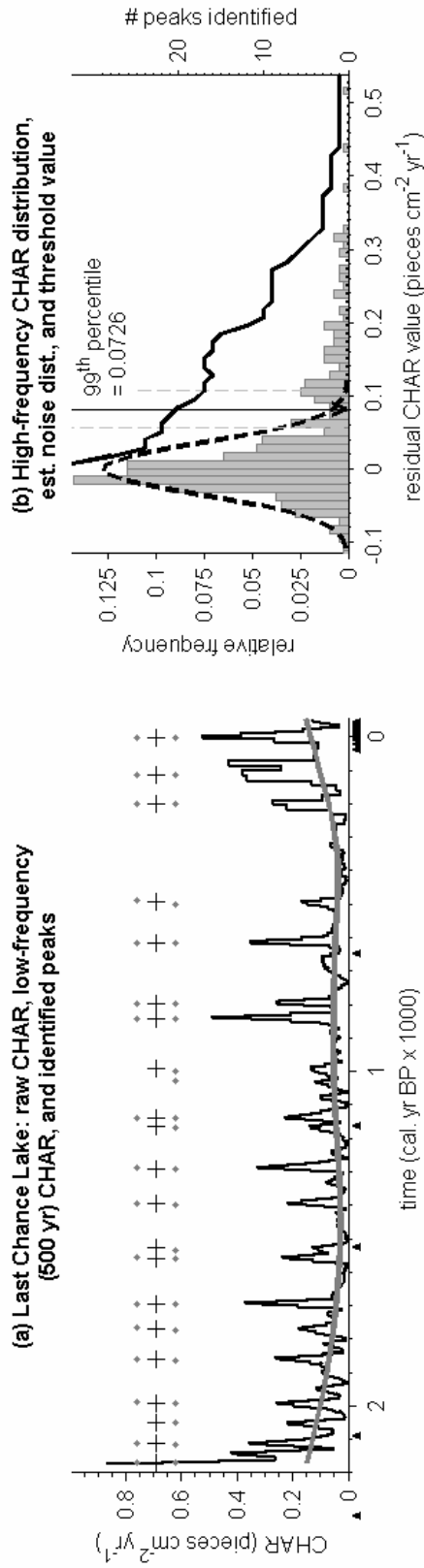
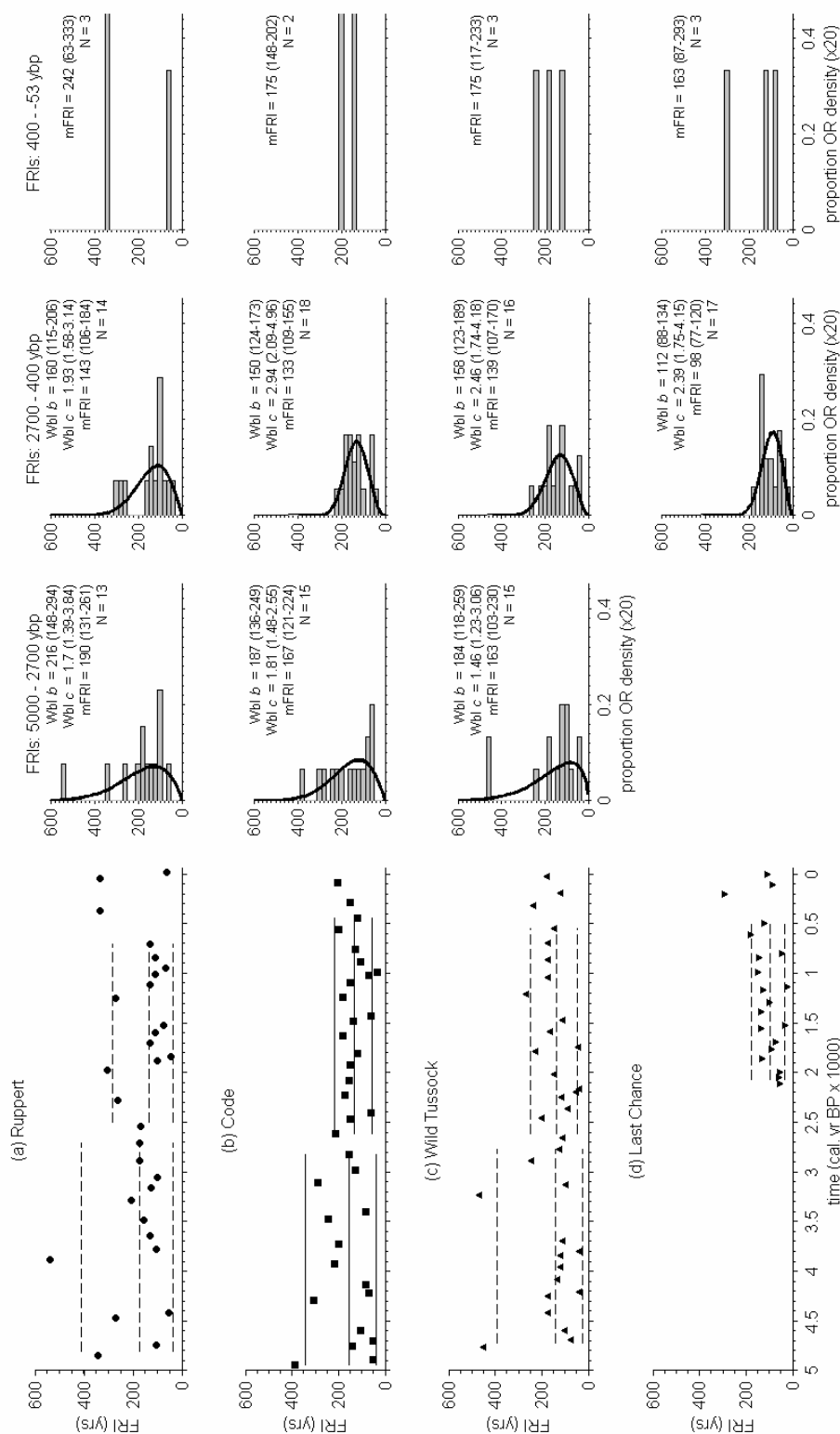


Figure 4.4 (d).



**Figure 4.5.** Left panel: Interpolated CHAR, low-frequency (500 yr) trend, and peaks identified with each of the three threshold criteria for Last Chance Lake (99<sup>th</sup> percentile criterion used for interpretation represented with '+'). Right panel: Histogram of residual CHAR,  $C_{peak}$  values, modeled distribution of the  $C_{noise}$  component (normal curve, thick dashed line), the number of peaks identified as a function of peaks identified value (thick solid line), and the three threshold values considered (vertical lines; dashed, solid, dashed corresponds to the 95<sup>th</sup>, 99<sup>th</sup> and 99.9<sup>th</sup> percentile of the  $C_{noise}$  distribution, respectively).



**Figure 4.6.** Time series of fire return intervals (FRIs; column 1), and the distribution of FRIs, fitted Weibull models with  $b$  and  $c$  parameter estimates (95% CI), mean FRI (mFRI, 95% CI), and number of fires ( $N$ ) identified within each of the three climatic zones maintained in the final partitioning (columns 2-3) for (a) Ruppert, (b) Code, (c) Wild Tussock, and (d), Last Chance lakes. The horizontal lines in the left column mark the 5<sup>th</sup>, 50<sup>th</sup>, and 95<sup>th</sup> percentiles of the Weibull distribution corresponding to each zone; solid (dashed) lines indicate that the FRIs within the period were (not) distinct from the preceding period.

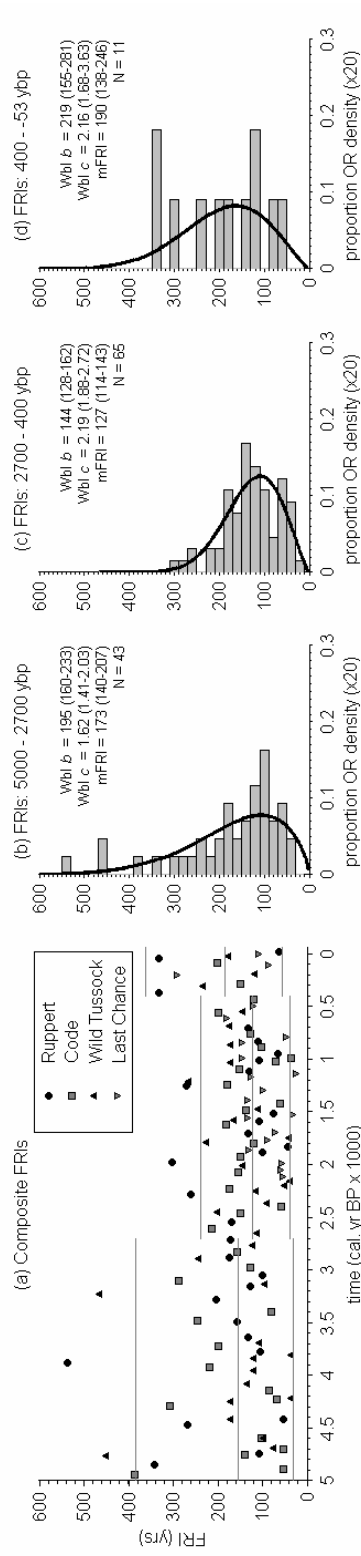


**Figure 4.7.** Composite record of FRIs with fitted Weibull models. Details are the same as in Figure 6. The climatic interpretation from Takahula Lake (bottom left) is provided for comparison.

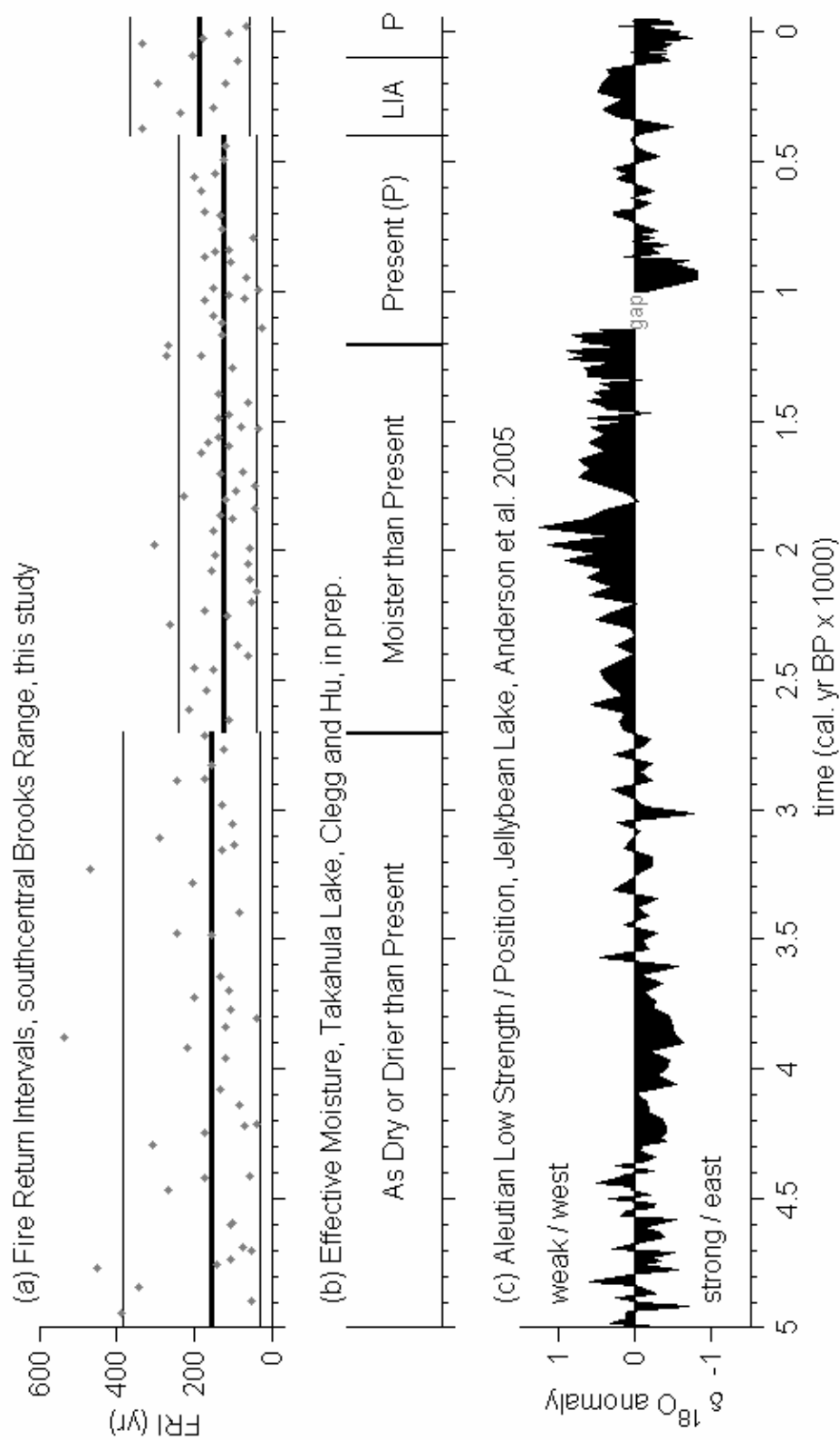


**Figure 4.8.** Fire return intervals (FRIs) and mean FRIs (mFRIs, 95% CD) from this study (a) in comparison to climatic interpretation for the study area (b) and the North Pacific region (c). Horizontal lines in (a) correspond to the 5<sup>th</sup>, 50<sup>th</sup>, and 95<sup>th</sup> percentile of the Weibull model fit to FRIs in each distinct period.

## REFERENCES

- Abbott, M. B., B. P. Finney, M. E. Edwards, and K. R. Kelts. 2000. Lake-level reconstruction and paleohydrology of Birch Lake, central Alaska, based on seismic reflection profiles and core transects. *Quaternary Research* **53**:154-166.
- AICI. 2004. *Impacts of a Warming Arctic: Arctic Climate Impact Assessment*. Cambridge University Press, Cambridge.
- Alaska Fire Service. 2004. Alaska Fire History. Bureau of Land Management. Available online at <http://agdc.usgs.gov/data/blm/fire/>.
- Alaska Fire Service. 2005. Alaska Fire History. Bureau of Land Management. Available online at <http://agdc.usgs.gov/data/blm/fire/>.
- Anderson, L., M. B. Abbott, and P. B. Finney. 2001. Holocene climate inferred from oxygen isotope ratios in lake sediments, Central Brooks Range, Alaska. *Quaternary Research* **55**:313-321.
- Anderson, L., M. B. Abbott, B. P. Finney, and S. J. Burns. 2005. Regional atmospheric circulation change in the North Pacific during the Holocene inferred from lacustrine carbonate oxygen isotopes, Yukon Territory, Canada. *Quaternary Research* **64**:21-35.
- Anderson, P. M., P. J. Bartlein, L. B. Brubaker, K. Gajewski, and J. C. Ritchie. 1989. Modern analogs of late-Quaternary pollen spectra from the western interior of North America. *Journal of Biogeography* **16**:573-596.
- Anderson, P. M., and L. B. Brubaker. 1993. Holocene vegetation and climate histories of Alaska. Pages 386-400 in H. E. Wright, J. E. J. Kutzbach, T. I. Webb, W. F. Ruddiman, F. A. Street-Perrott, and P. J. Bartlein, editors. *Global Climates Since the Last Glacial Maximum*. University of Minnesota Press, Minneapolis, MN.
- Anderson, P. M., and L. B. Brubaker. 1994. Vegetation history of northcentral Alaska: a mapped summary of Late-Quaternary pollen data. *Quaternary Science Reviews* **13**:71-92.
- Anderson, P. M., M. E. Edwards, and L. B. Brubaker. 2003. Results and paleoclimate implications of 35 years of paleoecological research in Alaska. *Development in Quaternary Science* **1**:427-440.

- Barnston, A. G., and R. E. Livezey. 1987. Classification, seasonality and persistence of low-frequency atmospheric circulation patterns. *Monthly Weather Review* **115**:1083-1126.
- Bartlein, P. J., P. M. Anderson, M. E. Edwards, and P. F. McDowell. 1991. A framework for interpreting paleoclimatic variations in eastern Beringia. *Quaternary International* **10-12**:73-83.
- Bergeron, Y., and S. Archambault. 1993. Decreasing frequency of forest fires in the southern boreal zone of Quebec and its relation to global warming since the end of the "Little Ice Age". *The Holocene* **3**:255-259.
- Bessie, W. C., and E. A. Johnson. 1995. The relative importance of fuels and weather on fire behavior in subalpine forests. *Ecology* **76**:747-762.
- Bigelow, N. H., L. B. Brubaker, M. E. Edwards, S. P. Harrison, I. C. Prentice, P. M. Anderson, A. A. Andreev, P. J. Bartlein, T. R. Christensen, W. Cramer, J. O. Kaplan, A. V. Lozhkin, N. V. Matveyeva, D. F. Murray, A. D. McGuire, V. Y. Razzhivin, J. C. Ritchie, B. Smith, D. A. Walker, K. Gajewski, V. Wolf, B. H. Holmqvist, Y. Igarashi, K. Kremenetskii, A. Paus, M. F. J. Pisaric, and V. S. Volkova. 2003. Climate change and arctic ecosystems: 1. Vegetation changes north of 55 degrees N between the last glacial maximum, mid-Holocene, and present. *Journal of Geophysical Research* **108**:ALT11-11-ALT11-25.
- Binford, M. W. 1990. Calculation and uncertainty analysis of <sup>210</sup>Pb dates for PIRLA project lake sediment cores. *Journal of Paleolimnology* **3**:253-267.
- Blackford, J. J. 2000. Charcoal fragments in surface samples following a fire and the implications for interpretation of subfossil charcoal data. *Palaeogeography, Palaeoclimatology, Palaeoecology* **164**:33-42.
- Bonan, G. B. 1989. Environmental factors and ecological processes controlling vegetation patterns in boreal forests. *Landscape Ecology* **3**:111-130.
- Bradbury, J. P. 1996. Charcoal deposition and redeposition in Elk Lake, Minnesota, USA. *The Holocene* **6**:339-344.
- Brubaker, L. B., H. L. Garfinkel, and M. E. Edwards. 1983a. A late Wisconsin and Holocene vegetation history from the central Brooks Range: Implications for Alaskan paleoecology. *Quaternary Research* **20**:194-214.

- Brubaker, L. B., H. L. Garfinkel, and M. E. Edwards. 1983b. A late Wisconsin and Holocene vegetation history from the central Brooks Range: Implications for Alaskan palaeoecology. *Quaternary Research* **20**:194-214.
- Brunelle, A., C. Whitlock, P. Bartlein, and K. Kipfmüller. 2005. Holocene fire and vegetation along environmental gradients in the Northern Rocky Mountains. *Quaternary Science Reviews* **24**:2281-2300.
- Bureau of Land Management, A. 2005. Wildland Fire Management Plan. Available online at [http://fire.ak.blm.gov/content/planning/BLM\\_Alaska\\_FMP\\_2005.pdf](http://fire.ak.blm.gov/content/planning/BLM_Alaska_FMP_2005.pdf).
- Calef, M. P., A. D. McGuire, H. E. Epstein, T. S. Rupp, and H. H. Shugart. 2005. Analysis of vegetation distribution in Interior Alaska and sensitivity to climate change using a logistic regression approach. *Journal of Biogeography* **32**:863-878.
- Calkin, P. E., G. C. Wiles, and D. J. Barclay. 2001. Holocene coastal glaciation of Alaska. *Quaternary Science Reviews* **20**:449-461.
- Carcaillet, C., and P. J. H. Richard. 2000. Holocene changes in seasonal precipitation highlighted by fire incidence in Eastern Canada. *Climate Dynamics* **16**:549-559.
- Carcaillet, C., Y. Bergeron, P. J. H. Richard, B. Frechette, S. Gauthier, and Y. T. Prairie. 2001a. Change of fire frequency in the eastern Canadian boreal forests during the Holocene: does vegetation composition or climate trigger the fire regime? *Journal of Ecology* **89**:930-946.
- Carcaillet, C., M. Bouvier, B. Frechette, A. C. Larouche, and P. J. H. Richard. 2001b. Comparison of pollen-slide and sieving methods in lacustrine charcoal analyses for local and regional fire history. *The Holocene* **11**:467-476.
- Carlson, L. J. 2003. Describing the postglacial pattern and rate of *Picea* expansion in Alaska using paleoecological records. Ph.D. dissertation. University of Washington, Seattle.
- Chamberlain, A. C. 1953. "Aspects of Travel and Deposition of Aerosol and Vapor Clouds". AERE-HP/R 1261, UK Atomic Energy Research Establishment Report, Harwell, Berkshire, United Kingdom.

- Chapin, F. S., G. R. Shaver, A. E. Giblin, K. J. Nadelhoffer, and J. A. Laundre. 1995. Responses of arctic tundra to experimental and observed changes in climate. *Ecology* **76**:694-711.
- Chapin, F. S., A. D. McGuire, J. Randerson, R. S. Pielke, D. Baldocchi, S. E. Hobbie, N. Roulet, W. Eugster, E. Kasischke, E. B. Rastetter, S. A. Zimov, and S. W. Running. 2000. Arctic and boreal ecosystems of western North America as components of the climate system. *Global Change Biology* **6**:211-223.
- Chapin, F. S., T. S. Rupp, A. M. Starfield, L. O. DeWilde, E. S. Zavaleta, N. Fresco, J. Henkelman, and A. D. McGuire. 2003. Planning for resilience: modeling change in human-fire interactions in the Alaskan boreal forest. *Frontiers in Ecology and the Environment* **1**:255-261.
- Christiansen, J. S. 1988. A Spruce-lichen Woodland in Northern Alaska: Post-fire Regeneration and Community Dynamics. Masters Thesis. University of Washington, Seattle.
- Clark, J. S. 1988a. Particle motion and the theory of charcoal analysis: source area, transport, deposition, and sampling. *Quaternary Research* **30**:67-80.
- Clark, J. S. 1988b. Stratigraphic charcoal analysis on petrographic thin sections: application to fire history in northwestern Minnesota. *Quaternary Research* **30**:81-91.
- Clark, J. S. 1989. Ecological disturbance as a renewal process: theory and application to fire history. *Oikos* **56**:17-30.
- Clark, J. S. 1990. Fire and climate change during the last 750 yr in northwestern Minnesota. *Ecological Monographs* **60**:135-159.
- Clark, J. S., and P. D. Royall. 1995a. Particle-size evidence for source areas of charcoal accumulation in late Holocene sediments of eastern North American lakes. *Quaternary Research* **43**:80-89.
- Clark, J. S., and P. D. Royall. 1995b. Transformation of a northern hardwood forest by aboriginal (Iroquois) fire: charcoal evidence from Crawford Lake, Ontario, Canada. *The Holocene* **5**:1-9.
- Clark, J. S., and P. D. Royall. 1996. Local and regional sediment charcoal evidence for fire regimes in presettlement north-eastern North America. *Journal of Ecology* **84**:365-382.

- Clark, J. S., P. D. Royall, and C. Chumbley. 1996. The role of fire during climate change in an eastern deciduous forest at Devil's Bathtub, New York. *Ecology* **77**:2148-2166.
- Clark, J. S., and W. A. Patterson. 1997. Background and local charcoal in sediments: scales of fire evidence in the paleorecord. Pages 23-48 *in* J. S. Clark, H. Cachier, J. G. Goldammer, and B. J. Stocks, editors. *Sediment Records of Biomass Burning and Global Change*. Springer, New York.
- Clark, J. S., J. A. Lynch, B. J. Stocks, and J. G. Goldammer. 1998. Relationships between charcoal particles in air and sediments in west-central Siberia. *The Holocene* **8**:19-29.
- Clegg, B. C., and F. S. Hu. in prep. A centennial-scale record of Holocene effective moisture in the southern Brooks Range, Alaska.
- Cleveland, W. S. 1979. Robust locally weighted regression and smoothing scatterplots. *Journal of the American Statistical Association* **74**:829-836.
- Cumming, S. G., F. K. A. Schmiegelow, and P. J. Burton. 2000. Gap dynamics in boreal aspen stands: Is the forest older than we think? *Ecological Applications* **10**:744-759.
- Cumming, S. G. 2001. Forest type and wildfire in the Alberta boreal mixedwood: What do fires burn? *Ecological Applications* **11**:97-110.
- Cwynar, L. S. 1978. Recent history of fire and vegetation from laminated sediment of Greenleaf Lake, Algonquin Park, Ontario. *Canadian Journal of Botany* **56**:10-21.
- D'Arrigo, R. D., and G. C. Jacoby. 1993. Secular trends in high northern latitude temperature reconstructions based on tree rings. *Climatic Change* **25**:163-177.
- de Groot, W. J., and R. W. Wein. 1999. *Betula glandulosa* Michx. response to burning and postfire growth temperature and implications of climate change. *International Journal of Wildland Fire* **9**:51-64.
- de Groot, W. J., and R. Wein. 2004. Effects of fire severity and season of burn on *Betula glandulosa* growth dynamics. *International Journal of Wildland Fire* **13**:287-295.

- Dissing, D., and D. L. Verbyla. 2003. Spatial patterns of lightning strikes in interior Alaska and their relations to elevation and vegetation. *Canadian Journal of Forest Resources* **33**:770-782.
- Duffy, P. A., J. E. Walsh, J. M. Graham, D. H. Mann, and T. S. Rupp. 2005. Impacts of large-scale atmospheric-ocean variability on Alaskan fire season severity. *Ecological Applications* **15**:1317-1330.
- Dugle, J. R. 1966. A taxonomic study of Western Canadian species in genus *Betula*. *Canadian Journal of Botany* **44**:929-&.
- Dyrness, C. T., L. A. Viereck, and K. Van Cleve. 1986. Fire in Taiga Communities of Interior Alaska. Pages 74-86 in K. Van Cleve, F. S. I. Chapin, P. W. Flanagan, L. A. Viereck, and C. T. Dyrness, editors. *Forest Ecosystems in the Alaskan Taiga*. Springer-Verlag, New York.
- Edwards, M. E., C. J. Mock, B. P. Finney, V. A. Barber, and P. J. Bartlein. 2001. Potential analogues for paleoclimatic variations in eastern interior Alaska during the past 14,000 yr: atmospheric-circulation controls of regional temperature and moisture responses. *Quaternary Science Reviews* **20**:189-202.
- Edwards, M. E., L. B. Brubaker, A. V. Lozhkin, and P. M. Anderson. 2005. Structurally novel biomes: a response to past warming in Beringia. *Ecology* **86**:1696-1703.
- Elias, S. A. 2000. Late Pleistocene climates of Beringia, based on analysis of fossil beetles. *Quaternary Research* **53**:229-235.
- Elias, S. A. 2001. Mutual climatic range reconstructions of seasonal temperatures based on Late Pleistocene fossil beetle assemblages in eastern Beringia. *Quaternary Science Reviews* **20**:77-91.
- Ellis, J. M., and P. E. Calkin. 1984. Chronology of Holocene glaciation, central Brooks Range, Alaska. *Geological Society of America Bulletin* **95**:897-912.
- Enache, M. D., and B. F. Cumming. 2006. Tracking recorded fires using charcoal morphology from the sedimentary sequence of Prosser Lake, British Columbia (Canada). *Quaternary Research* **65**:282-292.
- Esper, J., and F. H. Schweingruber. 2004. Large-scale treeline changes recorded in Siberia. *Geophysical Research Letters* **31**:doi: 10.1029/2003GL019178.

- Evison, L. H., P. E. Calkin, and J. M. Ellis. 1998. Late-Holocene glaciation and twentieth-century retreat, northeastern Brooks Range, Alaska. *The Holocene* **6**:17-24.
- Flannigan, M. D., and J. B. Harrington. 1988. A study of the relation of meteorological variables to monthly provincial area burned by wildfire in Canada (1953-80). *Journal of Applied Meteorology* **27**:441-452.
- Flannigan, M. D., and C. E. Van Wagner. 1991. Climate change and wildfire in Canada. *Canadian Journal of Forest Research* **21**:66-72.
- Flannigan, M. D., K. A. Logan, B. D. Amiro, W. R. Skinner, and B. J. Stocks. 2005. Future area burned in Canada. *Climatic Change* **72**:1-16.
- Gardner, J. J., and C. Whitlock. 2001. Charcoal accumulation following a recent fire in the Cascade Range, northwestern USA, and its relevance for fire-history studies. *The Holocene* **11**:541-549.
- Garfinkel, H. L., and L. B. Brubaker. 1980. Modern climate--tree-growth relationships and climatic reconstruction in sub-Arctic Alaska. *Nature* **286**:872-874.
- Gavin, D. G., L. B. Brubaker, and K. P. Lertzman. 2003. An 1800-year record of the spatial and temporal distribution of fire from the west coast of Vancouver Island, Canada. *Canadian Journal of Forest Research* **33**:573-586.
- Gavin, D. G., W. W. Oswald, E. R. Wahl, and J. W. Williams. 2005. A statistical approach to evaluating distance metrics and analog assignments for pollen records. *Quaternary Research* **60**:356-367.
- Gavin, D. G., F. S. Hu, K. Lertzman, and P. Corbett. 2006. Weak climatic control of stand-scale fire history during the late Holocene. *Ecology* **in press**
- Green, D. G. 1982. Fire and stability in the postglacial forests of southwest Nova Scotia. *Journal of Biogeography* **9**:29-40.
- Grissino-Mayer, H. D. 1995. Tree-ring reconstructions of climate and fire history at El Malpais National Monument, New Mexico. Dissertation. University of Arizona, Tucson.

- Grissino-Mayer, H. D. 1999. Modeling fire interval data from the American Southwest with the Weibull distribution. *International Journal of Wildland Fire* **9**:37-50.
- Hallett, D. J., D. S. Lepofsky, R. W. Mathewes, and K. P. Lertzman. 2003. 11,000 years of fire history and climate in the mountain hemlock rain forests of southwestern British Columbia based on sedimentary charcoal. *Canadian Journal of Forest Research* **33**:292-312.
- Hamilton, T. D. 1982. A late Pleistocene glacial chronology for the southern Brooks Range-stratigraphic record and regional significance. *Geological Society of America Bulletin* **93**:700-716.
- Hansen, B. C. S. 1994. Conifer stomate analysis as a paleoecological tool: an example from the Hudson Bay Lowlands. *Canadian Journal of Botany*:244-252.
- Harden, J. W., S. E. Trumbore, B. J. Stocks, A. Hirsch, S. T. Gower, K. P. O'Neill, and E. S. Kasischke. 2000. The role of fire in the boreal carbon budget. *Global Change Biology* **6**:174-184.
- Hely, C., M. Flannigan, Y. Bergeron, and D. McRae. 2001. Role of vegetation and weather on fire behavior in the Canadian mixedwood boreal forest using two fire behavior prediction systems. *Canadian Journal of Forest Research* **31**:430-441.
- Hess, J. C., C. A. Scott, G. L. Hufford, and M. D. Fleming. 2001. El Nino and its impact on fire weather conditions in Alaska. *International Journal of Wildland Fire* **10**:1-13.
- Higuera, P. E., D. G. Gavin, and M. E. Peters. 2004. When does a charcoal peak represent a fire? Insights from a simple statistical model. page 220 *in* Conference Proceedings from "89th Annual Meeting of the Ecological Society of America", Portland, Oregon.
- Higuera, P. E., L. B. Brubaker, P. M. Anderson, F. S. Hu, B. Clegg, T. Brown, and S. Rupp. 2005a. Vegetational and climatic controls on post-glacial fire regimes in the southern Brooks Range, Alaska. page 18 *in* Conference Proceedings from "Fire and Climate Synthesis in Western North America", Flagstaff, Arizona.
- Higuera, P. E., D. G. Sprugel, and L. B. Brubaker. 2005b. Reconstructing fire regimes with charcoal from small-hollow sediments: a calibration with tree-ring records of fire. *The Holocene* **15**:238-251.

- Hinzman, L. D., N. D. Bettez, W. R. Bolton, F. S. Chapin, M. B. Dyurgerov, C. L. Fastie, B. Griffith, R. D. Hollister, A. Hope, H. P. Huntington, A. M. Jensen, G. J. Jia, T. Jorgenson, D. L. Kane, D. R. Klein, G. Kofinas, A. H. Lynch, A. H. Lloyd, A. D. McGuire, F. E. Nelson, W. C. Oechel, T. E. Osterkamp, C. H. Racine, V. E. Romanovsky, R. S. Stone, D. A. Stow, M. Sturm, C. E. Tweedie, G. L. Vourlitis, M. D. Walker, D. A. Walker, P. J. Webber, J. M. Welker, K. Winker, and K. Yoshikawa. 2005. Evidence and implications of recent climate change in northern Alaska and other arctic regions. *Climatic Change* **72**:251-298.
- Hu, F. S., E. Ito, T. A. Brown, B. B. Curry, and D. R. Engstrom. 2001. Pronounced climatic variations in Alaska during the last two millennia. *Proceedings of the National Academy of Sciences of the United States of America* **98**:10552-10556.
- Hu, F. S., L. B. Brubaker, D. G. Gavin, P. E. Higuera, J. A. Lynch, T. S. Rupp, and W. Tinner. 2006. How climate and vegetation influence the fire regime of the Alaskan Boreal Biome: the Holocene perspective. *Mitigation and Adaptation Strategies for Global Change* **in press**.
- IPCC. 2001. Second Assessment - Climate Change 2001. A Report of the Intergovernmental Panel on Climate Change Intergovernmental Panel of Climate Change, Geneva, Switzerland.
- Jacobson, G. L., and R. H. W. Bradshaw. 1981. The selection of sites for paleovegetational studies. *Quaternary Research* **16**:80-96.
- Johnson, E. A. 1992. *Fire and Vegetation Dynamics: Studies from the North American Boreal Forest*. Cambridge University Press, Cambridge.
- Johnson, E. A., and S. L. Gutsell. 1994. Fire frequency models, methods and interpretations. *Advances in Ecological Research* **25**:239-287.
- Johnstone, J. F., and F. S. Chapin. 2006. Fire interval effects on successional trajectory in boreal forests of northwest Canada. *Ecosystems* **9**:268-277.
- Kasischke, E. S., D. Williams, and D. Barry. 2002. Analysis of the patterns of large fires in the boreal forest region of Alaska. *International Journal of Wildland Fire* **11**:131-144.
- Kaufman, D. S., T. A. Ager, N. J. Anderson, P. M. Anderson, J. T. Andrews, P. J. Bartlein, L. B. Brubaker, L. L. Coats, L. C. Cwynar, M. L. Duvall, A. S. Dyke, M.

- E. Edwards, W. R. Eisner, K. Gajewski, A. Geirsdottir, F. S. Hu, A. E. Jennings, M. R. Kaplan, M. W. Kerwin, A. V. Lozhkin, G. M. MacDonald, G. H. Miller, C. J. Mock, W. W. Oswald, B. L. Otto-Bliesner, D. F. Porinchu, K. Ruhland, J. P. Smol, E. J. Steig, and B. B. Wolfe. 2004. Holocene thermal maximum in the western Arctic (0-180 degrees W). *Quaternary Science Reviews* **23**:529-560.
- Larsen, C. P. S., and G. M. MacDonald. 1993. Lake morphology, sediment mixing, and the selection of sites for fine resolution palaeoecological studies. *Quaternary Science Reviews* **12**:781-192.
- Larsen, C. P. S., and G. M. MacDonald. 1995. Relations between tree-ring widths, climate, and annual area burned in the boreal forest of Alberta. *Canadian Journal of Forest Research* **25**:1746-1755.
- Larsen, C. P. S. 1996. Fire and climate dynamics in the boreal forest of northern Alberta, Canada, from AD 1850 to 1989. *The Holocene* **6**:449-456.
- Larsen, C. P. S. 1997. Spatial and temporal variations in boreal forest fire frequency in northern Alberta. *Journal of Biogeography* **24**:663-673.
- Lloyd, A. H., and C. L. Fastie. 2002. Spatial and temporal variability in the growth and climate response of treeline trees in Alaska. *Climatic Change* **52**:481-509.
- Lloyd, A. H., T. S. Rupp, C. L. Fastie, and A. M. Starfield. 2003. Patterns and dynamics of treeline advance on the Seward Peninsula, Alaska. *Journal of Geophysical Research* **108**:ALT2-1-ALT2-15.
- Lloyd, A. H. 2005. Ecological histories from Alaskan tree lines provide insight into future change. *Ecology* **86**:1687-1695.
- Long, C. J., C. Whitlock, P. J. Bartlein, and S. H. Millspaugh. 1998. A 9000-year fire history from the Oregon Coast Range, based on a high-resolution charcoal study. *Canadian Journal of Forest Research* **28**:774-787.
- Lynch, J. A., J. S. Clark, N. H. Bigelow, M. E. Edwards, and B. P. Finney. 2002. Geographic and temporal variations in fire history in boreal ecosystems of Alaska. *Journal of Geophysical Research* **108**:FFR8-1-FFR8-17.
- Lynch, J. A., J. S. Clark, and B. J. Stocks. 2004a. Charcoal production, dispersal and deposition from the Fort Providence experimental fire: Interpreting fire regimes

- from charcoal records in boreal forests. *Canadian Journal of Forest Research* **34**:1642-1656.
- Lynch, J. A., J. L. Hollis, and F. S. Hu. 2004b. Climatic and landscape controls of the boreal forest fire regime: Holocene records from Alaska. *Journal of Ecology* **92**:447-489.
- MacDonald, G. M., C. P. S. Larsen, J. M. Szeicz, and K. A. Moser. 1991. The reconstruction of boreal forest fire history from lake sediments: a comparison of charcoal, pollen, sedimentological, and geochemical indices. *Quaternary Science Reviews* **10**:53-71.
- MacDonald, G. M., A. A. Velichko, C. V. Kremenetski, O. K. Borisova, A. A. Goleva, A. A. Andreev, L. C. Cwynar, R. T. Riding, S. L. Forman, T. W. D. Edwards, R. Aravena, D. Hammarlund, J. M. Szeicz, and V. N. Gattaulin. 2000. Holocene treeline history and climate change across northern Eurasia. *Quaternary Research* **53**:302-311.
- Mack, M. C., E. A. G. Schuur, M. S. Bret-Harte, G. R. Shaver, and F. S. Chapin. 2004. Ecosystem carbon storage in arctic tundra reduced by long-term nutrient fertilization. *Nature* **431**:440-443.
- Mann, D. H., P. A. Heiser, and B. P. Finney. 2002. Holocene history of the Great Kobuk Sand Dunes, northwestern Alaska. *Quaternary Science Reviews* **21**:709-731.
- Marlon, J. 2003. A Meta-Analysis of Charcoal-based Fire History Records from the Northwestern United States. Masters Thesis. University of Oregon, Eugene.
- Millspaugh, S. H., C. Whitlock, and P. Bartlein. 2000. Variations in fire frequency and climate over the past 17000 yr in central Yellowstone National Park. *Geology* **28**:211-214.
- Mock, C. J., P. J. Bartlein, and P. M. Anderson. 1998. Atmospheric circulation patterns and spatial climatic variations in Beringia. *International Journal of Climatology* **18**:1085-1104.
- Mohr, J. A., C. Whitlock, and C. N. Skinner. 2000. Postglacial vegetation and fire history, eastern Klamath Mountains, California, USA. *The Holocene* **10**:587-602.

- Nash, C. H., and E. A. Johnson. 1996. Synoptic climatology of lightning-caused forest fires in subalpine and boreal forests. *Canadian Journal of Forest Research* **26**:1859-1874.
- Nowacki, G., P. Spencer, T. Brock, M. Fleming, and T. Jorgenson. 2000. Narrative Description for the Ecoregions of Alaska and Neighboring Territories. USGS, Reston, VA.
- Nowacki, G., P. Spencer, T. Brock, M. Fleming, and T. Jorgenson. 2001. Ecoregions of Alaska and Neighboring Territories. Online at <http://agdc.usgs.gov/data/projects/fhm/>, USGS, Reston, VA.
- Ohlson, M., and E. Tryterud. 2000. Interpretation of the charcoal record in forest soils: forest fires and their production and deposition of macroscopic charcoal. *The Holocene* **10**:519-525.
- Oswald, W. W., L. B. Brubaker, and P. M. Anderson. 1999. Late Quaternary vegetational history of the Howard Pass area, northwestern Alaska. *Canadian Journal of Botany* **77**:570-581.
- Overpeck, J., K. Hughen, D. Hardy, R. Bradley, R. Case, M. Douglas, B. Finney, K. Gajewski, G. Jacoby, A. Jennings, S. Lamourex, A. Lasca, G. MacDonald, J. Moore, M. Retelle, S. Smith, A. Wolfe, and G. Zielinski. 1997. Arctic environmental change of the last four centuries. *Science* **278**:1251-1256.
- Overpeck, J. T., T. Webb, and I. C. Prentice. 1985. Quantitative interpretation of fossil pollen spectra: dissimilarity coefficients and the method of modern analogs. *Quaternary Research* **23**:87-108.
- PALE\_members. 1994. Research Protocols for PALE: Paleoclimates of Arctic Lakes and Estuaries. PAGES workshop report:53.
- Patterson, W. A. I., K. J. Edwards, and D. J. Maguire. 1987. Microscopic charcoal as a fossil indicator of fire. *Quaternary Science Reviews* **6**:3-23.
- Payette, S., C. Morneau, L. Sirois, and M. Despons. 1989. Recent fire history of the northern Quebec biomes. *Ecology* **70**:656-673.
- Pisaric, M. F. J. 2002. Long-distance transport of terrestrial plant material by convection resulting from forest fires. *Journal of Paleolimnology* **28**:349-354.

- Pisaric, M. F. J., C. Holt, J. M. Szeicz, T. Karst, and J. P. Smol. 2003. Holocene treeline dynamics in the mountains of northeastern British Columbia, Canada, inferred from fossil pollen and stomata. *The Holocene* **13**:161-173.
- Racine, C., W. A. Patterson, and J. G. Dennis. 1985. Tundra fire regimes in the Noatak River Watershed, Alaska. *Arctic* **38**:194-200.
- Reimer, P. J., M. G. L. Baillie, E. Bard, A. Bayliss, J. W. Beck, C. J. H. Bertrand, P. G. Blackwell, C. E. Buck, G. S. Burr, K. B. Culter, R. E. Damon, R. L. Edwards, R. G. Fairbanks, M. Friedrich, T. P. Gulderson, A. G. Hogg, K. A. Hughen, B. Kromer, G. McCormac, S. Manning, C. B. Ramsey, R. W. Reimer, S. Remmelle, J. R. Southon, M. Stuiver, S. Talamo, F. W. Taylor, J. van der Plicht, and C. E. Weyhenmeyer. 2004. INTCAL04 terrestrial radiocarbon age calibration, 0-26 cal Kyr BP. *Radiocarbon* **46**:1029-1058.
- Rhodes, A. N. 1998. A method for the preparation and quantification of microscopic charcoal from terrestrial and lacustrine sediment cores. *The Holocene* **8**:113-117.
- Rupp, T. S., F. S. I. Chapin, and A. M. Starfield. 2000a. Response of subarctic vegetation to transient climatic change on the Seward Peninsula in northwest Alaska. *Global Change Biology* **6**:541-555.
- Rupp, T. S., A. M. Starfield, and F. S. I. Chapin. 2000b. A frame-based spatially explicit model of subarctic vegetation response to climatic change: comparison with a point model. *Landscape Ecology* **15**:383-400.
- Rupp, T. S., A. M. Starfield, F. S. I. Chapin, and P. Duffy. 2002. Modeling the impact of black spruce on the fire regime of Alaskan boreal forest. *Climatic Change* **55**:213-233.
- Samsonov, Y. N., K. P. Joutsenogii, V. I. Makarov, A. V. Ivanov, V. A. Ivanov, D. J. McRae, S. G. Conard, S. P. Baker, and G. A. Ivanova. 2005. Particulate emissions from fires in central Siberian Scots pine forests. *Canadian Journal of Forest Research* **35**:2207-2217.
- Serreze, M. C., J. E. Walsh, F. S. I. Chapin, T. Osterkamp, M. Dyurgerov, V. Romanovsky, W. C. Oechel, J. Morison, T. Zhang, and R. G. Barry. 2000. Observational evidence of recent change in the northern high-latitude environment. *Climatic Change* **46**:159-207.

- Shuman, B., P. Newby, Y. S. Huang, and T. Webb. 2004. Evidence for the close climatic control of New England vegetation history. *Ecology* **85**:1297-1310.
- Silipaswan, C. S., D. L. Verbyla, and A. D. McGuire. 2001. Land cover change on the Seward Peninsula: The use of remote sensing to evaluate the potential influences of climate warming on historical vegetation dynamics. *Canadian Journal of Remote Sensing* **27**:542-554.
- Stocks, B. J., J. A. Mason, J. B. Todd, E. M. Bosch, B. M. Wotton, B. D. Amiro, M. D. Flannigan, K. G. Hirsch, K. A. Logan, D. L. Martell, and W. R. Skinner. 2002. Large forest fires in Canada, 1959-1997. *Journal of Geophysical Research-Atmospheres* **108**.
- Stocks, B. J., J. A. Mason, B. J. Todd, E. M. Bosch, B. M. Wotton, B. D. Amiro, M. D. Flannigan, K. G. Hirsch, K. A. Logan, D. L. Martell, and W. R. Skinner. 2003. Large forest fires in Canada, 1957-1997. *Journal of Geophysical Research* **108**:FFR5-1 -FFR5-12.
- Stocks, B. J., M. E. Alexander, and R. A. Lanoville. 2004. Overview of the International Crown Fire Modeling Experiment (ICFME). *Canadian Journal of Forest Research* **34**:1543-1547.
- Stow, D. A., A. Hope, A. D. McGuire, D. L. Verbyla, J. Gamon, F. Huemmrich, S. Houston, C. Racine, M. Sturm, K. Tape, L. Hinzman, K. Yoshikawa, C. Tweedie, B. Noyle, C. Silapaswan, D. Douglas, B. Griffith, G. Jia, A. Petersen, L. Zhou, and R. Myneni. 2004. Remote sensing of vegetation and land-cover change in arctic tundra ecosystems. *Remote Sensing of Environment* **89**:281-308.
- Sturm, M., C. Racine, and K. Tape. 2001. Climate change - Increasing shrub abundance in the Arctic. *Nature* **411**:546-547.
- Sugita, S. 1993. A model of pollen source area for an entire lake surface. *Quaternary Research* **39**:239-244.
- Sutton, O. G. 1947a. The theoretical distribution of airborne pollution from factory chimneys. *Quarterly Journal Of The Royal Meteorological Society* **73**:426-436.
- Sutton, O. G. 1947b. The problem of diffusion in the lower atmosphere. *Quarterly Journal of the Royal Meteorological Society* **73**:257-281.

- Swain, A. M. 1973. A history of fire and vegetation in northeastern Minnesota as recorded in lake sediments. *Quaternary Research* **3**:383-396.
- Taylor, S. W., B. M. Wotton, M. E. Alexander, and G. N. Dalrymple. 2004. Variation in wind and crown fire behaviour in a northern jack pine-black spruce forest. *Canadian Journal of Forest Research* **34**:1561-1576.
- Telford, R. J., E. Heegaard, and H. J. B. Birks. 2004a. The intercept is a poor estimate of a calibrated radiocarbon age. *The Holocene* **14**:296-298.
- Telford, R. J., E. Heegaard, and H. J. B. Birks. 2004b. All age-depth models are wrong: but how badly? *Quaternary Science Reviews* **23**:1-5.
- Thoman, D. R., and L. J. Bain. 1969. Two sample tests in the Weibull distribution. *Technometrics* **11**:805-815.
- Tinner, W., S. Hofstetter, F. Zeugin, M. Conedera, T. Wohlgemuth, L. Zimmermann, and R. Zweifel. 2006. Long-distance transport of macroscopic charcoal by an intensive crown fire in the Swiss Alps - implications for fire history reconstruction. *Holocene* **16**:287-292.
- Trenberth, K. E., and J. W. Hurrell. 1994. Decadal Atmosphere-Ocean Variations in the Pacific. *Climate Dynamics* **9**:303-319.
- Viereck, L. A. 1973. Wildfire in the taiga of Alaska. *Quaternary Research* **3**:465-495.
- Viereck, L. A., K. Van Cleve, and C. T. Dyrness. 1986. Forest Ecosystem Distribution in the Taiga Environment. Pages 22-43 *in* K. Van Cleve, F. S. Chapin, P. W. Flanagan, L. A. Viereck, and C. T. Dyrness, editors. *Forest Ecosystems in the Alaskan Taiga*. Springer-Verlag, New York.
- Wahren, C.-H. A., M. D. Walker, and M. S. Bret-Harte. 2005. Vegetation response in Alaskan arctic tundra after 8 years of a summer warming and winter snow manipulation. *Global Change Biology* **11**:537-522.
- Walker, D. A., M. K. Reynolds, F. J. A. Daniels, E. Einarsson, A. Evlvebakk, W. A. Could, A. E. Katenin, S. S. Kholod, C. J. Markon, E. S. Melnikov, N. G. Moskalenko, S. S. Talbot, B. A. Yurtsev, and o. m. o. t. C. Team. 2005. The circumpolar Arctic vegetation map. *Journal of Vegetation Science* **16**:267-282.

- Weintraub, M. N., and J. P. Schimel. 2005. Nitrogen cycling and the spread of shrubs control changes in the carbon balance of arctic tundra ecosystems. *Bioscience* **55**:408-415.
- Weir, J. N. H., E. A. Johnson, and K. Miyanishi. 2000. Fire frequency and the spatial age mosaic of the mixed-wood boreal forest in western Canada. *Ecological Applications* **10**:1162-1177.
- Whitlock, C., and S. H. Millspaugh. 1996. Testing the assumptions of fire-history studies: an examination of modern charcoal accumulation in Yellowstone National Park, USA. *The Holocene* **6**:7-15.
- Whitlock, C., and R. S. Anderson. 2003. Fire history reconstructions based on sediment records from lakes and wetlands. Pages 3-31 *in* T. T. Veblen, W. L. Baker, G. Montenegro, and T. Swetnam, editors. *Fire and Climatic Change in Temperate Ecosystems of the Western Americas*. Springer, New York.
- Whitlock, C., C. N. Skinner, P. Bartlein, T. Minckley, and J. A. Mohr. 2004. Comparison of charcoal and tree-ring records of recent fires in the eastern Klamath Mountains, California, USA. *Canadian Journal of Forest Research* **34**:2110-2121.
- Whitmore, J., K. Gajewski, M. Sawada, J. W. Williams, B. Shuman, P. J. Bartlein, T. Minckley, A. E. Viau, T. I. Webb, S. Shafer, P. Anderson, and L. Brubaker. 2005. Modern pollen data from North American and Greenland for multi-scale paleoenvironmental applications. *Quaternary Science Reviews* **24**:1828-1848.
- Wiles, G. C., D. J. Barclay, and P. E. Calkin. 1999. Tree-ring-dated 'Little ice age' histories of maritime glaciers from western Prince William Sound, Alaska. *Holocene* **9**:163-173.
- Wiles, G. C., G. C. Jacoby, N. K. Davi, and R. P. McAllister. 2002. Late Holocene glacier fluctuations in the Wrangell Mountains, Alaska. *Geological Society of America Bulletin* **114**:896-908.
- Wright, H. E., D. H. Mann, and P. H. Glaser. 1984. Piston corers for peat and lake sediments. *Ecology* **65**:657-659.
- Yarie, J. 1981. Forest fire cycles and life tables: a case study from interior Alaska. *Canadian Journal of Forest Research* **11**:554-562.

Zar, J. H. 1999. Biostatistical Analysis, Fourth edition. Prentice Hall, Upper Saddle River.

Zimov, S. A., S. P. Davidov, G. M. Zimova, A. I. Davidova, F. S. Chapin, M. C. Chapin, and J. F. Reynolds. 1999. Contribution of disturbance to increasing seasonal amplitude of atmospheric CO<sub>2</sub>. *Science* **284**:1973-1976.

**APPENDIX A: EVALUATION AND EXPANSION OF A GAUSSIAN PLUME MODEL FOR  
QUANTIFYING THE SOURCE AREA OF MACROSCOPIC CHARCOAL**

Appendix A is a co-authored paper that tests and modifies the Gaussian plume model used in CharSim (Chapter 2). As of June 2006, the paper is in review.

**Evaluation and expansion of a Gaussian plume model for quantifying the source  
area of macroscopic charcoal**

Matthew Edward Peters<sup>1,2</sup> and Philip Edward Higuera<sup>3,4</sup>

<sup>13</sup>Department of Applied Mathematics

and

Department of Atmospheric Science

University of Washington

Seattle, WA 98195-1360

<sup>3</sup>College of Forest Resources

Box 352100

University of Washington

Seattle, WA 98195-1360

Key words: charcoal analysis, charcoal dispersal, charcoal source area, dispersal model,  
experimental burn, fire history

<sup>2</sup> Current address: Department of Earth and Planetary Sciences, Harvard University,  
Cambridge, MA 02138

<sup>3</sup> Author for correspondence: [phiguera@u.washington.edu](mailto:phiguera@u.washington.edu)

## ABSTRACT

To aid interpreting the source area of charcoal in lake-sediment records, we compare charcoal deposition from an experimental fire (Lynch et al. 2004a) to predictions from a Gaussian plume model. The model captures the two-dimensional patterns in the empirical data (predicted vs. observed  $r^2 = 0.67$ ,  $p < 0.001$ ). We expand the model to calculate the potential charcoal source area (PCSA) for several classes of fires. Results suggest that (1) variations in airborne charcoal deposition can be explained largely by the size of PCSAs relative to fire sizes and (2) PCSAs are larger than suggested by dispersal data from experimental fires.

## INTRODUCTION

Sediment-charcoal studies began with the analysis of charcoal on pollen slides in an effort to reconstruct watershed-scale fire history over centennial to millennial time scales (e.g. Swain 1973, Cwynar 1978, Green 1982). As summarized by Patterson et al. (1987), these and other early efforts found ambiguous relationships between charcoal abundance and either known or hypothesized fire histories. To explain these ambiguities, Clark (1988a) presented a one-dimensional model of charcoal transport and diffusion for particles of varying sizes and fall speeds. This model predicts that charcoal dispersal distances should increase with wind speed and injection height and decrease with particle size and particle density. Due to the physical differences between microscopic (pollen-slide) and macroscopic charcoal<sup>1</sup>, the former travels long distances ( $10^0$ - $10^2$  km) while the latter is more locally dispersed ( $10^1$ - $10^3$  m). The differences in dispersal distances led

---

<sup>1</sup> We use the term “microscopic charcoal” to refer to charcoal on pollen slides, typically  $< \sim 50$   $\mu$ m in diameter (Patterson et al. 1987). We use the terms “macroscopic charcoal” or “thin-section charcoal” to refer to charcoal pieces  $> \sim 50$   $\mu$ m quantified via the sieving method (Whitlock and Anderson 2003) or thin-section analysis (Clark 1988b).

Clark (1988a) to suggest that the two-dimensional source area of microscopic charcoal was substantially larger than that of macroscopic charcoal, with microscopic-charcoal records representing regional burning and macroscopic-charcoal records representing fires within several hundred meters of a lake. This suggestion has since received empirical support from many studies (Clark and Royall 1995a, Clark and Royall 1996, Whitlock and Millspaugh 1996, Gavin et al. 2003, Lynch et al. 2004a, Higuera et al. 2005b). Nevertheless, there is no strong theoretical foundation for predicting two-dimensional charcoal source areas and for understanding the effects of different source areas on sediment charcoal records.

To explicitly calculate charcoal source areas, Clark's (1988a) one-dimensional model must be expanded into its two-dimensional form. In this paper, we (1) present the two-dimensional form of the Gaussian plume model used by Clark (1988a); (2) evaluate the model's suitability for simulating charcoal dispersal by comparing its predictions to charcoal deposition from an experimental fire; and (3) expand the model to produce a visual and numerical representation of charcoal source area for several classes of fires. This exercise aids the interpretation of fossil charcoal records by illustrating relationships between charcoal source area, fire size, and temporal patterns of airborne charcoal deposition. The framework developed here also serves as a foundation for more complex modeling approaches (e.g. Higuera et al. 2004) that are needed to understand the effects of fire size, charcoal dispersal and charcoal taphonomy on charcoal accumulation in sediment records (Whitlock and Anderson, 2003).

## THEORY

Incidents of gas warfare during World War One led the British government to establish a research program in the 1930's to study the diffusion and transport of particles in the lower atmosphere. Results of this work were published in two papers by Sutton (1947b, 1947a), the second of which presents general formulas for the concentration of smoke particles reaching any point as a function of the particles emitted from a continuous point source at an arbitrary height. Particle deposition in these results was purposely ignored. Chamberlain (1953) generalized Sutton's work to allow for deposition and presented closed-form solutions for the concentration of particles deposited at the ground as:

$$c(x, y) = \frac{2v_g Q(x)}{u p C_y C_z x^{2-n}} \exp\left(\frac{-y^2}{C_y^2 x^{2-n}}\right) \exp\left(\frac{-h^2}{C_z^2 x^{2-n}}\right) \quad (1)$$

$$Q(x) = Q_0 \exp\left\{ \frac{4v_g}{nu C_z \sqrt{p}} \left[ -x^{n/2} e^{-\xi} + \left(\frac{h}{C_z}\right)^{2m} (\Gamma(-m+1) - \Gamma_\xi(-m+1)) \right] \right\} \quad (2)$$

Equations (1)-(2) depend on the parameters described in Table 1.  $\chi$  is the concentration of particles deposited on the ground at the point  $(x, y)$ , assuming the source to be at  $x = 0$ ,  $y = 0$ , and height  $h$ .  $Q(x)$  represents the concentration of emitted particles that have been transported beyond a distance  $x$ . Equation (2) is the same as equation (6) in Clark (1988a). Consequently, Clark's one-dimensional results (i.e. Fig. 4 in Clark 1988a) can be interpreted as the integral over all  $y$  of the two-dimensional results in Figure 1.

Equations (1)-(2) can be understood physically as a map of the proportion of charcoal deposited at varying distances from a single point source. For example, macroscopic charcoal released from a source at  $x = y = 0$ , height  $h = 14$  m, with a  $5 \text{ m s}^{-1}$  wind blowing from left to right would result in charcoal deposition illustrated in Figure 1a. The non-zero skip distance (i.e., no charcoal deposition) in Figure 1a results from the unrealistic

(but mathematically precise) release of particles from a single injection height. In the crosswind ( $y$ ) direction, the deposition is Gaussian for any  $x$  (Fig. 1b), and the integral over  $y$  (Fig. 1c) is analogous to Figure 4 in Clark (1988a).

Due to the symmetry inherent in the solutions of (1)-(2), Figure 1 has an alternate interpretation (also explained by Clark 1988a). It can also be viewed as a map of the proportion of total charcoal deposited at the point  $x = y = 0$  (i.e., the lake center) from each point in the surrounding landscape when the entire landscape burns in an infinitely large fire and wind blows from right to left. Thus Figure 1 also gives a visual depiction of the potential area contributing charcoal to the lake center under the stated assumptions on wind and injection height. Areas burned outside of the contoured source area do not contribute charcoal to the lake center via direct airborne fallout. To make this precise, we define potential charcoal source areas (PCSA) as two dimensional maps analogous to those in Figure 1(a). Each map is normalized by the total accumulated charcoal at the lake center, resulting in a probability density function (PDF)<sup>7</sup>. The term “potential” emphasizes that any single fire does not necessarily contribute charcoal from the entire source area.

## METHODS AND RATIONALE

### Comparison of Theory and Empirical Data

The PCSA described above gives the proportion of charcoal deposited at an arbitrary point from an arbitrary source location; the integral of the PCSA over the area of an

---

<sup>7</sup> The PCSA is defined to be  $PCSA(x,y) = \mathbf{c}(x,y) / \int_1^{\infty} \int_0^{\infty} \mathbf{c}(x,y) dx dy$

entire fire then yields the total charcoal deposited at a given point (i.e., a lake)<sup>8</sup>. To test the realism of this theoretical depiction, we evaluated the ability of equations (1)-(2) to reproduce two-dimensional charcoal deposition patterns from a prescribed fire in boreal Canada (Lynch et al. 2004a) by fixing observed parameters and computing optimum values of the remaining free parameters. In an effort to restrain the number of free parameters and to test the model in its most basic configuration, we assume single values for each of the dependent variables in (1) as in Figure 1.

The 2.25-ha fire studied by Lynch et al. (2004a) was one of several experimental fires in the International Crown Fire Modeling Experiment (ICFME, Stocks et al. 2004). Data from four evenly spaced transects of charcoal traps located 10-200 m from the edge of this fire showed significant variation in charcoal density ( $\text{mm}^{-2} \text{cm}^{-2}$ ) with distance from the fire edge (Fig. 2a, based on Fig. 2 in Lynch et al. 2004a). Lynch et al. (2004a) fit a negative-exponential curve to data from traps located inside as well as outside the fire, which confounded airborne deposition with *in situ* charcoal production. We disregard the data from traps inside fires, as our goal is to test the model for airborne charcoal dispersal away from burned areas. We do not use data from another experimental fire (Clark et al. 1998) because charcoal deposition in this study did not vary substantially within the distances sampled.

We calculated the expected fall speed for each piece of charcoal collected by Lynch et al. (2004a) using equation (1) from Clark et al. (1998). This equation predicts fall speed as a function of particle size, particle density, acceleration due to gravity, and the density and viscosity of air (Clark 1988a, Clark et al. 1998). Since (1)-(2) are relatively insensitive to

---

<sup>8</sup> The total accumulated charcoal from a fire is equal to  $\int \int_{fire} \text{PCSA}(x,y) dA$ .

variations in fall speed compared to injection height (see Results below), we used the mean fall speed of all samples in all transects in the subsequent analysis.

In the six fires of the ICFME, mean wind speeds at 10-m height varied between 3-7 m s<sup>-1</sup> during burning (Taylor et al. 2004); we use  $u = 5 \text{ m s}^{-1}$  as the estimated wind speed in the following analysis. Although the wind direction observed at the time of the burn was generally away from the fire and parallel to the direction of the transects (Jason Lynch, personal communication), the systematic difference in the magnitude of the charcoal deposited in transects 1, 2 vs. 3, 4 (Fig. 2) suggests wind direction was at some angle  $\theta$  to transect direction. We allow for this possibility by treating wind direction as a free parameter. The injection height and source strength  $Q_0$  (i.e. charcoal production) are less constrained by observations. Accordingly, we take the effective injection height  $h$  to be a free parameter and scale source strength  $Q_0$  to the maximum observed charcoal density ( $\text{mm}^{-2} \text{ cm}^{-2}$ ) in the charcoal traps. With these choices, we can calculate the total charcoal transported to each of the trap locations using equations (1)-(2). We then used the observed charcoal density in the traps to compute optimum values of  $\theta$  and  $h$  in the non-linear least-squares sense (i.e.  $\theta$  and  $h$  minimize the root-mean-square error of the difference between predicted and observed charcoal density in each of the 27 traps).

### **Sensitivity and Expansion of the Analytical Model**

The Lynch et al. (2004a) fire was small compared to naturally occurring wildfires in boreal forests (Kasischke et al. 2002). Given that plume heights are a function of heat release (Chandler et al., 1983, cited in Clark, 1988a), which in turn is related to fire intensity and arguably to fire size, the optimum injection height from our comparison with Lynch et al.'s (2004a) experimental burn is probably at the lower bound of actual

injection heights. We therefore consider the sensitivity of (1)-(2) to a range of injection heights  $h$ . In addition, fall speed  $v_g$  and wind speed  $u$  are expected to exhibit large variability both within and between fires. Since  $v_g$  and  $u$  only appear in (1)-(2) as the ratio  $v_g/u$ , we examine sensitivity to changes in either parameter from changes in  $u$  solely. We assess the sensitivity of (1)-(2) to both injection height  $h$  and wind speed  $u$  by varying each parameter independently while holding all other parameters constant.

Variations in wind direction become important as fire size and duration increase. To calculate PCSAs that include variations in wind direction, we assume that wind directions vary proportionally to the average June-August wind directions recorded in Bettles, Alaska (1971-2000) and that each fire lasts long enough to adequately sample this distribution. To include variations in injection heights, we assume a distribution of  $h$ , characterized by modal injection heights  $h_{mode}$  of 10, 100, 1000 m. We also assume that this distribution is negatively skewed, with a peak at large injection heights and a long tail at smaller heights (Fig. 4, row 1), based on two observations. First, small charcoal particles that dominate charcoal deposition in experimental burns (Clark 1988a, Lynch et al. 2004a) are lofted to greater heights in a fire's turbulent plume than are larger particles, leading to an upward bias in injection heights. Second, fire activity is favored in warm, dry atmospheric conditions, often accompanied by strong inversions. These inversions place a cap on plume height by trapping smoke below the inversion. In practice, the shape of the  $h$  distribution has a predictable effect on the shape of the PCSA as explained below. All other parameters for calculating each PCSA are the same as used for predicting the Lynch et al. (2004a) dataset.

We present PCSAs by displaying the (1) cumulative amount of charcoal reaching a lake from within a range of radial distances, and (2) map of total charcoal reaching a lake

from each part of the PCSA. Both approaches illustrate the size of the PCSA; the second shows the variability in charcoal deposition from within the PCSA due to varying wind direction and distance-from-lake.

## RESULTS

The two-dimensional model captured the spatial pattern of charcoal dispersal (with  $\theta = 55^\circ$  and  $h = 14$  m) by predicting the strong dependence of charcoal density ( $\text{mm}^{-2} \text{cm}^{-2}$ ) on both  $x$  and  $y$  distances (Fig. 2b). Quantitatively, the model explained 67% of the variation in the observed data ( $r^2 = 0.67$ ,  $p < 0.001$ ). The less-than-perfect correlation occurs because observed charcoal densities peak at 40 m but the model predicts nearly constant density from 10-40 m, with a rapid decrease at greater distances. The model also tends to under predict the lowest charcoal densities.

Both the size of the charcoal source area and the skip distance resulting from (1)-(2) are highly sensitive to injection height  $h$ , scaling approximately with  $h^2$  and  $h$ , respectively (Fig. 3a). In contrast, source area and skip distance are relatively insensitive to wind speed  $u$  (Fig. 3b). Thus the dependence of (1)-(2) on wind speed can be neglected given realistic variability in injection height.

Charcoal transport for the 10-, 100-, and 1000-m  $h_{mode}$  scenarios is inconsequential from distances greater than of  $\sim 200$ , 1500, and 15,000 m, respectively (Fig. 4, row 2), and skip distances are negligible as compared to those in Figure 3b. In each scenario, the center of the domain (i.e. the lake) receives a nearly constant proportion of charcoal from each distance, resulting in a nearly linear increase in cumulative charcoal deposition (Fig. 4, row 2). Most airborne charcoal deposited at the lake comes from pixels closest to the

lake and from pixels “up-wind” of the lake and along the dominant wind directions (darkest portions of Fig. 4, row 3).

## DISCUSSION

Our explicit method for computing charcoal deposition on a two-dimensional landscape reasonably depicts the charcoal deposited from an experimental fire. The largest drawback to our method is that it remains untested for large, wildland fires. Large fires would create greater spatial and temporal complexity than the experimental burn we examined, and it is unclear how this complexity would affect our assumptions (e.g. of injection heights). In addition, the theory underlying the analytical model was developed from smoke diffusion experiments and previously remained untested for particles as large as macroscopic charcoal. Despite these caveats, the agreement between predictions from the model and observed charcoal deposition patterns (Fig. 2; Lynch et al. 2004a) suggests that the model is a reasonable depiction of the processes of airborne charcoal dispersal and charcoal source areas.

Our simulated PCSAs motivate two simple hypotheses about conditions creating variable peak heights in sediment-charcoal records. First, the variability in airborne charcoal deposition to a lake depends on the relationship between PCSAs and fire sizes (i.e. the source-area to fire-size ratio). For example, if a 100-ha fire originates within a small PCSA (e.g. ~ 30 ha, represented by the 10 m  $h_{mode}$  scenario; Fig. 4, column 1), it will almost always cover the entire PCSA, resulting in charcoal peaks equal to one. In this scenario, multiple 100-ha fires would create a nearly binary pattern of airborne charcoal deposition through time, with distinct peaks when fires burn within the source area and no charcoal otherwise. With larger PCSAs (represented by 100 and 1000 m  $h_{mode}$

scenarios; Fig. 4, row 3), the potential locations of 100-ha fires within the PSCA increase. This would result in greater variability in airborne charcoal deposition due to location alone, because fires close to a lake deposit more charcoal than fires far from a lake. A larger PCSA also allows for more fires of varying sizes to occur within the PCSA, creating further variability in charcoal deposition through time.

Second, boreal-forest PCSAs are likely larger than those implied by Lynch et al. (2004a; Fig. 4) and similar charcoal-dispersal datasets (Clark et al. 1998, Ohlson and Tryterud 2000). In particular, the lack of binary patterns of charcoal deposition in boreal forest sediment records (e.g. Carcaillet et al. 2001a, Lynch et al. 2002, Lynch et al. 2004b), as describe above, argues against the short charcoal dispersal distances suggested by these studies. Larger PCSAs should result in variability in charcoal peak heights resembling empirical records, because a large range of fire sizes can burn within a PCSA. Given that the potential area for fires to burn increases by the square of radial distance, increased area at long distances provides more opportunities for long-distance (e.g. > 1-10 km; Whitlock and Millspaugh 1996, Pisaric 2002, Hallett et al. 2003) rather than short-distance dispersal. Thus, even while charcoal dispersal is strongly biased towards short distances, charcoal from long distances can ultimately comprise a significant proportion of overall charcoal reaching a lake (Fig. 4, row 2).

Overall, our results suggest that the variability in sediment charcoal records can largely be explained by the fundamental characteristics of charcoal deposition. Based on explicit representations of PCSAs, we propose that variations in the source-area to fire-size ratio and the size and location of fires within PCSAs significantly affect patterns of charcoal deposition. An explicit simulation-modeling approach should be fruitful for testing this hypothesis and understanding these patterns in greater detail. The theoretical framework

and analytical model developed here are a foundation for this next step in modeling the effects of charcoal deposition on sediment charcoal records.

#### **ACKNOWLEDGEMENTS**

Funding was provided by the National Science Foundation through a Graduate Research Fellowship to PEH and grant # 0112586 from the Arctic System Science program to Linda Brubaker. We thank Jason Lynch for providing the charcoal dispersal data, making this work possible. Discussions with J. Agee, L. Brubaker, D. Gavin, and D. Sprugel were tremendously helpful. The Bettles, AK wind data were provided by the Alaska Climate Research Center via their website <http://climate.gi.alaska.edu>.

## TABLES

Table 1. Description of the parameters in equations (1)-(2).

Parameter	Description / source
$x$	distance downwind
$y$	distance crosswind
$v_g$	deposition velocity
$Q_0$	source strength
$u$	mean wind speed (see Sutton 1947a)
$C_y, C_z$	Diffusion constants (we use $C_y = 0.21$ , $C_z = 0.12$ ; see Sutton 1947a)
$h$	source height
$n$	measure of turbulence near ground (we use 1/4; see Sutton 1947a)
$m$	$n/(4-2n)$
$\mathbf{x}$	$h^2/(x^{2-n}C_z^2)$
$(\Gamma(-m+1) - \Gamma_{\xi}(-m+1))$	$= -m \int_{\xi}^{\infty} e^{-t} t^{-m-1} dt$

### FIGURE CAPTIONS AND FIGURES

**Figure 1.** (a) Map of charcoal density on a flat landscape deposited from a continuous point source located at  $x = y = 0$  m and height  $h = 14$  m, with wind blowing from left to right with wind speed  $u = 5$  m s<sup>-1</sup>. The depositional velocity  $v_g = 1.56$  m s<sup>-1</sup> was calculated from empirical data collected by Lynch et al. (2004a), as described in “Methods”. (b) A cross section in the  $y$ -direction along the line labeled A-B in part (a). (c) The integral over all  $y$ .

**Figure 2.** Result of fitting the dispersal model (1)-(2) to the observed data from the ICFME fire studied by Lynch et al. (2004a). (a) Layout of the fire studied by Lynch et al. (2004a) trap locations with transect numbers, and the best-fit wind angle. (b) Predicted (lines) and observed (circles) charcoal densities for the four transects.

**Figure 3.** Sensitivity of the dispersal model (1)-(2) to injection height and wind speed. All plots as in Figure 1a, except note that the horizontal scale in (a) varies across two orders of magnitude, while the scale in (b) remains relatively constant. (a) Injection heights of 10 m, 100 m and 1000 m, from left to right, with the wind held constant at 5 m s<sup>-1</sup>. (b) Wind speeds of 0.5, 5 and 50 m s<sup>-1</sup>, from left to right, with the injection height held constant at 10 m,

**Figure 4.** Potential charcoal source area (PCSA) for three modal injection height scenarios (columns), including distribution of injection heights (row one), cumulative charcoal deposited at the lake at increasing distances (row two), and a map of the PCSA, including the empirical wind data from Bettles, Alaska, used to simulate variable wind direction (row three). Color bars in row three represent charcoal density.

Figure 1.

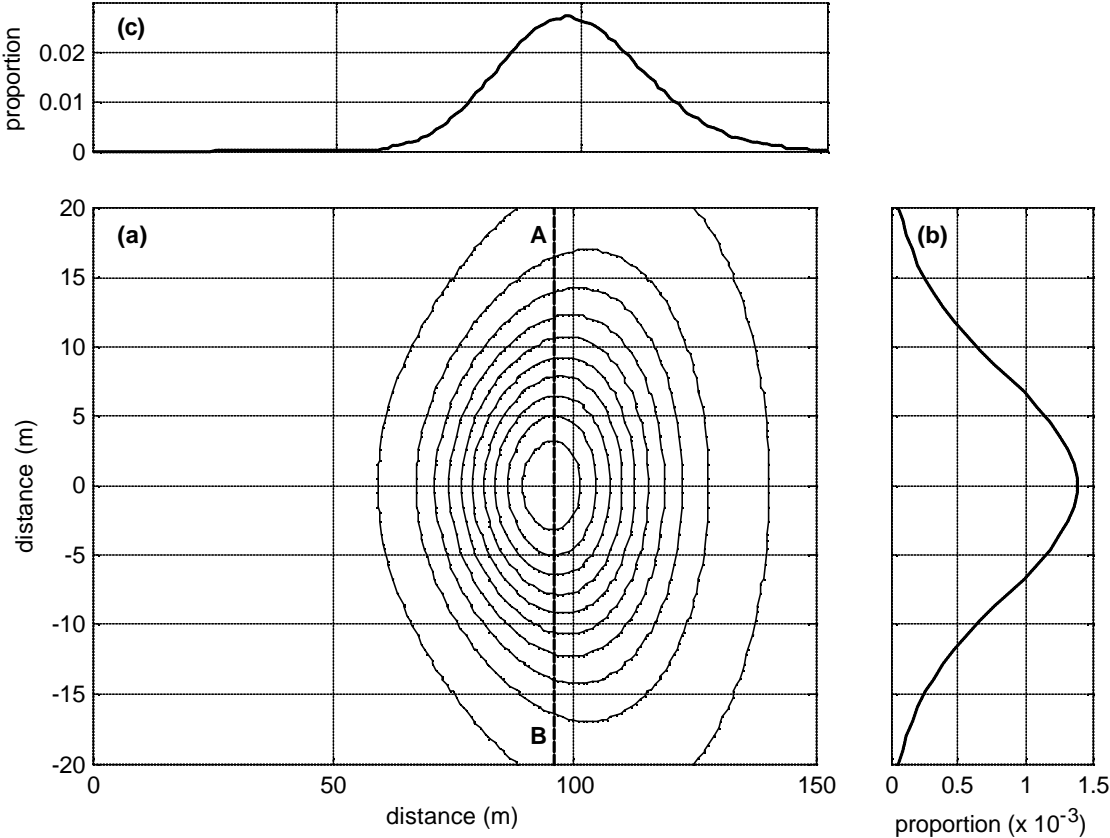
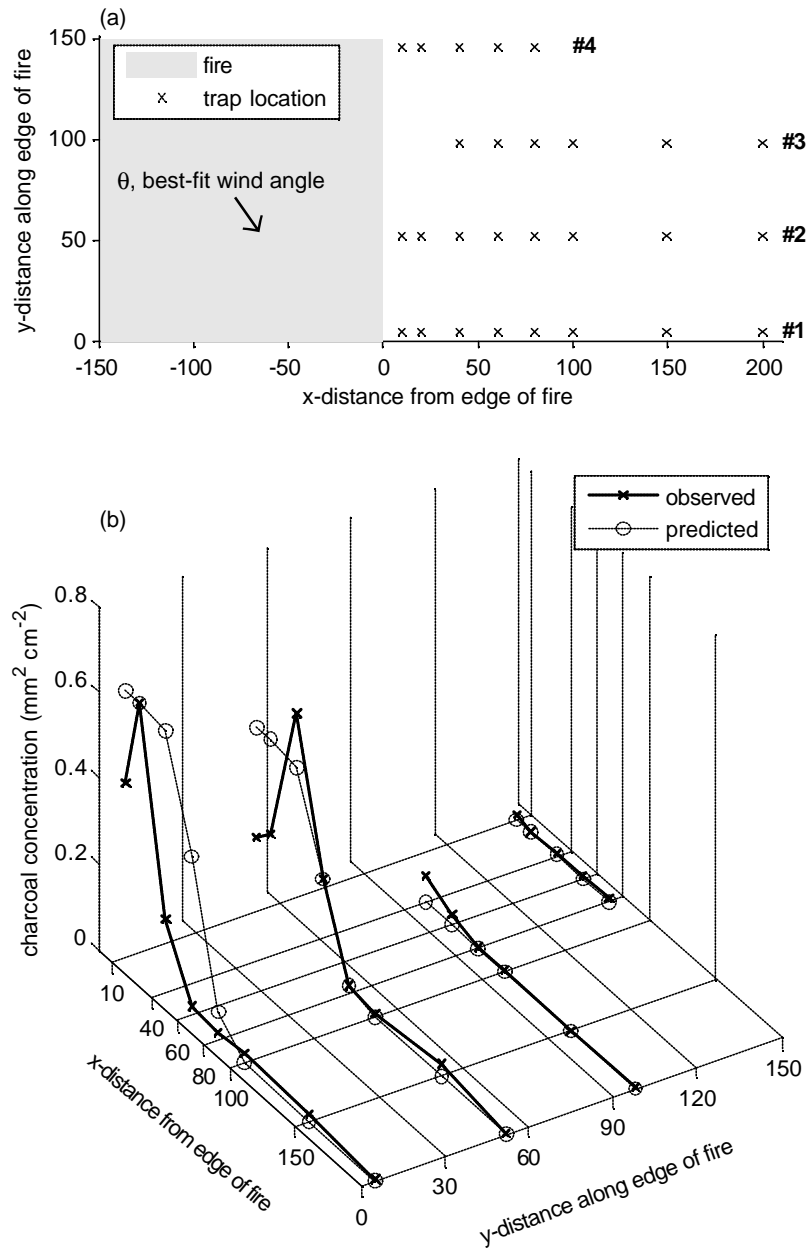


Figure 2.



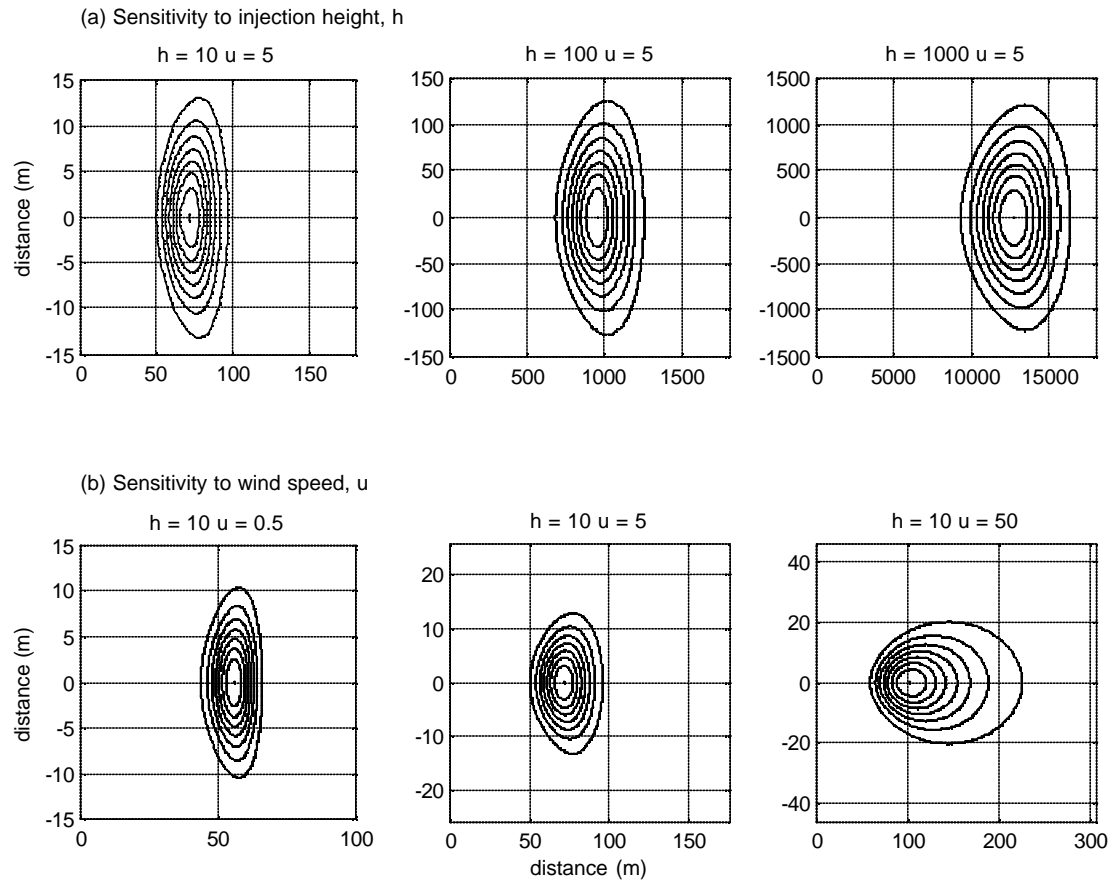
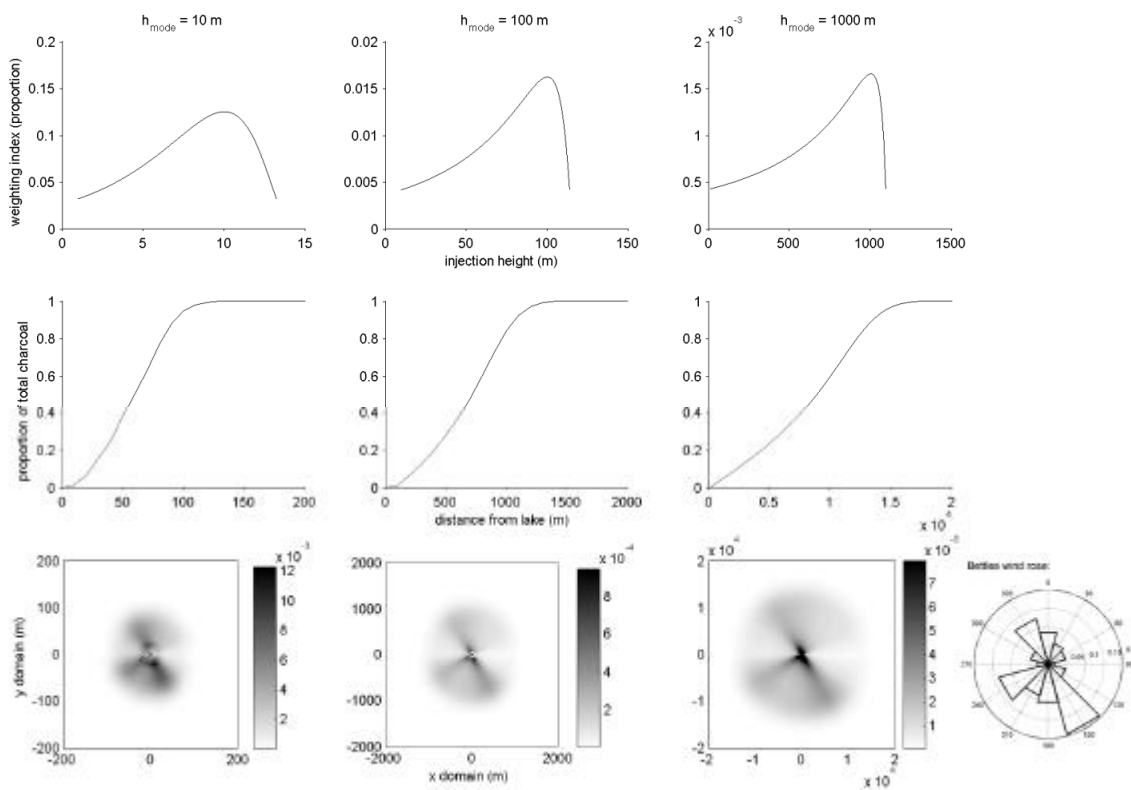
**Figure 3.**

Figure 4.



## APPENDIX B: SENSITIVITY TO ASSUMPTIONS ON WIND DIRECTION AND THE DISTRIBUTION OF INJECTION HEIGHTS

A single injection height is an unrealistic assumption for dispersal from a buoyant plume, and it results in large skip distances at relatively low injection heights (Clark 1988a). Thus, we assume the distribution of injection heights resulting from any single fire is continuous with negative skewness (a peak at large injection heights and a long tail at smaller heights; see Appendix A). We considered two other possibilities for the distribution of injection heights: (1) injection heights vary log-normally, with most particles exiting a plume at low elevations but a decreasing proportion exiting at much higher elevations and (2) injections heights vary normally, with most particles exiting a plume at a given elevation, and an equal number of particles exiting at given distances above and below this modal injection height. Together with the negatively skewed scenario, these three scenarios would result in three different cumulative distributions functions describing charcoal deposition with increasing radii from a lake (analogous to row two in Fig. 2.2 in Chapter 2).

We evaluated the effects of all three assumptions by creating generic dispersal tables resulting in cumulative distribution functions that are convex ( $y = r^{0.25}$ ), linear ( $y = r^1$ ), and concave ( $y = r^{1.75}$ ) (Fig. 6.1). The PCSA in each scenario, defined by the distance from which 100% of the total charcoal deposited at the lake originates, had a radius of 15 km. We also tested the sensitivity of the model to assumptions on wind direction by simulating identical fire regimes with and without variable wind.

The sensitivity tests have two important results. First, for any given dispersal scenario, variation in wind direction do little to change the fundamental relationship between  $C_{air}$  and area burned at a given spatial scale (Fig. 6.1). While wind reduces the maximum correlation between  $C_{air}$  and area burned, as expected, the degree of this reduction is minor compared to the variations associated with the changing radii considered. Second, assumptions on the distribution of injection heights change the degree to which a charcoal record is locally biased (or distance weighted), as illustrated

by the relationship between  $C_{air}$  and area burned (Fig. 6.1). While the radius of maximum correlation varies between scenarios, the more important difference is in the variations associated with different radii. The convex scenario is the most locally-biased record, followed by the linear and concave scenarios (Fig. 6.1).

We chose to simulate injection heights based on the assumptions that most particles exit a plume at a high elevation and proportionally smaller numbers of particles exist at lower elevations (the negatively skewed scenario in the first paragraph above). This is analogous to the linear cumulative charcoal distribution, the middle-of-the-road scenario. Although we model a single fall speed (which is a function of particle size), we also use the injection height distribution to implicitly represent some of the variation in particle sizes observed in empirical records (Clark et al. 1998, Lynch et al. 2004a). Smaller particles are lofted higher than larger particles, due to the same properties influencing particle dispersal. We assume that from any given 1 ha pixel in CharSim, the majority of particles injected in a plume are small and lofted to heights near the modal injection height, while a decreasing proportion of particles (assumed to be larger) are injected to proportionally smaller injection heights. The effect of particle size on subsequent transport is small and can be neglected compared to the effect on injection height (Appendix A).

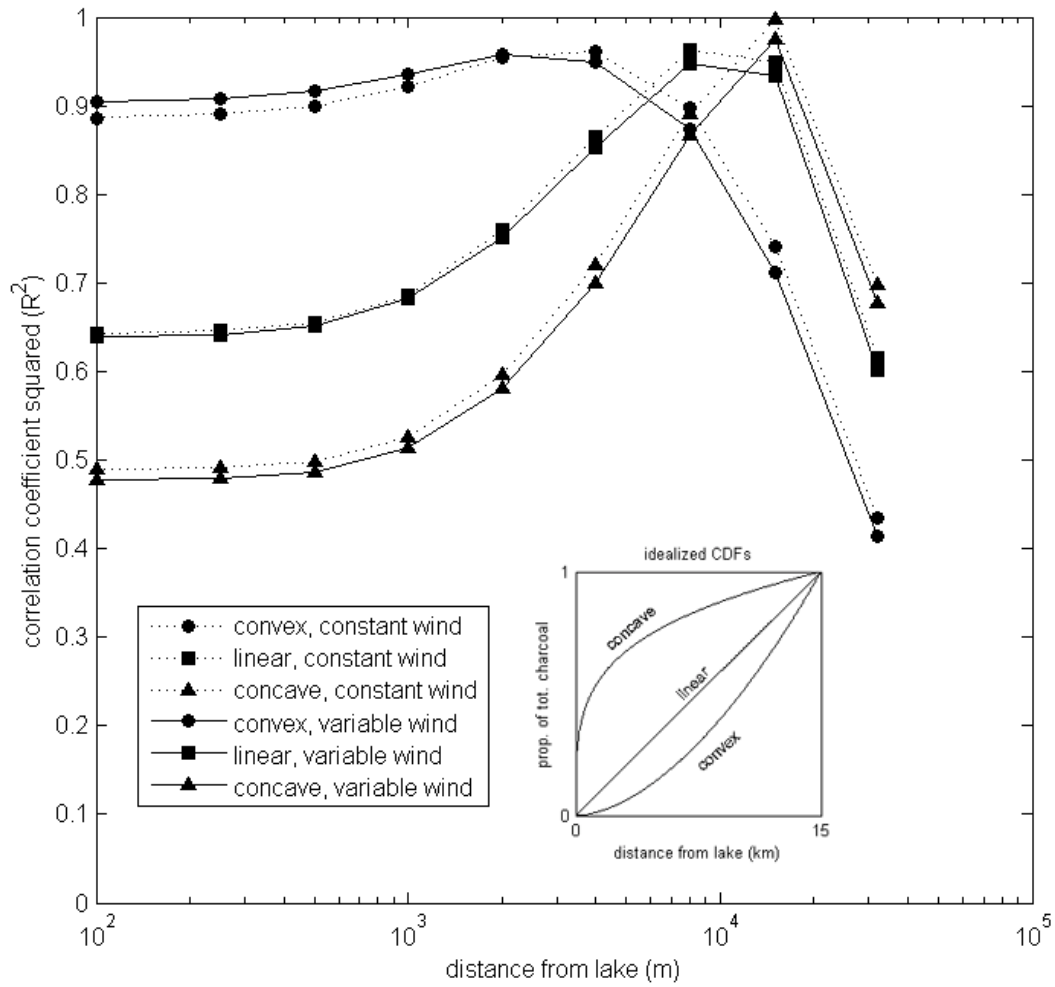


**Figure 6.1.** Correlation of airborne charcoal accumulation and area burned as a function of spatial scale for different cumulative charcoal distributions (symbols, see inset) and wind scenarios (dashed or solid line, variable or constant).

### APPENDIX C: MODERN ANALOG ANALYSIS WITH FOSSIL POLLEN SAMPLES

We used squared-chord distances (SCD) and receiver operating characteristic (ROC) curves (Gavin et al. 2005) to evaluate the similarity of fossil samples to the 3654 surface samples north of 40° N latitude from the North American Pollen Database (dataset summarized and described by Whitmore et al. (2005; Fig. 7.1). Only samples from Arctic Tundra ("Arctic" in Whitmore et al. 2005), Boreal Forest, and Forest Tundra were used for comparisons, because they yielded minimum SCD values (indicating maximum similarity) when comparing fossil samples to all modern samples in a preliminary analysis. ROC curves were constructed for each biome by comparing modern pollen assemblage (including 57 taxa) of every sample in each of the other two biomes to every sample in the Tundra (206 samples), Boreal Forest (856 samples), or Forest-tundra (405 samples) biome (Fig. 7.2). For example, for the Boreal Forest ROC curve, each sample in Tundra and Forest-tundra was compared to each sample in Boreal Forest. For each comparison, the mean of the lowest 1% of all SCD values was recorded. The area under the ROC curve (AUC) is an objective measure of the SCD metric to discriminate a given biome from the other two biomes, and ROC curves are useful when  $AUC > 0.05$  (no ability to discriminate pollen assemblages from a given biome);  $AUC = 1.0$  represents perfect discrimination between. AUC values for Arctic Tundra, Boreal Forest, and Forest-tundra were 0.88, 0.79, and 0.76, respectively (Fig. 7.2). For each SCD value (in 0.01-increment bins) a likelihood ratio was calculated from each ROC curve and fit with a negative exponential model ( $\log[\text{likelihood ratio}] = a\text{SCD}^b + c$ ; Fig. 7.2). Based on prior odds of 1/3 (i.e. each sample has a 1/3 chance of coming from 1 of the 3 biomes), the likelihood ratio values were used to calculate posterior odds (posterior odds = likelihood ratio x prior odds), and ultimately posterior probabilities (posterior probability = posterior odds / (1 + posterior odds) (Fig. 7.2; Gavin et al., 2005). To classify fossil samples, each sample (including 17 taxa) was compared to all modern samples within each of the three biomes. The mean of the lowest 1% of all SCD values was used to calculate the probability that the fossil assemblage was an analog to each of the three biomes used, based on the probably-of-analog calculations described above.

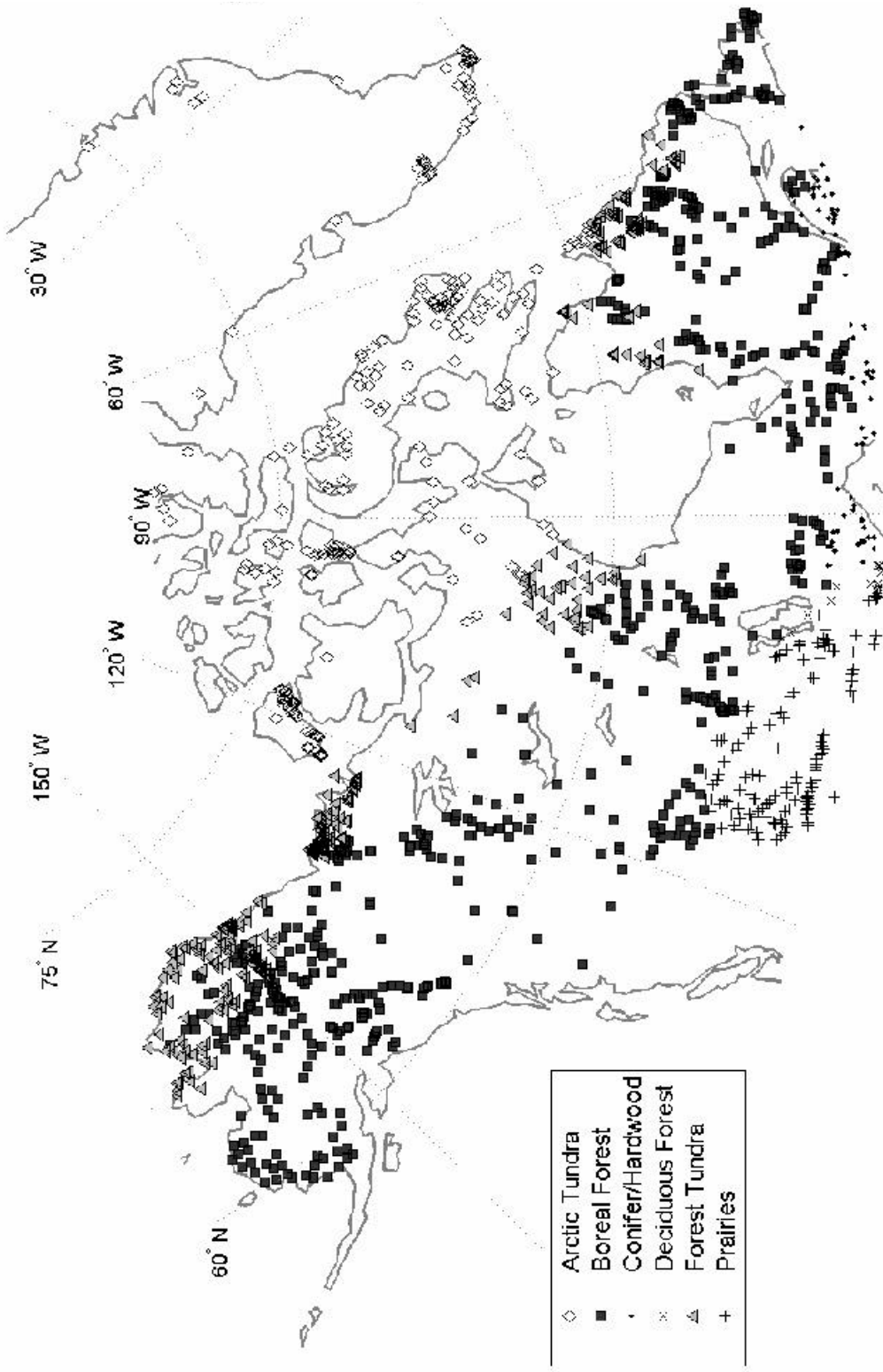


**Figure 7.1.** Distribution of modern pollen samples from the NAPD dataset, classified according to biome (as in Whitmore et al. 2005)

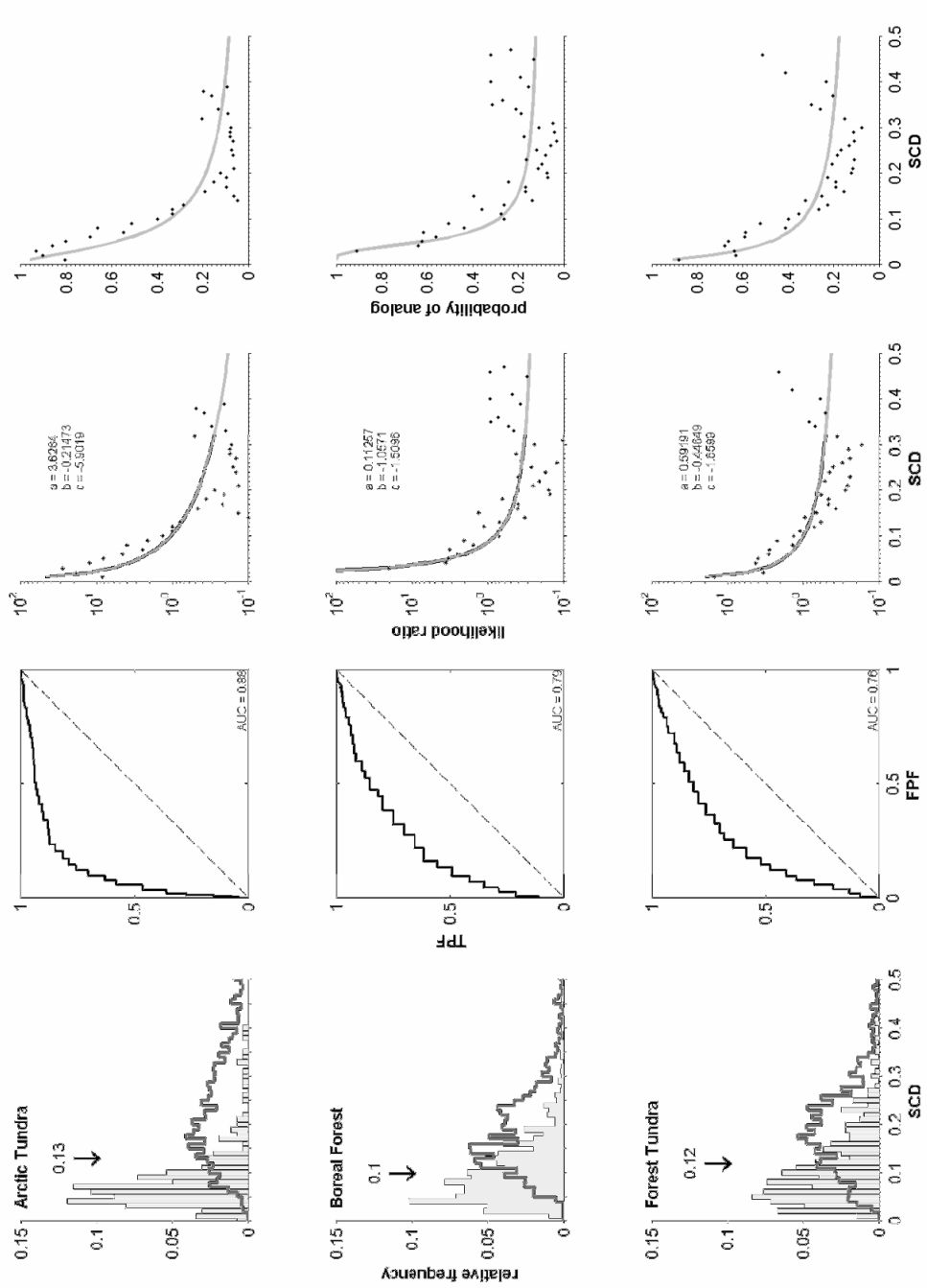


**Figure 7.2.** Distributions of SCD values for within- and between-biome comparisons, with the optimal threshold value identified (column 1), ROC curves with AUC value (column 2), likelihood ratios as a function of SCD values (column 3), and probability of analog as a function of SCD values (column 4) for each biome (rows). See text for details.

**APPENDIX D: DETECTING CHANGES IN FIRE-FREQUENCY REGIMES: SAMPLE SIZE AND STATISTICAL POWER**

**INTRODUCTION**

Fire occurrence at any point in time or space is controlled by a suite of factors, including climate (seasonal through decadal temperature and moisture patterns), weather (daily to monthly temperature and moisture patterns), topography, vegetation (abundance and flammability), and ignitions. Each variable contains a stochastic component creating variability in fire occurrence, and therefore changes in fire frequency can represent either a shift in the state of these systems or simply their inherent variability. In a statistical framework, comparing two fire regimes requires a null hypothesis that the differences observed between two “populations” (i.e. fire regimes) are due to chance alone, and an alternative hypothesis that the two populations truly differ. Interpretations of fire frequency regimes, if one aims to compare patterns in time or space, can therefore benefit from a statistical test to quantify the possibility of Type I and Type II errors. In this case, a Type I error is falsely concluding that two fire frequency regimes are not similar, and a Type II error is falsely concluding that two fire frequency regimes are similar.

Inferences on fire occurrence are often based on data from fire scars and sediment charcoal records, which provide direct evidence of fire timing, or from stand age and soil charcoal data, which provide time-since-fire estimates. Both types of data help characterize the distribution of fire return intervals for a given temporal and/or spatial domain. I term this characterization the “fire-frequency regime”, and it describes the probability of a site burning as a function of the time passed since the last fire occurred. Fire-return-intervals (yrs/fire) are simply the inverse of fire frequency (fires/yr). Often a

distribution of fire return intervals can be accurately described by a Weibull model, as has been done in both the Southwestern U.S. and North American boreal forests. The Weibull model is advantageous over simply reporting a single fire frequency or mean fire return interval because it contains information about the variability of fire occurrence, is easily converted into a hazard function, and can also be used for predictive purposes. Fitting fire occurrence data with a parametric model is also advantageous because it facilitates more powerful statistical comparisons than are possible with non-parametric methods (e.g. K-S test).

In this paper I (1) illustrate the risks of comparing fire occurrence data in the absence of statistical analyses, (2) present a likelihood ratio test to explicitly test the null hypothesis of no difference between two populations, and (3) calculate the relationships between sample size and statistical power for the likelihood ratio test and show that it is more powerful than two alternative statistical techniques. Finally, based on the sample-size power analyses, theoretical and practical conclusions are drawn for conceptualizing fire regimes and designing studies to detect changes in fire occurrence over space and time.

### **Quantifying fire-frequency regimes with Weibull distributions**

By fitting a parametric distribution, such as the Weibull, to fire-return intervals one makes two important assumptions. First, each fire-return-interval is assumed to be an independent sample. Therefore, one must account for the possibility that a single (large) fire burned two sampling sites at the same time. Counting this single fire return interval

twice would be pseudo-sampling and thus falsely increase sample size. Second, and perhaps more importantly, the variables that control fire occurrence (e.g. climate, vegetation, topography, etc.) are assumed to be constant over the entire sampling domain, which can be space and/or time. These assumptions are implicit in any comparison between two sets of fire-return intervals, and they can be tested by measuring physical and biological variables across space and/or time. The appropriateness of a Weibull distribution as a description of any set of fire return intervals can and should be tested with a goodness-of-fit test (e.g. a one-sample Kolmogorov-Smirnov [K-S] test; Johnson and Gutsell 1994, Grissino-Mayer 1999).

Grissino-Mayer (1999) illustrates the utility of the Weibull distribution as a descriptor of fire frequency regimes, with specific examples from ponderosa pine forests of the American Southwest. A similar approach has been used describe fire frequency regimes in boreal forests of eastern and northern North America (Clark 1989, Johnson 1992, Clark et al. 1996, Lynch et al. 2002). Weibull distributions can have two or three parameters, but I focus here on the two-parameter form because it is ecologically realistic, simplifies fitting the distribution to observed data, and more easily allows for comparisons between sites (Grissino-Mayer 1999).

The two-parameter Weibull has a scale parameter,  $b$ , and a shape parameter,  $c$ , and its probability density function (PDF), describing the probability of fire occurrence given the time-since-fire,  $t$ , is defined as:

$$f(t|b,c) = cb^{-b}t^{b-1} \exp(-[t/b]^c) \quad (1)$$

Two other expressions of the Weibull have unique ecological interpretations: the cumulative distribution function,  $F(x)$ , and the hazard function,  $A(x)$  (see Clark, 1989, Johnson 1992, Grissino-Meyer, 1999, for a detailed description of these forms and their interpretations). The scale parameter defines the 63<sup>rd</sup> percentile of the Weibull distribution and is directly related to the modal fire return interval ( $MOI = b [(c-1)/c]^{1/c}$ , Grissino-Mayer, 1999). The shape parameter,  $c$ , determines the skeweness of the distribution and also has an associated ecological interpretation:  $1 < c < 3$  indicates that the probability of fire increases with time-since-fire and suggests that fuel build up is an important factor controlling fire occurrence (Clark 1989).  $c \sim 1$  yields a negative exponential PDF, which indicates that the probability of fire does not change as time-since-fire increases and suggests that variables not associated with fuels control fire occurrence (e.g. large-scale climate variability; Johnson 1992). When  $3.25 < c < 3.61$  the Weibull distribution is approximately normal.

Clark (1989) described a method of fitting observed data with a two-parameter Weibull distribution that utilizes maximum likelihood techniques, and the frequently used program FHX(2) (Grissino-Mayer 1995) employs a similar maximum-likelihood based technique for fitting fire-return-intervals distributions with Weibull models. Additionally, analytical packages such R, S+ and MatLab have pre-made functions that fit Weibull parameters to observed data using maximum likelihood techniques. The maximum likelihood approach is thus a commonly used means for fitting fire-return-interval data with Weibull models. The likelihood ratio test described below relies on maximum likelihood estimates and can thus be used on any set of distributions that were fit with maximum likelihood techniques.

### **Comparing distributions of fire return intervals**

Figure 8.1 illustrates the random variability inherent in fire occurrence data and the potential to draw false conclusions from visual comparisons of fire frequencies. While many studies have quantified fire-return-interval data using Weibull distributions, few make explicit comparisons between different distributions (e.g. Clark et al. 1996, Lynch et al. 2002, Gavin et al. 2006). There are at least three possible methods for comparing two populations of fire-return-intervals: (1) use a non-parametric test, such as the K-S test (e.g. Clark 1989, Gavin et al. 2006); (2) bootstrap confidence intervals for each Weibull parameter generated from maximum likelihood fitting (e.g. Lynch et al. 2002); (3) utilize a likelihood-ratio test. The third method is the focus of this paper, and it utilizes both parameters of the Weibull distribution. Non-parametric tests are less powerful than parametric tests, and generating confidence intervals and comparing individual Weibull parameters only addresses one aspect of the distribution, in isolation from the other parameter. Therefore, so long as the Weibull distribution yields a satisfactory fit to the observed data, the likelihood ratio test described here should provide a more powerful test than previously used methods by utilizing information on both the  $b$  and  $c$  parameters.

### **A likelihood ratio test for comparing Weibull distributions**

When comparing two populations of fire return intervals with the likelihood ratio test we explicitly test the following null hypothesis against its alternative:

$$H_0 : b_1 = b_2 \text{ AND } c_1 = c_2$$

$$H_a : b_1 \neq b_2 \text{ OR } c_1 \neq c_2$$

The likelihood-ratio test relies on a test statistic,  $T$ , computed by taking the ratio of (1) the maximum likelihood estimate (MLE) under the constraints of the null hypothesis and (2) the MLE with the constraints of the null hypothesis relaxed. This is analogous to conceptualizing the null hypothesis as a simplified model with only two parameters (i.e. a single Weibull  $a$  and  $b$  parameter), and the alternative hypothesis as a more complex model, with four parameters (i.e. two distinct Weibull  $a$  and  $b$  parameters). The MLEs are those parameters that maximize the likelihood function, which itself depends upon the unknown parameters ( $b$  and  $c$ ) of the probabilistic data-generating process. In practice, the logarithm of the likelihood function is used, but MLEs maximize both the ordinary likelihood and the log likelihood function. The log-likelihood function for the two-parameter Weibull transformation is:

$$l = \log L = \log \prod_{i=1}^n f(b, c | t_i) = \sum_{i=1}^n \log f(b, c | t_i) \quad (2)$$

The test statistic for the likelihood ratio test,  $T$ , is:

$$T = 2(l_{H_1} - l_{H_0}) = 2(l_{1H_1} + l_{2H_1} - l_{H_0}) \quad (3)$$

where  $l_{1H_1}$  and  $l_{2H_1}$  are the MLEs obtained by fitting a separate Weibull model to the data from each population, and  $l_{H_0}$  is obtained by fitting a single Weibull model to the combined dataset. If the true parameters for each population are equal, then the distribution of  $T$  should be approximately Chi-Square with  $k$  degrees of freedom, where  $k$  is the total number of parameters that differ between  $H_0$  and  $H_1$  ( $k = 2$  when comparing a two-parameter model to a four-parameter model). The null hypothesis is rejected when  $T$

is greater than a Chi-Square value with  $k$  degrees of freedom at the  $1 - a$  percentile, where  $a$  is the pre-specified significance level.

In practice, and particularly for small sample sizes, the true distribution of  $T$  under the null hypothesis is unknown, but it can be estimated using permutations. Under the assumption of the null hypothesis (i.e. no difference between two populations), one can permute the labels of Population 1 and Population 2 and obtain a new data set as likely as the original data set. Repeat this for  $J$  trials, for each trial compute a new statistic  $T_j$ , and record  $H_j$ :

$$\begin{aligned} H_j &= 1 & T_j < T \\ H_j &= 0 & T_j \geq T \end{aligned}$$

where 1 and 0 correspond to rejecting or failing to reject the null hypothesis, respectively. Using the newly computed statistics,  $T_j$ , one can approximate the probability that the two populations do not differ by taking the proportion of trials where the null hypothesis was rejected. If the two populations truly differ, then  $T_j$  should be smaller than  $T$  most of the time (i.e.  $H_j = 1$ ) and thus the approximated p-value should be small. Using the permutation test, the null hypothesis is rejected when the approximated p-value is smaller than  $a$ , where  $a$  is the pre-specified significance level (Fig. 8.1).

## METHODS

### Sample-size power analysis for the likelihood ratio test

To determine (1) the relationship between sample size and statistical power for the likelihood ratio test, and (2) the power of the likelihood ratio test relative to two

alternative techniques, I used a simulation approach to calculate statistical power for a variety of sample sizes and population-to-population comparisons. Analytical approaches are not available for all three methods, and therefore the simulation approach was desirable. Each sample-size – power comparison was done using a single Weibull shape parameter,  $c$ .

For a given shape parameter,  $c$ , I constructed a base population by generating  $n$  random numbers from a Weibull distribution with a given scale parameter,  $b$ . This base population was compared to five other populations, generated in the same fashion, but where  $b$  increased by 25% each time. Thus, the base population was compared to Weibull populations with a  $b$  parameter that increased by 25,50...125%. For each comparison, I conducted one of three “tests” to test the null hypothesis that the two populations came from the same Weibull distribution (tests are described below). I repeated this process 1000 times and used the proportion of times the null hypothesis was rejected as an estimate of statistical power:  $1-\beta$ , where  $\beta$  is the probability of falsely accepting the null hypothesis. To evaluate how statistical power changed with sample size, the above procedure was repeated for 10 different sample sizes,  $n$ , where  $n = 10, 20...100$ .

I used three different statistical tests to test the null hypothesis of no difference between each population compared, with an alpha level of 0.10 for each test. First, I used the likelihood ratio test, as described earlier, with the p-value estimated via 100 permutations. Second, I used 1-alpha percent confidence intervals on the Weibull  $b$  parameters estimated via maximum likelihood techniques, and I rejected the null hypothesis when these confidence intervals did not overlap (Lynch et al. 2002). The confidence intervals were generated by resampling the original data, with replacement,

100 times. The third approach was simply a two-sample K-S test, which makes no assumptions about the underlying distribution from which the data came (Clark 1989).

Finally, for the likelihood ratio test only, I repeated the sample-size power analysis using  $c = 1, 2, 2.5,$  and  $3,$  to illustrate how varying  $c$  parameters affect sample-size – power relationships. This serves as a tool for coarsely evaluating the statistical power of comparisons made via the likelihood ratio test and for designing future studies that seek to discriminate between two potentially different fire-frequency regimes.

## RESULTS

For any given comparison at any sample size, the likelihood ratio test is the most powerful statistic, followed by the “confidence interval” test and lastly by the K-S test (Fig. 8.2). At sample sizes below  $< c. 50,$  the likelihood ratio test utilizing permutations to estimate p-values is slightly more conservative with respect to rejecting  $H_0$  (i.e.  $\sim 5\%$  less powerful) than the likelihood ratio test using p-values derived from a Chi-Square distribution. Statistical power increases by approximately  $5\%$  or more for any comparison between these different tests. In some cases the difference between the K-S, “confidence interval”, and likelihood ratio test is greater than  $15\%.$  All methods share the same characteristic relationships between sample size and power: power increases with sample size, and the rate of increase becomes greater as difference between two populations increase (Fig. 8.2). When comparing populations with a  $+25\%$  or  $-20\%$  change in the mean fire-return interval (mFRI), particularly for the two least powerful tests, the results did not stabilize after 1000 simulations (Fig. 8.2). With this small difference between populations, all methods have generally low power for most sample sizes.

The relationship between sample size and power is strongly dependent upon the shape of the FRI distribution, characterized by the Weibull  $c$  parameter (Fig. 8.3). As  $c$  increases, the variance in the distribution decreases, and it therefore becomes easier to separate two distributions with fewer samples. The impacts of varying  $c$  parameters on statistical power are not negligible and can be as large as the impacts of samples size itself.

### CONCLUSIONS

Comparing two fire-frequency regimes implicitly tests the null hypothesis that the two populations do not differ. Given the high variability of fire-return-interval data, statistical tests accounting for this variability are useful tools for drawing inferences on fire regimes. In the absence of an explicit statistical comparison, the possibility of drawing false inferences on change (Type I error) or lack of change (Type II error) in fire regimes are unknown. Given that fire history studies frequently use Weibull models to describe fire-return-interval data, it is logical to utilize all the parameters associated with this model when making statistical comparisons, so as to maximize statistical power. The likelihood ratio test presented here does just that, and the sample-size power analysis clearly indicates that it provides a more powerful test than those previously used (Clark 1989, Lynch et al. 2002, Gavin et al. 2006)). This test is applicable to datasets generated from stand-ages, fire scars, or sediment-charcoal records, so long as the assumptions outlined above are met (see “Comparing distributions of fire return intervals”). The choice to use a permutation test or a Chi-Square distribution to obtain the probability of Type I error (i.e. p-value) has negligible effects at larger samples sizes ( $\sim 50$  samples per

population). At smaller samples sizes, however, the permutation test is a more conservative estimate of p-values, and may be more appropriate than assuming a Chi-Square distribution.

The relationships between sample size and statistical power (Fig. 8.2) have important theoretical and practical relevance. First, detecting small changes in fire-frequency regimes (e.g. <25% change) will require unusually large sample sizes (> 50 fires per population). This is relevant to studies attempting to quantify impacts of short-term climatic changes (e.g. Little Ice Age, or current global warming) on fire-frequency regimes. In order to obtain sufficient statistical power, one must increase the time and/or space over which fires are sampled, which forces researcher to evaluate the assumptions of uniform variability in these domains. Eventually, a maximum temporal and/or spatial domain will be reached, and it will be impossible to sample additional fires without violating assumptions of uniform variability. Thus, over short time periods, it is entirely possible that the impacts of climate on fire-frequency regimes (NOT fire occurrence) could never be detected.

Theoretically, a minimum sample size required to discriminate between two fire-frequency regimes implies that the concept of a fire regime is only relevant at particular spatial and temporal scales. That is, if one cannot meaningfully define a fire regime without X number of return intervals, then the fire regime does not exist practically until X+1 fires occur. Ecologically, this fact will be magnified in systems where fires are infrequent. It makes little sense, therefore, to think about changes in fire regimes at some spatial and temporal scales. This scale should depend upon the spatial variability in biotic

(e.g. vegetation) and abiotic (e.g. topography) features, and on the temporal variability in fire occurrence (relative to the temporal variability of climatic changes).

Finally, the sample-size power analyses conducted here serves as a tool for planning future research that aims to detect changes in fire-frequency-regimes. Specifically, based on the potential or anticipated changes in fire frequencies between two populations (e.g. time periods, or geographic regions), one can assess the number of fires needed to obtain sufficient statistical power for discriminating different regimes. The lower four x-axes in Fig. 8.2 indicate the approximate time needed to sample in order to obtain the number of fires indicated on the primary x-axis, and thus to obtain the statistical power indicated on the y axis. Fig. 8.3 can be used to estimate statistical power for a wide range of comparisons, where sample size and both Weibull  $b$  and  $c$  parameters vary.

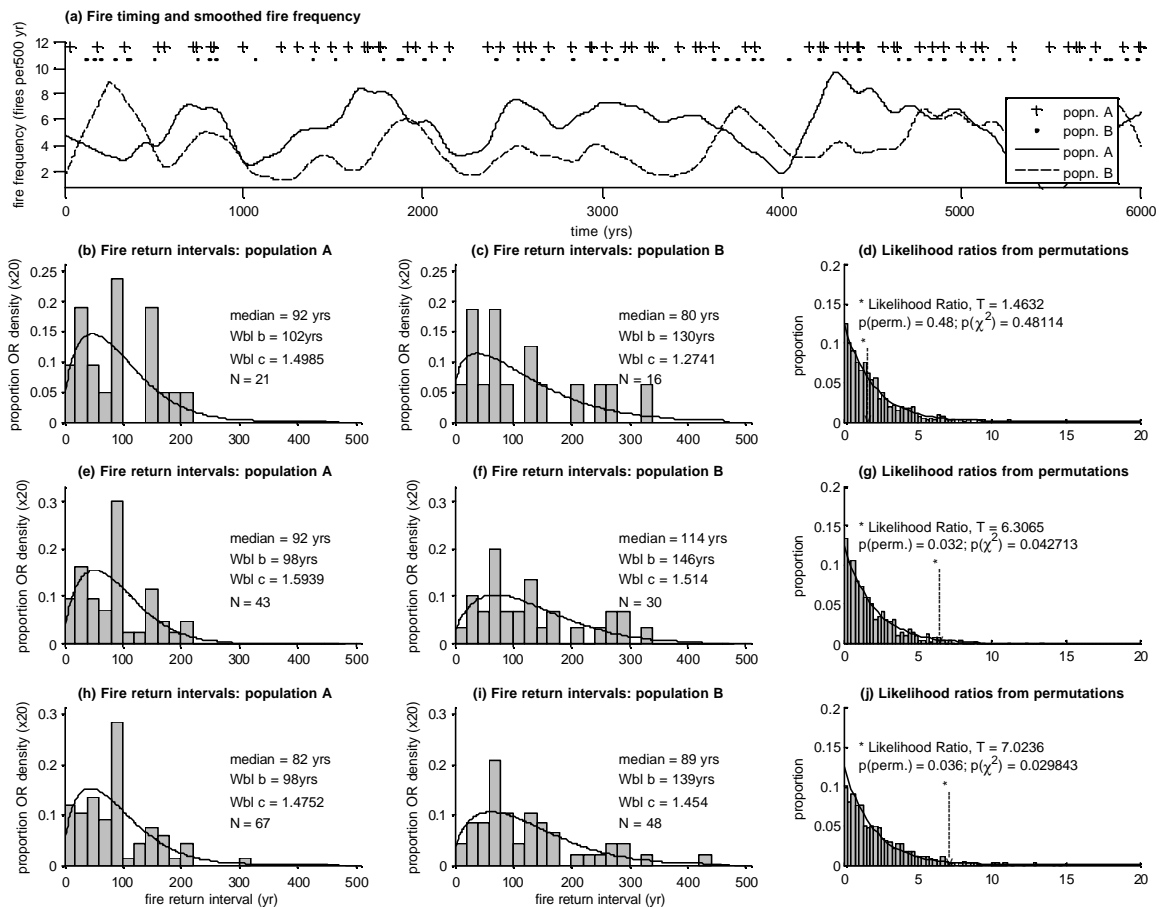


**Figure 8.1.** (a) Fire events derived from random samples of two Weibull distributions (population A, Weibull  $b = 100$  yrs,  $c = 1.5$ ; population B, Weibull  $b = 150$  yrs,  $c = 1.5$ ) illustrating the variability inherent in fire occurrence data and the potential to draw false conclusions from visual comparisons of fire frequencies. Fire frequencies, in this case at 500 year time scales, vary randomly despite no change in the distribution parameters from which the samples came from, and thus the two populations appear similar at times and distinct at other times. The same principle holds when the sampling unit is space instead of time. The two left columns summarize fire-return intervals from 0-2000 (b, c), 0-4000 (e, f), and 0-6000 years (h, i), for populations A and B (left and center column, respectively), illustrating the effects of sample size on characterizing fire-frequency regimes. The right column illustrates the decision rule used in the likelihood ratio test to reject or accept the null hypothesis of no difference between populations. The likelihood ratio,  $T$ , from one comparison is compared to (1) the distribution of  $T_j$  values from 1000 permutations (grey bars), representing the same test under the constraints of the null hypothesis of no difference between populations, or (2) the probability of obtaining the given  $T$  value from a Chi-Square distribution with  $k = 2$  degrees of freedom (black line). If the two populations are truly different, the observed  $T$  will be unlikely to occur in the permutation tests. Each row (d, g, j) illustrates the increased power obtained as sample sizes increase: although the null hypothesis is truly wrong, comparisons from 0-2000 yrs fails to detect this difference (d vs. g, j).

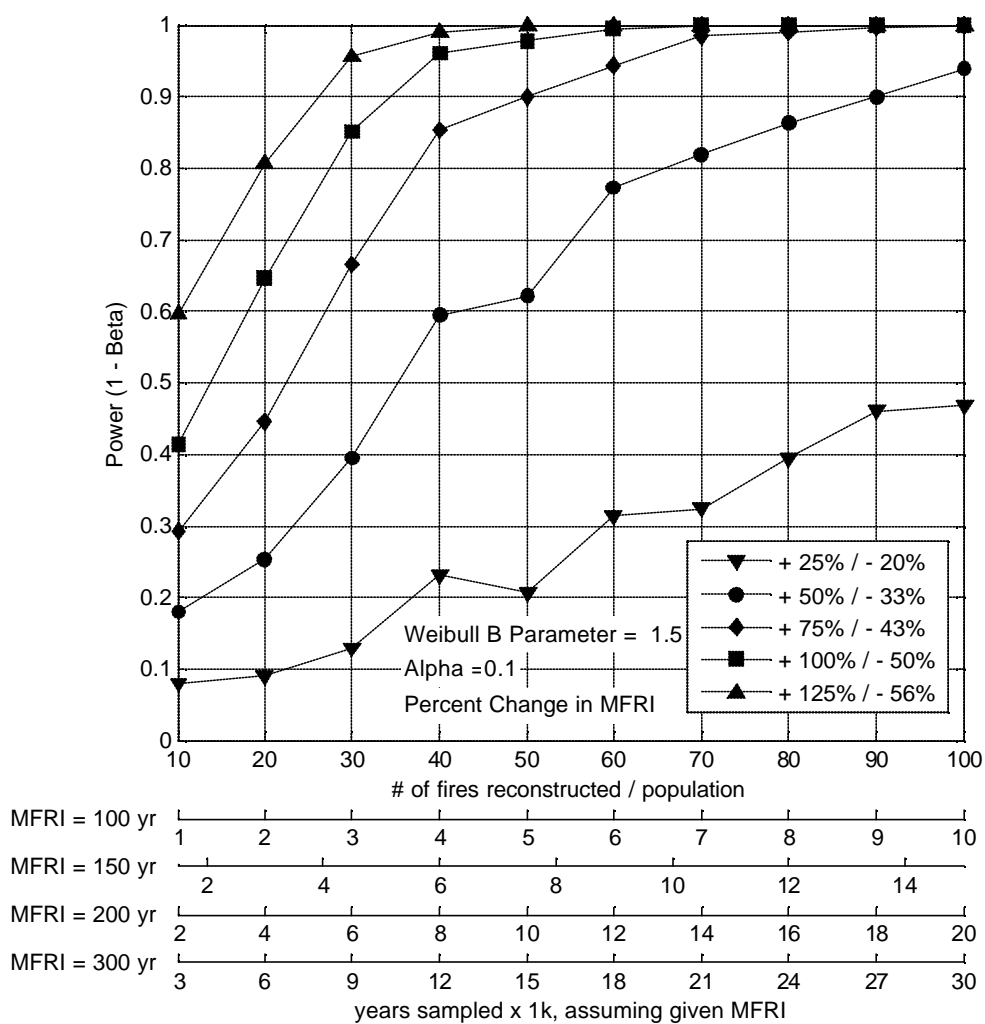


**Figure 8.2 (a).** Power as a function of sample size for (a) the two-sample K-S test, (b) comparing  $100 \cdot (1 - \alpha)$ -percent confidence intervals, (c) the likelihood ratio test using 1000 permutations to calculate p-values, and (d) the likelihood ratio test using a Chi-Square distribution to calculate p-values. Each line represents a different magnitude of change in Weibull  $b$  parameters (directly related to the median return interval). The lower four x-axes indicate how many years are required to obtain the number of fires indicated on the primary x-axis, assuming the mean fire return interval (MFRI) indicated on the left of the given secondary x-axis.

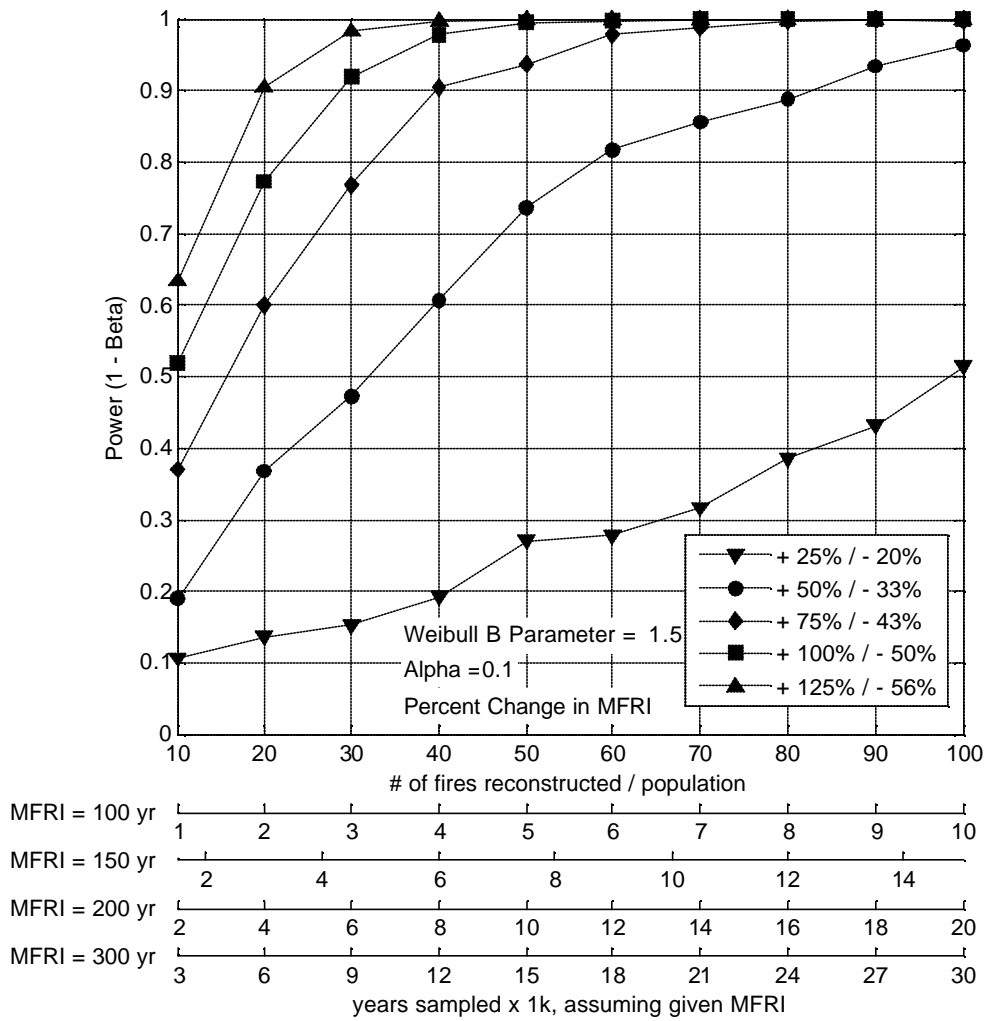


Figure 8.2 (b).

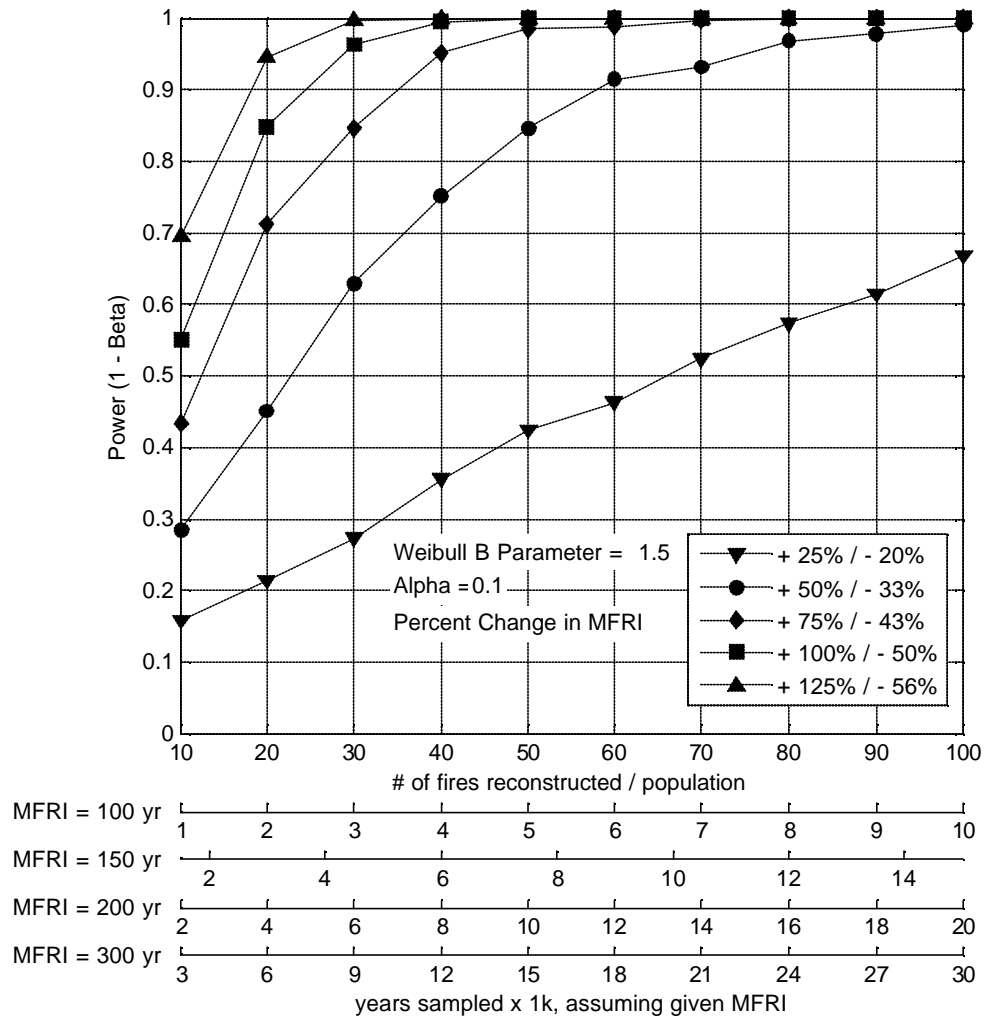


Figure 8.2 (c).

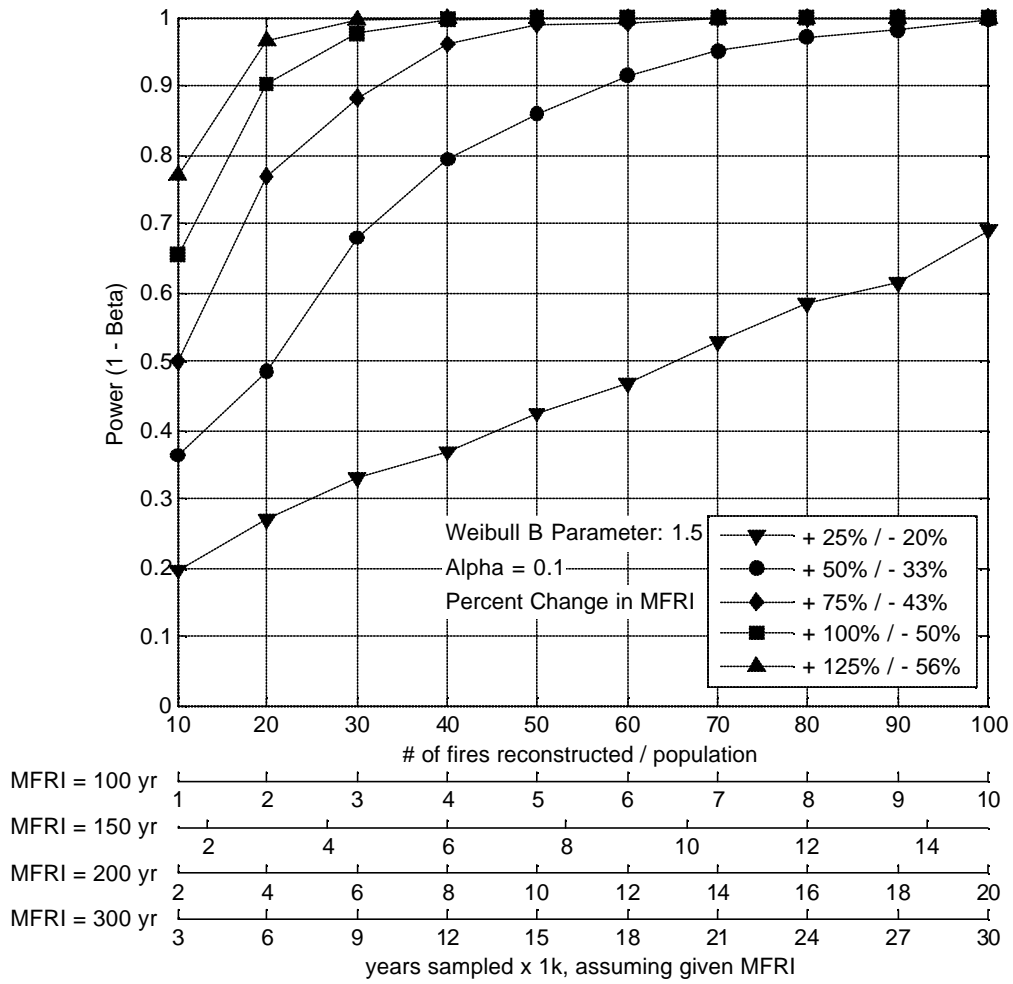
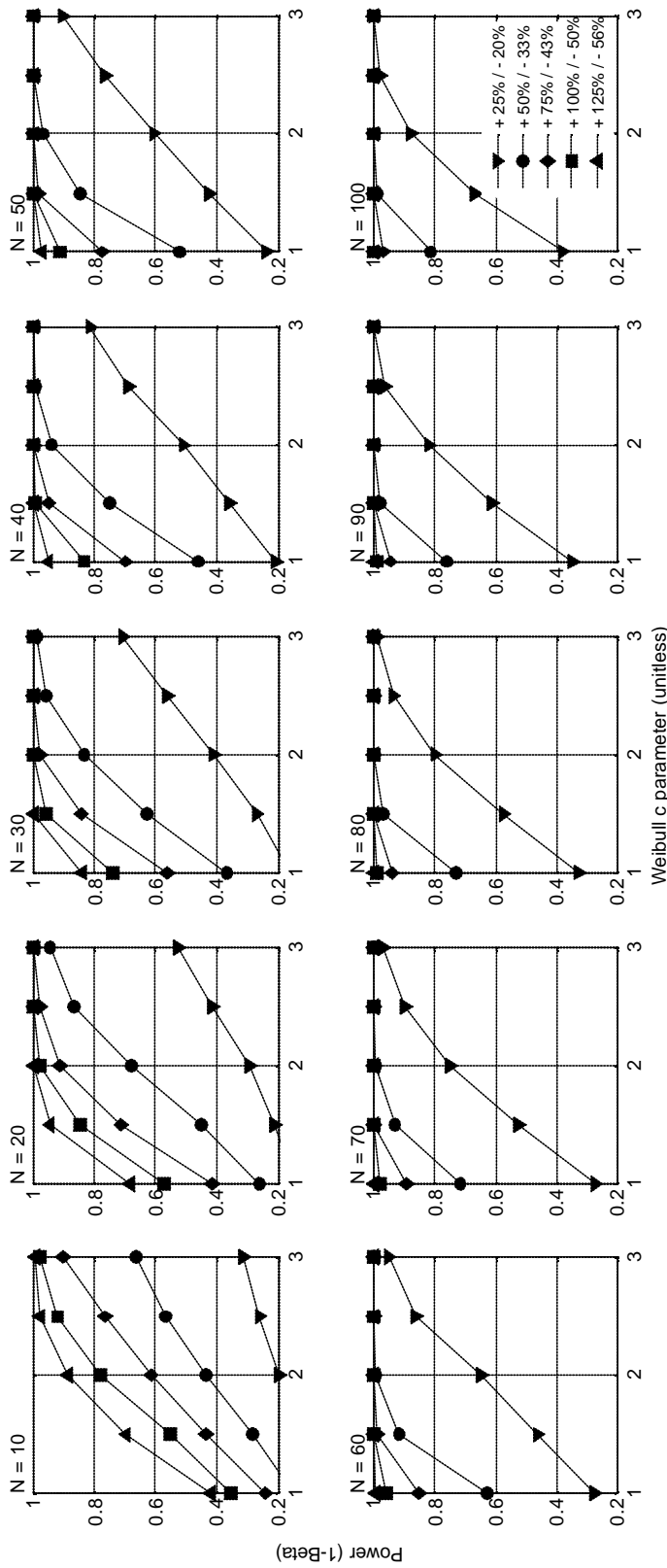


Figure 8.2 (d).



**Figure 8.3.** Power as a function of Weibull  $c$  parameter for different sample sizes (each sub-plot) and different magnitudes of change in Weibull  $b$  parameters, using the likelihood ratio test with permutation-derived  $p$ -values (as in Figure 8.2 [c]).

### MATLAB FUNCTION FOR THE LIKELIHOOD RATIO TEST

To use the following function, save the scrip below as a Matlab function (\*.m) and put in the current working directory. You must pass the function three variables:

1. FRI\_data: observed (fire) return intervals organized in columns, where each column (j) represents one population that will be compared to all other populations, and each row (i) is an observed return interval. Empty cells must contain “NaN”, such that the final matrix has no blank values.
2. alpha: specifies the significance level for the test, e.g. 0.05.
3. n\_perm: specifies the number of permutations to use in the permutation test to estimate the probability of Type I error,  $p$ . If sample sizes are large (e.g.  $> 30$ ), you can set n\_perm equal to 0, in which case  $p$  is calculated from a Chi-squared distribution.

For example, in Matlab, you would define these variables, and then enter in the command

line: `[H,P,N] = wbl_LRT (com_FRIs,alpha,n_perm)`

After the function has run (which can take a few minutes, depending on the value of n\_perm), this will return two matrices, H and P, where each row (i) corresponds to populations 1 through n-1, where n is the total number of populations being compared (i.e. columns in FRI\_data), and each column (j) corresponds to populations 2 through n. The values in the matrix are the results of comparing population i to population j, and therefore half of the matrix will be blank (NaN). The variable P contains the probability of Type I error, and the matrix H contains a “1” where the probability of Type I error is  $\leq$  alpha, and a 0 otherwise. The variable N contains the number of return intervals in each population (column) in FRI\_data.

The symbol “%” signifies code that is commented out. Text following “%” is to be read to help understand what the function is doing.

```

function [H, P, N, T] = wbl_LRT (FRI_data, alpha, n_perm)
% wbl_LRT.m
% Compare two populations fit with Weibull distributions using a
% Likelihood-ratio Test to test Ho: b1 = b2 AND c1 = c2 against Ha: a1 ~ a2
% OR b1 ~ b2, where b and c are the maximum likelihood estimates for the
% scale and shape parameters, respectively, for each hypothesized
% population (1, 2...n).

% The likelihood-ratio test statistic, T, = 2(logLike(H1) + logLike(H2) -
% logLike(Ho))
% If the true parameters of Ho and Ha are equal, then the distribution of T
% is approximately chi-square with n-2 degrees of freedom, where n is the
% number of observations in both populations.
% If n_perm is set to 0, then:
% This T is compared to a Chi-squared distribution with k degrees of
% freedom (where k = 2 = # of additional parameters in H1 relative to H0),
% and a p-value is derived. If p < 1-alpha, then H0 is rejected.
% If n_perm > 0, then:
% In practice, the distribution of T under Ho is unknown, so we estimate
% it using a permutation test. Under the assumption of Ho, we select N1,
% N2, and N1+N2 samples from a permuted Ho dataset. We then calculate the
% likelihood ratio statistic in the same fashion as under Ha.
% We do this n_perm times and compute a new statistic T(j) for each
% permutation. Using the newly computed statistics (T(j), T(j+1)...
% T(n_perm)) we can approximate the p-value to test Ho:
% p = 1/n_perm * (sum(T(j) > T)), where '(sum(T(j) > T))' represents the
% number of times a randomly generated permutation results in a log
% likelihood difference greater than the log likelihood difference observed
% in the original dataset. If the two distributions are truly different,
% then the statistics from the permutations, T(j), should be smaller
% than T most of the time.

% CREATE VARIABLES AND SPACE FOR NEW VARIABLES
[n m] = size(FRI_data); % dimensions of incoming dataset, with n rows
% of fire return intervals, and m columns
% of populations
H = NaN(m-1, m-1); % space for hypothesis test results: 1 = reject
% 0 = fail to reject, assuming alpha
P = NaN(m-1, m-1); % space for p-value to go for each comparison
N = NaN(1, m); % space for N (sample size) of each population

% COMPARE EACH POPULATION TO EACH OTHER
for i = 1:m-1 % for each population, popn1
    disp(['popn. comparison ', num2str(i), ' of ', num2str(m-1)]) % display
    % the comparison being made on screen
    for k = i+1:m % for each population being compared to popn1, popn2
        % define the populations
        popn1 = FRI_data(FRI_data(:, i) > 0, i); % population 1
        popn2 = FRI_data(FRI_data(:, k) > 0, k); % population 2
        popn_Ho = [popn1; popn2]; % combined population, Ho
        n1 = length(popn1); % N for population 1
        n2 = length(popn2); % N for population 2
        nHo = n1+n2; % N for Ho population

        % estimate Weibull a and b parameters with maximum likelihood method
        param_popn1 = wblfit(popn1); % MLE for Weibull b and c parameters
        % for popn1
        param_popn2 = wblfit(popn2); % same for popn2
        param_Ho = wblfit(popn_Ho); % same for popn_Ho

        % compute negative log-likelihood values for each population
        NLL_popn1 = -1*wbllike(param_popn1, popn1); % negative log-likelihood
        % for popn1
        NLL_popn2 = -1*wbllike(param_popn2, popn2); % negative log-likelihood
        % for popn2
        NLL_popn_Ho = -1*wbllike(param_Ho, popn_Ho); % negative log-likelihood
        % for popn_Ho
        % Calculate likelihood ratio statistic, T
        T = 2*(NLL_popn1 + NLL_popn2 - NLL_popn_Ho);

        if n_perm == 0 % if n_perm = 0, derive p-value from Chi^2 distribution
            % compute likelihood ratio statistic, T
            T = 2*(NLL_popn1 + NLL_popn2 - NLL_popn_Ho);
            P_val = 1-chi2cdf(T, 2); % p-value derived from chi squared
        end
    end
end

```

```

                                % distribution
P(i, k-1) = P_val;    % fill in P matrix with p-values
if P_val < alpha
    H(i, k-1) = 1;    % if P is less than alpha, make H = 1
else
    H(i, k-1) = 0;    % else make H = 0
end
else % if n_perm ~= 0, derive p-value from permutations
% Calculate n_perm T(j) statistics to calculate p-value for each
% comparison
for j = 1:n_perm % for each permutation, j
    perm = randperm(length(popn_Ho)); % random permutation of the
    % combined dataset (popn_Ho)
    Ho_perm = popn_Ho(perm); % Ho population for this permutation
    % is the permutations selected from popn_Ho
    popn1_perm = Ho_perm(1:length(popn1)); % popn1 for this
    % permutation is the first length(popn1) values from Ho_perm
    popn2_perm = Ho_perm(length(popn1)+1:length(Ho_perm)); % popn2 for
    % this permutation is the remaining values from Ho_perm

    % compute negative log likelihood values for each population
    NLL_Ho_perm = -1*wbllike(wblfit(Ho_perm), Ho_perm); % negative
    % log-likelihood values for Ho_perm
    NLL_popn1_perm = -1*wbllike(wblfit(popn1_perm), popn1_perm);
    % negative log-likelihood values for popn1_perm
    NLL_popn2_perm = -1*wbllike(wblfit(popn2_perm), popn2_perm);
    % negative log-likelihood values for popn2_perm

    T_perm(j) = 2*(NLL_popn1_perm + NLL_popn2_perm - NLL_Ho_perm);
    % T statistic for this permutation, j
end
% Find p-value for this comparison
P_val = 1/n_perm * sum(T_perm > T); % P is the number of time T_perm is
% greater than T, divided by the total number of permutations.

P(i, k-1) = P_val;    % fill in P matrix with p-values
if P_val < alpha
    H(i, k-1) = 1;    % if P is less than alpha, make H = 1
else
    H(i, k-1) = 0;    % else make H = 0
end
end % end code to calculate p-value
N(i) = n1;            % fill in N with n of popn1
end
end
N(length(N)) = n2;    % fill in the last value in N with n of popn2

```

**VITA****Philip Edward Higuera****Date of Birth**

12 February, 1976

**Place of Birth**

Royal Oak, Michigan, U.S.A.

**Education**

B.A. Middlebury College (*magna cum laude*), Biology (high honors), Environmental Studies-Geology (high honors), 1998

M.S. University of Washington, College of Forest Resources, Forest Ecosystem Analysis, 2002

Ph.D. University of Washington, College of Forest Resources, Forest Ecosystem Analysis, 2006

**Publications**

**Higuera, P. E.**, D. G. Sprugel, and L. B. Brubaker. 2005. Reconstructing fire regimes with charcoal from small-hollow sediments: a calibration with tree-ring records of fire. *The Holocene* **15**:238-251.

Hu, F. S., L. B. Brubaker, D. G. Gavin, **P. E. Higuera**, J. A. Lynch, T. S. Rupp, and W. Tinner. 2006. How climate and vegetation influence the fire regime of the Alaskan Boreal Biome: the Holocene perspective. *Mitigation and Adaptation Strategies for Global Change* **in press**.

Trombulak, S. C., **P. E. Higuera**, and M. DesMeules. 2001. Population trends of wintering bats in Vermont. *Northeastern Naturalist* **8**:51-62.